STUDY OF HYDROGEN PORT INJECTION SI ENGINE

Thesis

Submitted in partial fulfilment of the requirements for the degree of

DOCTOR OF PHILOSOPHY

by

JAYASHISH KUMAR PANDEY

DEPARTMENT OF MECHANICAL ENGINEERING

NATIONAL INSTITUTE OF TECHNOLOGY KARNATAKA,

SURATHKAL, MANGALORE -575025

February 2023

STUDY OF HYDROGEN PORT INJECTION SI ENGINE

Thesis

Submitted in partial fulfilment of the requirements for the degree of

DOCTOR OF PHILOSOPHY

by

JAYASHISH KUMAR PANDEY

DEPARTMENT OF MECHANICAL ENGINEERING

NATIONAL INSTITUTE OF TECHNOLOGY KARNATAKA,

SURATHKAL, MANGALORE -575025

February 2023

DECLARATION

I hereby *declare* that the Research Thesis entitled "**Study of hydrogen port injection SI engine**" which is being submitted to the National Institute of Technology Karnataka, Surathkal in partial fulfilment of the requirements for the award of the Degree of **Doctor of Philosophy** in "Department of Mechanical Engineering" is a *bonafide report of the research work carried out by me*. The material contained in this Research Thesis has not been submitted to any University or Institution for the award of any degree.

Registration Number   : 187008

Name   : Jayashish Kumar Pandey

Signature   : *Jayashish Kumar*

Department of Mechanical Engineering
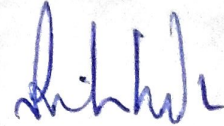
Place: NITK-Surathkal

Date: 07/02/2023

CERTIFICATE

This is to *certify* that the Research Thesis entitled "**Study of hydrogen port injection SI engine**" submitted by **Jayashish Kumar Pandey, (Register Number: 187008)** as the record of the research work carried out by him, *is accepted as the Research Thesis submission* in partial fulfilment of the requirements for the award of the degree of Doctor of Philosophy.

Dr. Kumar G. N.

(Research Guide)

Date: 07/02/2023

Chairman – DRPC

Date: 9.2.2023

प्रपञ्चोपशमंशान्तंशिवमद्वैतं चतुर्थंमन्यन्तेसआत्मासविज्ञेयः, ज्ञानमिच्छेत्महेश्वरात्

इन्द्रंमित्रंवरुणमग्निमाहुरथोदिव्यःससुपर्णोगरुत्मान्।

एकंसद्विप्राबहुधावदन्त्यग्निंयमंमातरिश्वानमाहुः॥ Rg Veda 1.164.46

∥ Shiva is the fountain head of all types of knowledge ∥

ACKNOWLEDGEMENT

ABSTRACT

The rapidly growing energy demands and environmental concern of transportation sector, primarily powered by hydrocarbon-based fossil fuelled IC engines are looking for a sustainable energy economy. Among the alternates, the carbonless hydrogen is the most suitable fuel that can be adopted with minute changes. Most of the hydrogen properties, such as a high autoignition temperature and a high-octane rating, find it suitable for the SI engine. However, low volumetric energy content and higher diffusivity limit power output. Hence, an increased CR helps overcome the volumetric losses. Besides, equivalence ratio (ϕ) plays a vital role in SI engines. Another primary concern is NO_x, which worsens by increasing CR and ϕ. Many researchers concluded that retarded ignition timing (IT) reduces NO_x emissions. However, it is not explicit about falling under the permissible limit. Hence, effective NO_x reduction tool EGR is preferred, and the power drop due to EGR can be improved by boosting MAP.

The experimental study is conducted in two stages under WOT conditions at three engine speeds, 1400rpm, 1600rpm and 1800rpm for hydrogen PFI SI engine. In the first stage, the effect of varying CR from 10 to 15 at various ϕ from 0.4 to 1.0, keeping the IT fixed at 20ºCA bTDC is studied as first phase. An optimal operating parameter is decided based on the trade-off between BTE and NO_x emissions. Later, the effect of variable IT from 24ºCA bTDC to 14ºCA bTDC is studied at the selected CR for ϕ varying ±0.05 from ϕ decided from first phase. The optimised IT and ϕ are decided for the next stage. Various EGR ratios (from 5% to 15%) at variable MAP (from N/A to 110kPa) are studied for NO_x control at minimal power loss in the last stage.

BP and BTE, η_{vol} dropped rapidly. At high CR (>13), a rich mixture ($\phi \geq 0.9$) has adverse effects, reducing BTE. P_{max} and HRR_{max} are increased by increasing CR for $\phi < 0.9$. While, for $\phi = 0.9$ at 1800rpm, they are nearly static for CR14 and CR 15, at $\phi = 1.0$, dropped slightly at CR 15. CA10 was reduced with increasing CR and ϕ, while CA10-90 shortens with increasing CR for $\phi < 0.8$. CA10-90 is increased slightly for $\phi \geq 0.8$ after CR13. CoV_{IMEP} was reduced by increasing CR for $\phi \leq 0.8$, while after $\phi = 0.8$, there is a slight increase noticed after CR13. The specific NO_x emissions are increased with ϕ,

CR and speed. However, for $\phi=1.0$ at CR15, NO_x emission is dropped insignificantly. CR14 has the best trade-off between BTE and NO_x at $\phi=0.7/0.8$.

Delaying IT improved BP and BTE till maximum and then deteriorates at any speed and ϕ. The optimal IT retards with increasing ϕ and speed. CA10 is reduced, while CA10-90 reduces till certain IT. The IT of minimum combustion duration is retarded with increasing ϕ and speed. P_{max} and HRR_{max} are reduced by retarding IT, while the rate of rise in CP and HRR before TDC is increased. T_{max} is reduced by retarding IT, and CoV_{IMEP} is reduced till a certain IT. EGT is increased gradually with IT retard at low speed and low ϕ, and rapidly at high speed. Retarding IT reduces NO_x emissions. The rate of reduction increases with increasing ϕ and speed. 16ºCA bTDC, IT at $\phi=0.8$, is efficient for controlling NO_x moderately without BTE compromise.

BP and BTE are improved for low EGR (5-7.5%) but dropped rapidly with a further increase in EGR. η_{vol} is reduced continuously with EGR. Boosting MAP increases BP, BTE, and η_{vol}; even at high EGR, power is regained by 5% by boosting MAP to 110kPa. CP, and HRR are increased slightly for low EGR but dropped rapidly with higher EGR. Boosting MAP increased CP and HRR due to large fuel supplied to maintain ϕ. Similarly, increasing η_{vol} supplies more air, increasing CA10, and a large fuel mass increased CA10-90. A slight EGR has reduced CA10 and CA10-90, but a higher EGR deteriorated combustion. Similarly, T_{max} and EGT increased with EGR up to 5%. A net 34% NO_x reduction is observed at MAP 110kPa by 15% EGR than N/A conditions.

The hydrogen-fuelled SI engine competes equally with the gasoline SI engine at a relatively higher CR, retarded ignition, and has efficient NO_x control by EGR implemented parallelly with MAP boost. Further, based on the current findings, research can be advanced in a more complicated but efficient technology, such as high-pressure hydrogen DI SI system, variable MAP control through supercharging, and split high-pressure hydrogen DI.

CONTENTS

LIST OF TABLES

LIST OF FIGURES

x

NOMENCLATURE

A/F	Air-Fuel Ratio
A/F_{sto}	Stoichiometric Air-Fuel Ratio
A/F_{actual}	Actual Air-Fuel Ratio
ATR	Auto Thermal Reforming
BMEP	Brake Mean Effective Pressure
BP	Brake Power
BSEC	Brake Specific Energy Consumption
BSFC	Brake Specific Fuel Consumption
bTDC	before Top Dead Centre
BTE	Brake Thermal Efficiency
^{o}CA	Crank angle in degree
CA10	Crank angle travelled corresponding to 10% fuel mass burnt
CA10-90	Crank angle travelled between 10% to 90% fuel mass burnt
CA90-100	Crank angle travelled between 90% to 100% fuel mass burnt
CA50	Crank angle travelled corresponding to 50% fuel mass burnt
CA5	Crank angle travelled corresponding to 5% fuel mass burnt
cc	cubic centimetre
CDI	Capacitive Discharge Ignition
CH_4	Methane
CI	Compression Ignition
CNG	Compressed Natural Gas

CO	Carbon Mono-oxide
CO_2	Carbon Di-oxide
CoV_{imep}	Coefficient of Variations in IMEP
CP	Cylinder Pressure
CR	Compression Ratio
DAQ	Data Acquisition System
DI	Direct Injection
DME	Di Methyl Ether
ECU	Engine Control Unit
EER	Energy Efficiency Ratio
EGR	Exhaust Gas Recirculation
EGT	Exhaust Gas Temperature
g/kWh	gram per kilo-watt-hour
GDI	Gasoline Direct Injection
H_2	Molecular Hydrogen
H_2O	Water
HC	Unburnt Hydrocarbon
HICE	Hydrogen Internal Combustion Engine
HOT	Half Open Throttle
HP	High Pressure
HPFI	Hydrogen Port Fuel Injection
HPI	Hydrogen Port Injection
HRR	Heat Release Rate

HRR$_{max}$	Peak Heat Release Rate
ICE	Internal Combustion Engine
IMEP	Indicated Mean Effective Pressure
ITE	Indicated Thermal Efficiency
IT	Ignition Timing
kPa	Kilo Pascal
LP	Low Pressure
lph	litres per hour
lpm	litres per minute
MAP	Manifold Absolute Air Pressure
MBT	Maximum Brake Torque
MGP	Mean Gas Pressure
MGT	Mean Gas Temperature
mJ	Millijoule
MJ	Mega Joule
mm	Millimetre
MW	Megawatt
N	Engine speed in rpm
N/A	Naturally Aspirated Conditions
NHR$_{max}$	Peak Net Heat Release Rate
NO	Nitrous Oxide
NO$_x$	Oxides of Nitrogen
P	Load in kg

PEM	Proton Exchange Membrane
PFI	Port Fuel Injection
PM	Particulate Matter
P_{max}	Peak Cylinder Pressure
POX	Partial Oxidation
RGF	Residual Gas Fraction
RON	Research Octane Number
RPR	Rate of Pressure Rise
rpm	Revolutions per Minute
RTD	Resistance Temperature Detector
SFC	Specific Fuel Consumption
SI	Spark Ignition
SMR	Steam Methane Reforming
TDC	Top Dead Centre
TDP	Thermal Dilution Parameter
T_{max}	Peak Cylinder Temperature
TPS	Throttle Position Sensor
WGS	Water Gas Shift
WHR	Water Injection Rate
WOT	Wide Open Throttle
η_{th}	Brake Thermal Efficiency
η_{vol}	Volumetric Efficiency
λ	Air-excess Ratio

ϕ	Equivalence Ratio
l	Arm-length in mm
$\dot{m}_{EGR}$	EGR Mass Flow Rate (g/min)
$\dot{m}_{exhaust}$	Mass Flow Rate of Exhaust (g/min)
$\dot{m}_{air}$	Mass Flow Rate of intake air (g/min)
$\dot{m}_{H_2}$	Mass Flow Rate of hydrogen (g/min)
g	Gravitational Acceleration (m/s^2),
ρ_{air}	Density of Air (kg/m^3)
ρ_{water}	Density of Water (kg/m^3)
h_{water}	Differential Pressure Reading (air pressure sensor, mm of water column)
A_m	Orifice Area (3.142×10^{-4} m^2 for both airbox and EGR throat)
C_d	Coefficient of Discharge (0.6 for both airbox and EGR throat)
M_{ex}	Molecular Weight of Exhaust (kg/kmol)
SE_i	Specific emission of any entity (g/kWh)
VE_i	Emission data recorded by the analyzer of any entity
M_i	Molecular Weight of the entity (kg/kmol)
$T_{w_{in}}$	Cooling Water Temperatures at the inlet to the calorimeters
$T_{w_{out}}$	Cooling Water Temperatures at the outlet to the calorimeters
$T_{exhaust_{in}}$	Exhausted Air Temperatures at the inlet to the calorimeter
$T_{exhaust_{out}}$	Exhausted Air Temperatures at the outlet to the calorimeter,
$\dot{m}_{water}$	Mass Flow Rate of cooling water in the calorimeter

CHAPTER 1

INTRODUCTION

The existence and success of any civilization depend upon energy and its efficient conversion from one form to another. The thought of growth always drives the human mindset from the start of the human race until today. Energy is needed for developing such a demanded atmosphere of technology. With the advancement in people's living standards, transportation has taken an ample space in everyone's life. Goods produced in one place are sold in a wide range of areas; similarly, people travel to other places for many specific reasons. All of these sicknesses of transportation demand more consumption of energy sources. In modern days the vast majority of these energy demands are fulfilled by internal combustion engines. The primary energy sources supplied to these engines are fossil fuels, which are available in nature in limited quantity and usually are hydrocarbon constituents. These fossil fuels are a limited energy source, depleting rapidly towards its end with increasing energy demands, finding a way hard to fulfil the energy demands after a certain period.

1.1. Drawbacks of fossil fuels

Fossil fuels are carbon-based in structure and slender in quantity, which increases energy insecurity. Apart from that, these fuels have another limitation: emission. Hydrocarbon basically after burning leaves CO_2 theoretically, while in operation to the powertrains, it has unavoidable other emissions such as NO_x, Particulate Matters(s), some Sulphur contents, and unburnt hydrocarbons. Small size (less than 2.5) PMs can easily penetrate human blood vessels and harm the respiratory and cardiovascular systems (Technologies, 2013). Several researchers believe that air pollution can cause congenital disabilities too. The burden of air pollution is not limited to economic zones; it has nearly the same impact on low-, middle- and high-income grade nations. However, a developing nation is less aware of the danger; Figure 1.1 shows a glimpse of the death rate due to air pollution in 2019. India, a developing nation, faces the worst consequences of air pollution, recording a very high number of causalities due to air

pollution. According to the centre of science and environment India's report, out of9 66.7lakh deaths due to air pollution in 2021, 25lakh deaths are recorded in India. In modern days, the government and society are also concerned about the environment, making stricter norms concerned with air pollution by vehicles.
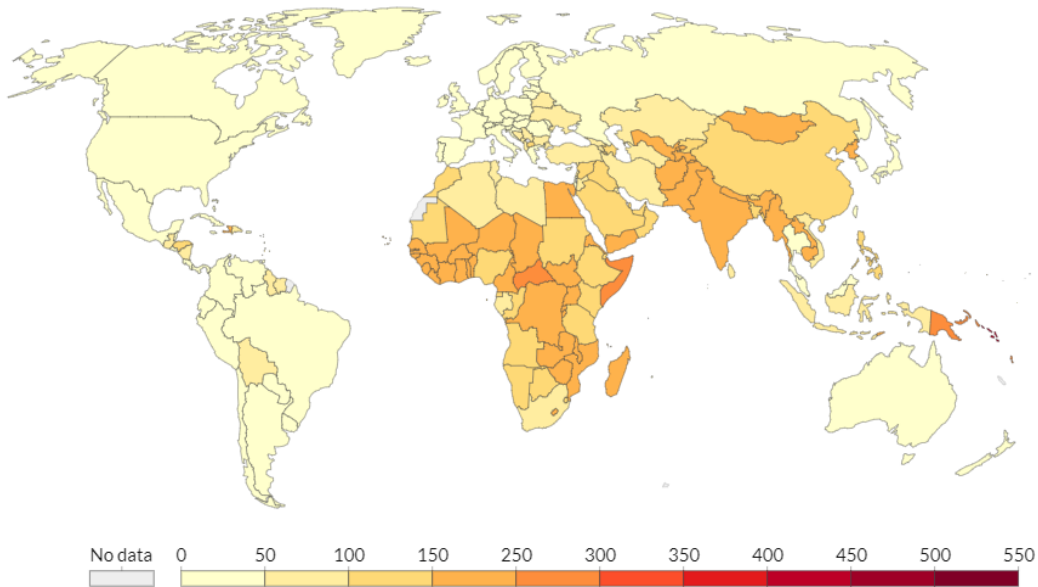
Figure 1.1.The death rate per 1,00,000 people from air pollution (2019, Source: IHME, Global Burden of Disease)

Apart from pollution, the rapid rise in population and the enhancing living standards ask for rapid growth in energy supply to the transportation sector, but the conventional petroleum fuel resource is limited to a specific geographic area. Therefore, other nations are bound to import from the producer nations, adversely impacting the economy. India is no exception; imports meet over 85% of the petroleum demand in the financial year 2020-21. If we look at the crude oil demand of India, we have nearly reached ten times our oil imports in 2020 than 1990 (shown in Figure 1.2). It impacts our economy even more intensively due to rising oil prices, primarily due to reduced production to demand ratio and depletion of the reserves. We can understand it more specifically in terms of the budget, which rose to $11920crores in the financial year 2021-22 from $313crores in the financial year 1987-88(Panagariya, 2004).
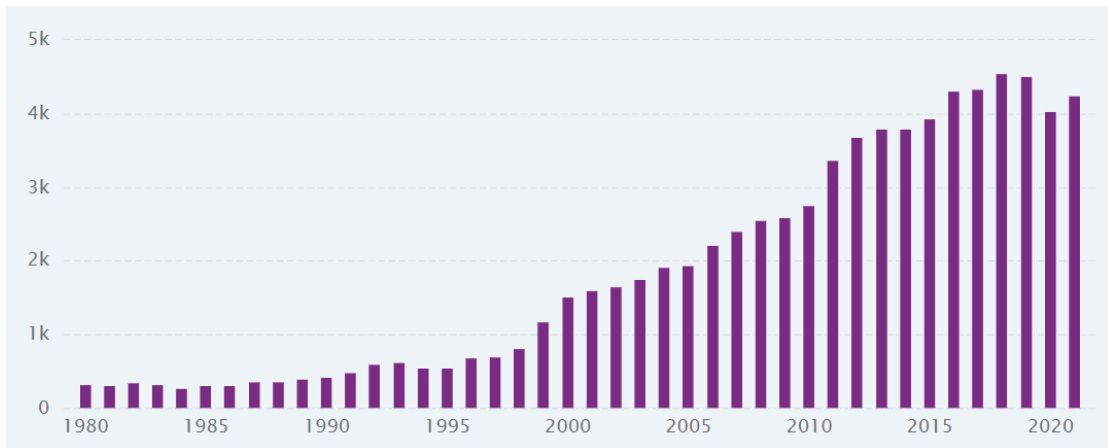
Figure 1.2.Net daily oil import of India over the years (1980-2021, source: - www.ceicdata.com, Organization of the Petroleum Exporting Countries)

1.2. Need for an alternative source of energy

The primary consequence of dependence on petroleum products is energy insecurity and economic fragility. There is only one option to overcome such hurdles, to be energy independent. There are several ways researchers have proposed and worked on to relieve the energy insecurity in the transportation sector, including primarily renewable technology. There are two primary proposals for renewable energy technology given; the first alternative fuels, including biofuels or hydrogen, and another is electric vehicles. There are two kinds of electric vehicle technology available, fuel cell and battery-powered vehicles, which get the energy from renewable energy sources such as solar and wind(Nouni et al., 2021; Pollet, Kocha, & Staffell, 2019). On the other hand, electric vehicle technology demands a complete makeover of the existing IC engine technology, a huge investment. Therefore, in the intermediate phase of shifting, biofuels are considered a suitable alternative(Verma et al., 2021).

1.3. Limitations of alternative technology

The attraction of battery-powered and fuel cell vehicles is zero-emission and noiseless operation. However, the primary source of energy supply to batteries is still conventional fuels like coal and nuclear. If the non-convention energy production technology is adapted like solar, wind, or ocean, it is bounded to territorial conditions. In addition, the battery technology is also often questioned, and there are several environmental concerns raised, including consequences of lithium mining and unsafe

disposal of decayed batteries(Lebrouhi et al., 2021; Liu, Placke, & Chau, 2022). Apart from that, another issue is the availability of surplus energy in developing countries like India, where the scarcity of energy still leads to frequent load shedding(Goel, Sharma, & Rathore, 2021). Hence, most researchers think hydrogen fuel cells are a long-term solution, which also comes up with a condition of highly pure hydrogen(Pollet et al., 2019). It is a costly affair, increasing the operating and vehicle costs in the current situation. Therefore, the intermediate solution, the biofuels, is better, which does not require a complete makeover of the existing technology, saving a considerable sum invested. The problem associated with biofuels, like biodiesels and alcohol, is similar to conventional fuels. These hydrocarbon-based fuels lead to high carbon emissions (Bergthorson & Thomson, 2015).

Hence, for the economy not to suffer critical modification and overcome emission drawbacks, there is a requirement for a perfect or almost perfect fuel with nearly zero carbon emission. Therefore, the fuel's essential property required is to be carbon-free. There is a general belief among researchers that hydrogen could be the fuel of the future, which is virtually zero-emission and has got all the potential of fuel to use in the existing engine technology with negligible modifications directly.

1.4. Hydrogen

Hydrogen is a colourless and odourless non-toxic gas with the least density of any material. It is vastly available in nature but in the form of compounds only. The atom consists of a non-neutronic nucleolus bearing only one proton surrounded by an alone electron. The normal state of the gas is diatomic, possessing two hydrogen atoms in aggregation with sharing electron cloud. Hence the gas has a molecular weight of 2, the lightest. In nature, it is found in compound forms, such as hydrocarbons, hydrides, and water. Water surrounds over two-thirds of the earth's surface, being the largest source of hydrogen. Hydrogen is widely used as a constituent chemical in many industrial processes, from ammonia and methanol production to refining petroleum products, from electric to metallurgic industries. It is also used as rocket propellants with oxygen in aerospace applications. Recently, the properties of hydrogen are being researched for its application as fuel.

1.5. Hydrogen as a fuel

Hydrogen is a beautiful substance that possesses several attractive features of an energy carrier. It is a clean fuel as it does not consist of any carbon atom and releases water vapors due to combustion. One of its greatness is the wide range of production, which involves synthesis from fossil fuels, biomass, solar energy, wind, and nuclear. Compared to other available alternatives like biofuel, the energy yield land area is relatively lower. Though hydrogen as a fuel to IC Engines goes for unquiet employment and the overall efficiency is far less than fuel cell, hydrogen fuel has many advantages in combustion engines. The IC engine is working fine with various fuels, so hydrogen can be one of them, which will not burden the existing economic structure. The fuel purity is also not strict compared to the fuel cell(S Verhelst, 2013).

Table 1.1.Properties of hydrogen-air mixture compared to methane and octane fuel (Sebastian Verhelst & Wallner, 2009)

Property	H_2	Gasoline
Molecular Weight (g/mol)	2.016	114.236
Density (kg/m^3)	0.08	692/740[b]
Autoignition temperature (K)	858	690
Adiabatic flame temperature (K)	2390	2276
Thermal diffusivity (mm^2/s)	42.1	18.3
Ratio of specific heats	1.401	1.389
Laminar burning velocity, ~360 K (cm/s)	290	45
Flammability limits (volume % in air/ φ)	4-75/ 0.1-7.1	1.1-6/ 0.66-3.85
Minimum ignition energy (mJ)	0.02	0.28
Minimum quenching distance (mm)	0.6	3.5
Lower heating value (MJ/kg)	120	44.3
Stoichiometric air-fuel ratio (kg/kg)	34.2	15
Heat of combustion (MJ/kg-air)	3.37	2.83[b]
Research octane number (RON)	>130	100/ 88-99[b]

b stands for commercial gasoline properties

Hydrogen has certain advantages over the existing IC engine fuels like gasoline and diesel. It has been widely tested for CI and SI engines. The research summarizes its properties to be the best fit in the SI engine respective to CI engines. The hydrogen's self-ignition temperature is higher than gasoline (Table 1.1), allowing for high CR

operation leading to less pumping loss, better thermal efficiency, and low specific fuel consumption. The mass diffusivity of hydrogen is higher than other fuels, which helps in a homogenous charge formation. The laminar flame speed is higher than other fuels, enables rapid burning, and allows the engine to run smoothly at higher speeds. The minimum quenching distance allows the flame to reach the closest to the combustion chamber wall. The adiabatic flame temperature is also higher, which means the quality of energy delivered is better than other gaseous fuels. It has wider flammability limits, meaning rich and lean operations are also possible. However, the minimum ignition energy respective to other fuels is also a benefit over others, which means the cold start issues are not viable for hydrogen. The heating value of hydrogen is also higher than others, which means the quantity of fuel needed is also less.

1.6. Global initiative on Hydrogen adoption

Hydrogen has been seen as a renewable energy carrier globally in recent years. Institutions around the globe have emphasized developing a sustainable hydrogen economy. Many governments have made initiatives with specific rules, laws, or research motivations to increase the substitution of hydrogen for present sources. The United States Department of energy has motivated hydrogen fuel through its mission of developing more energy-efficient and environmentally friendly highway transportation technologies to use less petroleum(Davies, 2012). The research and development related to hydrogen fuel and fuel cells are also supported by the Japanese government's Ministry of Economic, Trade, and Industry(Government of Japan, 2017). The Indian Ministry of New and Renewable Energy has supported many projects in Its and other institutions and the corporate sector to develop hydrogen infrastructure(Murthy, 2016). The Indian Institute of Technology Delhi has developed a hydrogen-fuelled IC engine-based three-wheeler and generator(Das, 1990).

1.7. Hydrogen Production

Hydrogen production is quite flexible and involves renewable sources like gasification of hydrocarbon-based biofuels and biomass, water electrolysis using solar energy or wind energy, and non-renewable fossil fuels by steam reforming auto-thermal oxidation, partial oxidation, and gasification(Abdalla, Hossain, Nis, & Azad, 2018). In

India, because of its vast land area and massive population with very high diversity, there are opportunities and necessities to find out locally best-fit sources of hydrogen. A similar condition is also persistent in the case of global technology for hydrogen production.

1.7.1. Steam Methane Reforming (SMR)

SMR is the most followed hydrogen production technique, using methane-based gases, producing 70-75% hydrogen-rich gas(S. Singh et al., 2015). It is a catalytic process that involves multistage reactions, where light hydrocarbons like methane and steam are fed to react at different stages. The first stage is the reforming of methane and steam fed to the reactor at a very high temperature of 1100K-1300K and 14-20 atm pressure in the presence of a nickel-based catalyst. This endothermic reaction provides nearly 75% pure hydrogen. In the next stage, the reformat is fed to the WGS reactor, where the endothermic reaction at 500K-750K takes place (Barelli, Bidini, Gallorini, & Servili, 2008).

$$CH_4 + H_2O \leftrightarrow CO + 3H_2 \quad \Delta H^o{}_{298} = 206.2 \; kJ/mol$$
$$CH_4 + 2H_2O \leftrightarrow CO_2 + 4H_2 \quad \Delta H^o{}_{298} = 165 \; kJ/mol$$

Steam Methane Reforming Reaction

$$CO + H_2O \leftrightarrow CO_2 + H_2 \quad \Delta H^o{}_{298} = -41.2 \; kJ/mol$$

WGS Reaction
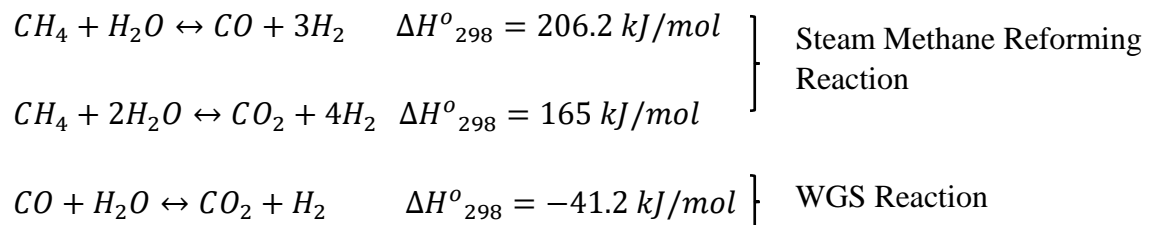
The SMR is not a sustainable and environment-friendly method as it is equally polluting as the burning of methane because of CO_2 release(S. Singh et al., 2015).

1.7.2. Partial oxidation (POX)

Partial oxidation is another method of reforming hydrogen from hydrocarbon, similar to the SMR method. This method can be implemented in both a catalytic and non-catalytic manner. Unlike SMR, a wide range of hydrocarbons can be reformed from methane to heavy oils. The typical operating temperature ranges 1400K-1700K for non-catalytic type and 1100K-1200K for the catalytic operation(Abdalla et al., 2018). The catalytic process often involves noble metal and transition metal-based catalysts. Generalized POX reactions are as follows.

Reformer	$C_nH_m + nH_2O \leftrightarrow nCO + \left(n + \frac{m}{2}\right)H_2$
Water Gas Shift Reactor	$CO + H_2O \leftrightarrow CO_2 + H_2$
Methanator	$CO + 3H_2 \leftrightarrow CH_4 + H_2O$
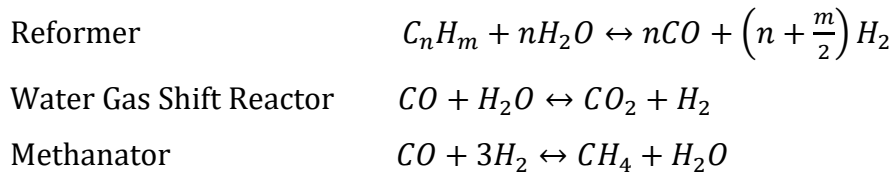
1.7.3. Auto thermal reforming (ATR)

The ATR process combines SMR and POX, where auto-thermal stands for the ability to self-stabilize heat requirement by balancing endothermic and exothermic reactions. Hence, no external heat source is needed for this process. It is advantageous over SMR and POX as its low energy requirement and high gas hourly pace-velocity. There are two varieties of ATR reformers, one which has only a catalyst bed in which SMR and combustion co-occur, and the other has two completely separate sections. The first chamber has POX reactions without catalyst and the second chamber has SMR catalyst placed downstream of the POX chamber.

1.7.4. Gasification

The gasification process is similar to the POX, with a slight difference in feedstock being coal. Several types of coal gasification operations are done; however, all involve converting carbon to gas by using high temperature entrained flow. In this process, H_2 and CO are produced in the first stage, where H_2 is extracted, and CO helps produce H_2 by WGS reaction. Gasification is an endothermic process that needs high heat. The fundamental reaction of gasification is,

$$C(coal\ solid) + H_2O + heat\ energy \rightarrow CO + H$$
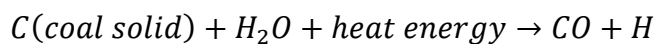
1.7.5. Biomass pyrolysis

The pyrolysis of biomass for hydrogen production involves heating the biomass at a very high temperature in a short time. This results in the thermal decomposition of the biomass, generating the liquid mixture and the gaseous product. The extent of the product phase depends entirely on the residence time, heating rate, and temperature range. At a temperature range of 1500K-3000K at a very high heating rate for 1s residence time, the gaseous product is obtained through flash pyrolysis. Further,

methane and CO are processed to get more hydrogen(Bakhtyari, Makarem, & Rahimpour, 2018). The typical reaction during flash pyrolysis is,

$$Biomass + heat \rightarrow H_2 + CO + CH_4 + other\ organic\ vapors + unorganic\ products$$
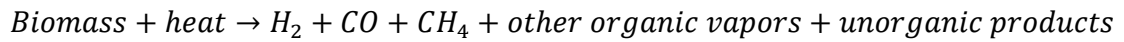
1.7.6. Water Electrolysis

Electrolysis is a process of breaking water molecules into their constituents, pure hydrogen and pure oxygen molecules, by using electric energy in an electrolyser. The electricity supply to the electrolyser can be from any renewable source like solar, wind, or biomass. There are two types of electrolysers used generally, alkaline and PEM. Hydrogen produced by this method is pure with no emission during the production. Figure 1.3 represents a basic overview of an alkaline electrolysis cell. The alkaline water electrolysis is considered a superior technology that can range up to a few MW of electricity used for large-scale hydrogen production, producing around 60kg/h. however, the present technology is challenged for low current density operation, specifically at load varying conditions(Millet & Grigoriev, 2013).
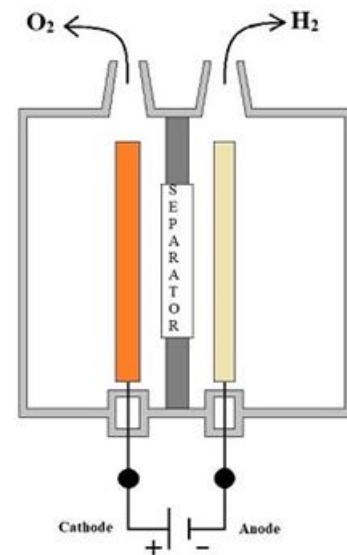
Figure 1.3.Alkaline water electrolysis

The PEM technology of hydrogen production is slightly different from Alkaline electrolysis and is similar to polymer electrolyte membrane (PEM) fuel cell; here, water breaks into oxygen, electrons, and protons on only positive electrodes after the application of DC voltage above thermoneutral voltage. These protons are passed through the membrane by water transport to the cathode, where it combines with electrons and form hydrogen gas. The electrodes used in PEM are porous along with polymer membrane, separator plates, end plates, current collector, and bus plates. It overcomes the drawbacks of alkaline electrolysis; however, only a few manufacturers of PEM are available(Barbir, 2005).

9

1.7.7. Biological hydrogen production

The bio-hydrogen production is a process of hydrogen liberation from waste materials or water with the help of microorganisms at a temperature near ambient. This process can use sunlight or not. Hydrogen is a by-product of fermentation with wild and mutant bacteria, green algae, and cyanobacteria, which melt water into oxygen and hydrogen in sunlight through certain enzymes. The feedstock used in bioproduction is known as substrate; usually, it is represented as carbohydrate. The dark fermentation process does not need sunlight and is processed by strictly anaerobic bacteria. This process is considered to have the potential to be a pre-treatment process in hydrogen production through photo fermentation. The bio photolysis is done through green algae (*Scenedesmus obliquus, Chlorella fusca, Chlamydomonas reinhardtii, and Platymonas subcordiformis*), where oxygen with 0.1% concentration is avoided as it hinders the hydrogen production. However, in the case of cyanobacteria, CO_2 acts as a carbon source to produce a cellular substance in sunlight, which is later used to produce hydrogen(Martínez-Merino, Gil, & Cornejo, 2013).

1.8. Hydrogen Storage

The advancement of technology permits hydrogen storage in all three phases, solid, liquid, and gas. There are four ways to store hydrogen, compressed gas, cryogenic liquids, metal hydride, and carbon absorption, dependent solely on the end-use scheme.

The transportation sector needs a low-cost and safer technology, for which compressed gas technology is adaptive. Usually, hydrogen is compressed from 200 to 800 bar in the steel make 50L storage tank, depending upon the weight and type of the tank(Abdalla et al., 2018). Roughly the amount of hydrogen-filled in these tanks is 1-7% of the total weight of the tank. Almost 20% of the energy is consumed at the filling stations to fill the cylinders. Though the volumetric density of hydrogen gas is proportional to the applied pressure, the density of gas-filled 800bar is also around $40kg/m^3$; hence, the energy density is also less.

The liquified hydrogen is stored at 21K temperature only at atmospheric pressure following precooling by the Linde cycle flowsheet. The mass of hydrogen stored is 16%

of the tank's mass(Keçebaş & Kayfeci, 2019). Liquid hydrogen contains an energy density three times that of petrol. There is always a chance of continuous leakage despite any insulation and safety of the vessel, storage cost, and hydrogen delivery rate at required conditions.

In search of a solution to such cases, solid storage in the form of metal hydrides is developed. Metal hydrides are formed through the lattice imperfections of metal by filling hydrogen to the interstices of lattice cavities. Here are two ways to act, one is chemical adhesion, and the other is the electrochemical separation of water. These are exothermic reactions.

(chemical adhesion) $M + \frac{x}{2}H_2 \rightarrow MH_x + Q$

(electrochemical separation) $M + \frac{x}{2}H_2O + \frac{x}{2}e^- \rightarrow MH_x + \frac{x}{2}OH^-$
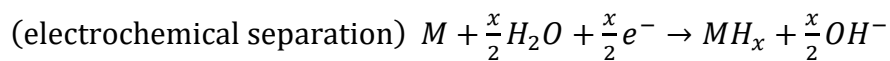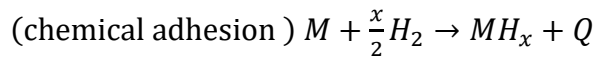
Metal hydride can store hydrogen at 5-7% of the total weight at 2800K. However, to absorb hydrogen, the required temperature is 400-650K. Another method of solid storage of hydrogen is nanostructure and porous material. Carbon nanotubes, zeolites, metal-organic frameworks, and covalent organic framework technology are used. The carbon nanotubes, made up of tiny particles with high porosity, have higher elasticity than steel and behave as semiconductors. Zeolites are a group of crystalline microporous aluminosilicate compounds. The organic frameworks use packs of organic binders, which are highly porous and crystalline structures. Solid-state hydrogen storage in format of metal hydrides such as $FeTiH_2$ and $LaNi5H_6$, uses nanocarbon or activated carbon as absolvents(Murthy, 2016). Here, hydrogen adsorption in carbonaceous materials corresponds to adsorption amount near carbon surface only due to the physical forces by carbon atoms on hydrogen molecules, called physisorption. The porous carbons with a specific surface area of 3220 m^2/g are capable of storing hydrogen of 1.3 wt%. Nanostructured-carbon systems like nanotubes and nano-magnesium based hydrides are considered for storing large quantities of hydrogen.

The separate hydrogen production and storage is a slightly complicated process for IC engine fuel. Hydrogen being light, faces challenges of available infrastructure, filling, and consumption for intermittent application. Therefore, researchers started looking for

alternative solutions, such as onboard hydrogen generation (Polverino, D'Aniello, Arsie, & Pianese, 2019). The onboard hydrogen generation technology mainly involves water electrolysis, steam reforming, and dry reforming technology(Martin, Millington, Campbell, Barron, & Fisher, 2019). However, further research is still mandatory to develop a sustainable and portable hydrogen unit for the onboard application.

1.9. Challenges associated with hydrogen fuelling

Despite all these pros with hydrogen as fuel, some cons are also there. One of those is its energy concentration. Since the density of hydrogen is the least, the volumetric energy concentration is also less than gasoline. The increasing leanness of mixture concentration leads to a rapid drop in the energy concentration, and the laminar burning velocity reduces. This is a significant drawback with hydrogen as a fuel. There are several techniques to overcome such limitations to a large extent. The best-accepted technique is increasing CR from gasoline operational conditions.

1.9.1. Probable techniques to target challenges

CR is one of the critical properties deciding combustion in SI engines, reducing pumping losses and improving engine breathing(Nuthan Prasad, Pandey, & Kumar, 2020). The volumetric losses can be compensated for a lighter fuel like hydrogen by increasing the CR to a specific limit. The high autoignition temperature of hydrogen is an advantage to operating on a high CR that improves the lean limit. Since hydrogen port injection replaces a large amount of air and reduces the η_{vol}, increasing CR helps induct a larger air mass. Besides, it has better action of pumping out the burnt gases, resulting in increased η_{vol} (Salvi & Subramanian, 2016a). Hence, more hydrogen can be injected, leading to better combustion and high BP. At increased CR, CA10 and CA10-90 decrease, reducing the total combustion duration(Maintenance, Şöhret, Gürbüz, & Akçay, 2019). Thus, it reduces the CoV of IMEP, which helps maintain stable combustion and increases the ITE and EER. With increased combustion speed and stability, the P_{max} and the HRR are also advancing, enhancing BTE and MGT (Alrazen & Ahmad, 2018). The heat loss through cylinder walls reduces with increasing CR due to short combustion for a hydrogen-fuelled engine. However, after a certain CR, the MGT achieves too high values, quickly achieving the autoignition condition,

promoting knock(Seungmook Oh et al., 2019). Here, a significant change in spark advance could avoid knock. However, increasing CR to 15 or above makes it difficult to avoid frequent knocks at λ near 1. The other face of increasing the CR faces a high emission level, specifically NO_x. Stable combustion leading to higher MGT and T_{max} favors the NO_x formation. An increase in CR increases T_{max} proportionally, which increases the NO_x emission. Further, the increase in hydrogen fraction surges T_{max} and leads to even higher NO_x (Krishna, Reddy, Kumar, & Raghu, 2020).

IT is another prominent factor in deciding combustion characteristics of SI engines, which governs performance and emission. An early ignition increases the CP during the compression stroke, increasing compression negative work (Sayin, 2012). While, a delayed ignition pushes a large portion of combustion away from TDC, reducing the peak pressure and the work output (Binjuwair & Alkudsi, 2016). Cyclic variations also depend on IT to a large extent, as a too-retarded or too advanced ignition leads to abnormal combustion. A hydrogen-fuelled engine prefers a retarded ignition compared to other fuels at the same CR due to hydrogen's high laminar flame speed (Gao, Tian, Ma, Huang, & Xing, 2021). While operating on elevated CR, the pressure and temperature increase at ignition; hence, preferred IT gets affected too. In addition, the operating equivalence ratio also governs the selection of optimal IT (Yousufuddin & Masood, 2009). Though the ignition delay gets reduced by retarding the ignition due to increased MGT at ignition, the total combustion duration may increase due to shifting the major combustion zone in expansion stroke that increases the CA10-90. The elongated combustion after retarding ignition results in higher MGT at the end of the expansion, which increases EGT (Gong et al., 2019). The CP falls rapidly, and the peak gets reduced and retarded, reducing T_{max}. Since T_{max} is a prime cause of NO_x formation, delayed ignition reduces NO_x emissions. However, the NO_x reduction by ignition retard has a particular limitation, as if we consider minimal compromise in power output, the NO_x benefit is not significant. Nevertheless, power output falls drastically to achieve a comprehensive NO_x control (Zareei, Rohani, Mahmood, & Abdullah, 2020).

There are several techniques to reduce NO_x with a small impact on engine performance; researchers believe EGR is the most effective method. EGR is a method of recirculating a portion of the exhaust gas back to the intake manifold, either after-treated or not.

Therefore, it replaces a chunk of air, reducing available oxygen and elongating the combustion period; hence NO_x formation is restricted. However, EGR has a different effect on combustion depending upon the fuel strength; combustion improves under lean ($\lambda<1.2$) conditions at low EGR rates. Increasing the EGR strength reduces the available fresh air and increases stratification due to increased heterogeneity by thermal differences between air and EGR. Therefore, some locally rich and some locally lean zones are formed, destabilizing combustion and cyclic variations increase. Similarly, the deteriorated combustion reduces P_{max}, reducing the BMEP and power output (S. Lee, Park, Park, & Kim, 2013). However, the NO_x emissions are heavily reduced to near-zero emissions.

Researchers have reported that a large amount of power is lost at EGR of over 15%. Hence, they suggested that EGR accompanied by inlet boosting through supercharging or turbocharging to overcome the losses efficiently. Intake boost increases fresh air in the combustion chamber, which helps NO_x formation; however, when accompanied by EGR, it helps overcome power loss without affecting NO_x significantly (S. Lee et al., 2013). Also, intake boosting marginalizes the two-way expansion of high-pressure exhaust and improves homogeneity; however, after a specific limit, the random turbulence increases, increasing cyclic variations and combustion instability. There is already a significant amount of air replaced by hydrogen; EGR further reduces air, severely impacting performance. Therefore, intake boosting proves to be more effective, improving volumetric capacity and increasing working fluid mass. The extra amount of cold air supplied reduces cylinder wall temperature. However, CA10 may increase due to sensible heat gain by the excess air; besides, the total combustion duration also increases by the extra fuel supplied to maintain the same equivalence ratio.

1.10. Thesis structure
The entire thesis is disserted in six chapters, briefing about pre-experimental to post-experimental exertion.

Chapter 1 belongs to the introduction, which explains the present energy scenario, importance, and contribution of ICE challenges associated with ICE, probable solution,

affinities of hydrogen for ICE, and preface of the importance of some engine parameters concerning the present work.

Chapter 2 summarizes the literature survey that provides a lineout for the experimentation. It includes six subsections related to modes of hydrogen fuelling and parametric variations. In the end research gap is highlighted followed by objectives of the present research.

Chapter 3 describes the methodology followed for the experiments, the systematic work plan of experimentation, objectives set, and experimental setup preparation. It describes, in brief, the equations used for calculation and the different types of equipment used for building the test rig.

Chapter 4 briefs the experimental results with probable causes. This chapter has three subsections, where 4.1 and 4.2 belong to stage I experiments targeting the first three objectives. While section 4.3 describes stage II experiments belongs to NO_x control by EGR at regained power through MAP boost.

Though subsequent conclusions are provided in chapter 4 at the end of all subsections, a summary of experimental results is included in *Chapter 5*, which points out an optimal operating condition. It also describes the future scope of the present work.

Chapter 6 lists different references cited in the entire thesis, providing the backbone of the research.

CHAPTER 2

LITERATURE SURVEY

Understanding and decision-making ability are motivated by the inspiration grasped from experience. Obeying the concept of "standing on the shoulders of the giant," a scholastic review of near similar work is done to contrive objectives for the research. The research work and findings of these papers are categorized in three ways depending on the mode of hydrogen intake and briefly summarized here.

2.1. Consequences of hydrogen enrichment

Combustion is the prime factor behind all operational characteristics of an engine, depending mainly on the fuel qualities. Out of the three phases, flame development or delay period (CA10) is the first phase, flame propagation (CA10-90) is the second, and after burning is the last phase. Hydrogen possesses a high reputation for its combustion qualities, benefitting all three phases. (X. Sun et al., 2022) mentioned in their study on hydrogen enrichment of natural gas-fuelled SI engines that CA10-90 was reduced by hydrogen, and the flame kernel volume was increased.

(Zhen, Tian, Wang, Liu, & Li, 2021) explored the flame behaviour even more deeply in a direct injection type SI engine. They observed that the increasing hydrogen fraction resulted in higher laminar flame speed and flame temperature at the same flame kernel radius. CA10 and CA10-90 were also increased, resulting in lower EGT and higher power development. However, NO_x and HC emissions were reported to be high, but CO and CO_2 were reduced with hydrogen.

The excellent combustion qualities of hydrogen help the rapid burning of other fuels. (Raviteja & Kumar, 2015) concluded in their research on low CR, 338cc, PFI engine fuelled with butanol at 3000rpm that BSFC is improved by hydrogen enrichment. Combustion duration is shortened proportionally while NO_x emissions have increased drastically. Though hydrogen helps fast combustion of butanol, net HC and CO emissions have been reduced.

The high adiabatic flame temperature increases the CP and temperature, improving the quality of energy delivered. In addition, a shorter combustion period reduces cooling losses and improves performance. (Shivaprasad, Chitragar, & Kumar, 2015) had reported an improvement in HRR up to 20% hydrogen enrichment, which reflects in BTE. Though they reported a drop in BTE after 20% hydrogen due to scarcity of available oxygen, NO_x is proportionally increased.

The conventional fuel like gasoline also gets benefitted by enriching incoming air, which reduces the delay period and improves lean limit. (H. Zhao, Stone, & Zhou, 2010) had a similar experience on a 561.8cc GDI engine, where MBT IT is noticed to retard with hydrogen enrichment. Similarly, the high combustion rate reduces cyclic variations, reducing the PM emissions by 90% at just 5% hydrogen addition.

Hydrogen has wide flammability, which helps efficient burning in rich and lean conditions. However, the combustion speed depends on flame travel speed, which depends on fuel strength in the air (Kim, Min, Song, Baek, & Woo, 2018) had a similar experience. Though they observed an improvement in CA10 and CA10-90 at all the loads, increasing λ is noticed to work inversely. The CoV was reduced drastically by hydrogen addition, affecting the load proportionally; the λ was less significant. NO_x was reported to increase with hydrogen but reduced with λ.

A similar study was performed by (Elsemary, Attia, Elnagar, & Elsaleh, 2017) for a more extensive range of hydrogen (up to 49%), where they observed that the BSFC was reducing with hydrogen addition to 31%; after that, it started increasing at 30º spark timing; similarly, the hydrogen addition improves thermal efficiency. At 30º spark timing and 31% of hydrogen addition, BTE was found the best. The hydrogen addition also helped to decrease HC and CO emissions.

Apart from the conventional fuel, renewable fuels like bio-ethanol & bio-methanol, which have high heat of vaporization, hydrogen is observed to improve combustion. Basically, the stoichiometric air requirement of such fuels is shallow, and the lean limit is also narrow. Hence, under WOT, engine chilling reduces the cylinder temperature, creating combustion instabilities improved by hydrogen enrichment. (Greenwood, Erickson, Hwang, & Jordan, 2014) have concluded it by enriching the air with 30%

hydrogen, they noticed ethanol performance and lean limit were improved. Hydrogen promoted combustion, and NO_x emission reduction by increasing λ was reduced.

In other research by (García-Morales, Cervantes-Bobadilla, Escobar-Jimenez, Gómez-Aguilar, & Olivares-Peregrino, 2017), the control strategy of hydrogen enrichment in E10 fuel is studied. They concluded that the combustion and thermal efficiencies were improved, but power was maintained. They suggested that the engine brake power is unaffected until hydrogen enrichment is maintained up to 6-7%.

Hydrogen enrichment is advantageous for pure ethanol fueled engines, (Ayad et al., 2020) examined it experimentally on a 4-cylinder 2-liters engine at CR10. They observed a continuous reduction in SEC and EGT with hydrogen at all the loads. The mechanical and thermal efficiency increased while CO, CO_2, and HC emissions were reduced. The NO_x emissions were increased with hydrogen.

(Prasad, Pandey, & Kumar, 2021) compared hydrogen enrichment on methanol SI engine with gasoline fueled engine. They noticed improved engine efficiency for methanol fuel by up to 12.5% of hydrogen enrichment. CA10 was noticed to reduce continuously with hydrogen while CA10-90 and after the burning phase were reduced till EGR 12.5%. They observed that a higher speed has a larger effect on enrichment.

In addition, the low heating value of alternative fuels like methanol and ethanol had an adverse effect on performance, limiting power generation at higher BSFC; hydrogen enrichment helps improve the energy content. Even a partial enrichment of merely 20% hydrogen in a methanol fueled engine helps improve BSFC. (Sarıkoç, 2021) has also commented on a steeper rise in CP than gasoline as a credit to the fast combustion rate. However, he criticized the elevated NO_x emission of methanol engines by hydrogen.

(Cong, Ji, & Wang, 2021) had compared the performance of various premix hydrogen-DME combos with the premixed hydrogen-fueled operation. HRR was noticed to drop by DME addition up to 3%, then a sudden rise is noticed. DME increased the CA10 and CA10-90. Similarly, DME increased CoV and IMEP, but ITE was reduced to a minimum at 2.9%DME. NO_x followed ITE while HC and CO emissions are increased with DME.

Cyclic variations are the indicator of stable engine operation resulting from combustion quality. Hydrogen helps in improving combustion, reflecting the reduction of cyclic variations. (X. Duan et al., 2020) noticed a continuous reduction in CoV of IMEP and cyclic variations with hydrogen enrichment. The pressure distributions are concentrated, and CP changes sharply due to hydrogen. They observed that the start of combustion was advanced by hydrogen enrichment, and cyclic variations in CA50 were reduced.

The mass diffusivity of hydrogen allows it to mix with air readily; when charged in the intake line, a homogenous mixture form. Hence, flame propagation is uniform, which assures rapid mass burning, increasing HRR, which increases T_{max}. Therefore, NO_x formation gets motivated (Shi, Ji, Wang, Yang, & Wang, 2021) observed a steep increase in NO_x with increasing hydrogen fraction due to a rapid rise in T_{max} in their experimental study on the Wankel engine. They noticed a reduced turbulent kinetic energy due to increased λ; however, increasing hydrogen also intimated low kinetic energy. The Cov of P_{max} was reduced while BTE was improved.

In a similar study (Kosmadakis, Rakopoulos, & Rakopoulos, 2021) experimentally studied cyclic variation under methane-hydrogen fueling. They noticed a reduction in CA5 continuously with hydrogen, but CA90 was reduced by up to 30% hydrogen enrichment. However, NO_x was observed to increase continuously with hydrogen and reduce ϕ. They noticed an improvement in combustion by increasing hydrogen and ϕ, reducing cyclic variations.

According to (Akif Ceviz, Sen, Küleri, & Volkan Öner, 2012), gasoline fuel strength in the mixture significantly impacts CoV, which deteriorates with increased and decreased λ. However, hydrogen enrichment broadens the range and reduces cyclic variations. Their experimental study improved power and thermal efficiency and increased T_{max} and NO emissions. They also concluded that the effect of λ reduces with increasing hydrogen fraction because of the wide flammability limit of hydrogen.

Hydrogen is known for high knock resistance with a very high octane rating, which improves the knock limit of other fuels. (Naruke, Morie, Sakaida, Tanaka, & Konno, 2019) experimentally analyzed knock tendency at various λ at a fixed IMEP. They

noticed that the spark timing of the knock limit was retarded and indicated thermal efficiency (ITE) is improved at λ=1.8 with hydrogen addition; however, with a higher hydrogen percentage, it started falling rapidly. The knock limit was also decreased with hydrogen following the same trend of ITE. There was a significant drop in CA10 and CA10-90 by hydrogen addition, while CoV was improved. Hydrogen addition is observed to increase efficient lean operation limit.

2.2. Hydrogen port injection

In comparison to the continuous hydrogen supply to the intake line, which has a probability of two-way hydrogen expansion, backfire, and higher air replacement, electronically governed port injection is a good choice.

2.2.1. Parallel hydrogen injection with other fuels

The cyclic variations use to reduce too. (B. G. Sun, Zhang, & Liu, 2013) had reported a narrow band cyclic variation in IMEP while the ignition was advanced. The CoV was observed to increase with λ; however, an advanced ignition helps reduce it.

The air/fuel ratio is crucial in SI engines, usually running near stoichiometric for gasoline. However, hydrogen has good efficiency while fed under lean conditions (S. Wang, Ji, Zhang, & Liu, 2014) observed in their experimental study that thermal efficiency improves by hydrogen addition under lean fueling. However, CA10 and CA10-90 were increased with increasing λ in hydrogen operation, while it was difficult for gasoline to run smoothly under increased λ. Even CoV was observed near static values for hydrogen addition but increasing rapidly with gasoline. They concluded that the lean operation limit of gasoline was increased by injecting hydrogen.

Though the parallel hydrogen injection benefits over carburation, the highly diffusive fuel still restricts air induction. (Açikgöz, Çelik, Soyhan, Gökalp, & Karabał, 2015) experimentally investigated the beneficial hydrogen limit, fed parallelly with methane. They observed excellent brake power improvement until 20% hydrogen; however, even at 30% hydrogen, significant improvement was noticed. Thermal efficiency was also improved due to rapid combustion. While concerning λ alongside hydrogen addition, they noticed 20% as the optimal hydrogen supply limit.

(Akansu, Tangöz, Kahraman, İlhak, & Açıkgöz, 2017) had hydrogen addition to gasoline-ethanol blend (80-20, G80E20) in a 1.8 SI engine. Thermal efficiency was reported less for the G80E20 than gasoline, increased by hydrogen addition. The CP was increased and advanced with hydrogen. CO was reported to reduce to 0 when hydrogen added up to 20%, while HC continuously decreased with hydrogen. NO_x increased sharply with hydrogen until 33.8%, but after that, it dropped suddenly.

Often the higher autoignition temperature of hydrogen is seen as a chance to increase the efficiency of the SI engine by elevating CR while primarily fueling gasoline or natural gas. (Tangöz, Kahraman, & Akansu, 2017) had a similar experience, where CR is elevated to 12.5, brake power and thermal efficiency were increased by hydrogen addition up to 10%. The CP and HRR were increased and advanced with hydrogen addition. The HC and CO emissions were reduced with hydrogen addition to 10. λ limit of emissions is broadened with hydrogen. The NO_x emission was increased with hydrogen addition, speed, and spark advance; however, for λ, it decreased sharply at λ over 1.

(Nitnaware & Suryawanshi, 2016) had a similar analysis of hydrogen addition to natural gas on a small capacity 3-cylinder engine. They reported that the η_{vol} was decreased with hydrogen addition, more at lower ϕ. The η_{th} was increased with hydrogen addition till a 5% EGR rate, but for a higher hydrogen supply, CNG had a better η_{th}. The MBT spark gets retarded by hydrogen addition, and with ϕ increasing, it is further retarded. The CO emission was reduced with hydrogen but increased with ϕ, and NO_x emission was increased with hydrogen and ϕ. The combustion duration and HRR were reduced while the peak of HRR was advanced with hydrogen addition. The CoV of IMEP was reduced with hydrogen addition.

(R. Singh & Das, 2019) had studied the hydrogen addition in CNG effects. The CNG torque was reduced compared to gasoline, but hydrogen addition had increased it. Power was also decreased with CNG replacing gasoline, but hydrogen addition increased the power below gasoline. The η_{th} was increased for CNG from gasoline and further increased with hydrogen. However, the η_{vol} was reduced with CNG and further reduced by hydrogen. CNG reduced the EGT, but adding hydrogen had increased it slightly below gasoline; similarly, engine oil temperature decreased with CNG and

increased with hydrogen addition. The HC, CO, and CO_2 emissions were reduced with CNG and further reduced with hydrogen addition, but NO_x has increased a lot with gaseous fuels.

(Nadaleti et al., 2018) had analyzed the parallel port injection of hydrogen alongside biogas (95% and 60% methane-based). They reported that the η_{th} of biogas was increased by inducing hydrogen. The CoV was reported to increase with λ but improved by hydrogen addition. The combustion duration was increased with λ and decreased with hydrogen addition and methane quantity. The HC and CO emissions were increased with methane and decreased with λ for pure biogas; however, for hydrogen, it increased with λ. The cylinder temperature was decreased with λ but increased with hydrogen addition. NO_x was found to increase with hydrogen and decrease with λ and methane.

(Yilmaz & Taştan, 2018) explained port injection of hydrogen on methanol-gasoline. The BSFC was found to decrease by hydrogen. The combustion characteristics such as CP, dropped by methanol, here adding hydrogen benefited it. Peak had increased and advanced with hydrogen increased. The CO and CO_2 emissions were found to decrease with hydrogen; HC emission was also reported decreasing with hydrogen; however, NO_x was reported increasing moderately with methanol but severely with H_2 fraction.

(Gong, Li, Sun, & Liu, 2020)evaluated combustion and lean burn limit of a methanol/hydrogen-fueled SI engine under variable IT. They observed a continuous rise in P_{max} and HRR_{max} with ignition advanced, while the corresponding angle was advanced too. However, increasing hydrogen fraction led to an increase and advance P_{max} and HRR_{max}. CA10 was reduced with ignition advanced to a minimum and then increased while CA90 was reduced continuously. CA10, CA90and CoV were observed to get reduced with hydrogen fraction. On the other hand, increasing excess air ratio (λ) has opposite effects. The CoV was drastically increased after λ increasing 1.2 without hydrogen, which improved to 2.4 with 9% hydrogen.

In another study, (Gong, Li, Yi, Huang, & Liu, 2020) explained hydrogen addition effects on methanol fueled engines under three λ. He noticed a continuous reduction in SFC with increasing λ as well as hydrogen fraction at all the loads. However, the CP

and HRR were increased with hydrogen but reduced with λ. The EGT was reduced with λ; however, depending upon load, as at low load, it was reduced with hydrogen, while at full load, it was increased. CO and HC emissions are reduced with λ and drastically dropped with hydrogen. The NO_x emissions were increased with λ till λ=1 at low load and λ=1.2 at full load, while hydrogen addition further boosted the emissions.

(Fu et al., 2021) studied hydrogen addition effects on liquid methane fueled heavy-duty engine at CR13.6. They noticed an increment in CP and HRR while a continuous reduction in ignition delay, CA10-90, and total combustion duration with increasing hydrogen fractions. The ITE was increased first and then dropped with hydrogen addition; however, T_{max} and NO_x increased continuously with hydrogen.

In a similar study on a 4-cylinder inline engine, (Yu et al., 2021) analyzed energy and exergy for combined injection strategy, hydrogen PFI and gasoline DI at low CR (9.6). They observed increments in BTE with hydrogen fraction, while with increasing ϕ, first BTE increased to peak and then dropped. The ϕ value corresponding to peak BTE was dependent on hydrogen fraction. The exhaust heat losses were reduced to a minimum and then increased while cooling water heat loss increased with ϕ increased.

2.2.2. Pure hydrogen port fuel injection (H-PFI)

Knocking and backfire are considered the worst phenomenon for SI engines; with hydrogen addition to the port, the chances of backfire are thought to arise. (Dhyani & Subramanian, 2018) observed relation between knock and backfire, they found the low-intensity knock after 100cycles which gradually turned severe after 400 cycles. The increasing knock was responsible for the slight speed drop and the sudden rise of CP; the CP started varying a lot; for the 444th cycle, it was around 70bar, but for the 445th cycle, it was 25bar, and the 446th cycle 40bar. As a result of the knock, the sudden rise of component temperature occurred, leading to the hot spot and for the next cycle backfire. It was also observed that the delayed hydrogen injection reduced the backfire probability.

In another research (Dhyani & Subramanian, 2019b) characterized the backfire and knock in hydrogen PFI engine through numerical and experimental analysis. They

proposed that the backfire probability depends upon hotspot temperature, leading to an unavoidable knock after 950K. The hot spot location does not have significance in backfire; however, it affects the timing of its origin. The turbulent velocity of the backfire was reported to be very high (230m/s), and the maximum pressure-rise rate was 0.3bar. They also proposed that backfire occurs in three-phase like combustion, ignition delay, propagation, and termination.

(Xu, Ji, Wang, Bai, & Cong, 2018) examined the cold start NO_x emission of a hydrogen PFI SI engine at various λ. They reported that the speed rise was decreased with increasing λ. Similarly, with λ, the early pressure rise decreased, and the peak pressure shifted from idle speed to higher speed, reflecting the combustion probability shifted to a higher speed. The maximum pressure P_{max} and maximum pressure rise rate decreased with λ. Similarly, CA10 and CA10-90 were found to increase with λ. EGT was reduced, but the NO_x emission was increased with λ.

Though the probability of backfire in PFI is less than carburation-typed, it still contains a big challenge towards the success of hydrogen engines. (Dhyani & Subramanian, 2021) had developed an online control system to avoid backfire in their case. They designed the control circuit such that it follows ignition variation with ϕ. Their study observed that increasing ϕ increases the chances of backfire by increasing lubricating oil temperatures and EGT. They set these two parameters following the crank position to control injection timing to avoid backfire.

(Qing he Luo et al., 2019) studied ϕ variation on a turbocharged hydrogen PFI engine; power was reported increasing with ϕ at low speed till ϕ is near 1; after that, it remains constant; however, the η_{th} was increased with ϕ till peak near 0.7. The turbocharge pressure was also increased with ϕ at a certain level, and after that, it was constant. The air mass flow was increased until ϕ became 0.7 and then decreased. The η_{mech} was increased with ϕ, but the burning duration and ITE were decreased. The CoV was increased with ϕ and speed. The IMEP was reported to be 0.83% higher for the start cycle. The NO_x had increased first and then decreased with ϕ, but it was reduced to 10% with turbocharging.

The idle characteristics of hydrogen PFI were studied by (Ji & Wang, 2013); they reported that both CA10 and CA10-90 were gradually prolonged with increasing λ, and the energy flow rate was reduced. COV_{IMEP} was reported low, and pressure and cooling loss were reduced with increasing λ. At higher λ, the low combustion temperature resulted in low NO_x emission.

(Ma et al., 2011) tested the idle characteristics of a SI engine fueled with pure hydrogen for various ϕ and IT. They observed a continuous reduction in ITE, CA10, CA10-90, and CoV with increasing ϕ. HRR, CP, P_{max}, rate of pressure rises, and the NO_x emissions increase continuously. The ignition angle corresponding to the optimum ITE was observed to retard with increasing ϕ. However, NO_x, and P_{max}, reported reduced with ignition retard, while CA10-90 was increased. The CA10 was observed to reduce with ignition retard to a minimum and then increased; the optimum angle was retarded with ϕ.

(Ceper, 2012) had experimented with various spark plug gaps (0.4mm to 0.8mm) on a hydrogen-fueled heavy-duty engine for two ITs (10ºCA and 15ºCA bTDC) at CR13.5. He noticed maximum thermal efficiency at 0.6mm under both wide-open throttle (WOT) and half-open throttle (HOT). A significant reduction in NO_x emissions was reported by increasing throttle from HOT to WOT.

(R. Zhang et al., 2021) on the other hand, they had a discrete theory related to the combustion of hydrogen PFI engine; they emphasized the importance of injection strategy. In their experimental study, they optimized it; during optimization, they noticed improving efficiency with ignition retard till maximum. The CoV was reduced with hydrogen strength. The CP and HRR were improved with an early injection, while CA10 and CA10-90 increased. The flame length, as well as flame area, also improved with an early injection.

A comparative study of combustion of HICE with gasoline PFI was performed by (Bai-Gang, Hua-Yu, & Fu-Shui, 2014) for a wide range of speeds. They notified that the combustion duration of HICE is much shorter than gasoline above ϕ=0.6. When hydrogen fed was lean (below 0.4), lower laminar velocity caused huge variations in combustion duration. They observed that the combustion duration is independent of

speed after ϕ=0.6. CA50 is observed to advance from gasoline above ϕ=0.6, but ϕ below 0.4, it was retarded.

(L. Wang et al., 2017) had numerically studied the influence of injection parameters in hydrogen PFI; they observed a large amount of residual hydrogen in the intake line due to late injection. Even a too early injection provided a larger retention time for a rich gas mixture. Hence, the mixture is not uniform, and the high concentration gas mixture is accumulated at the inlet valve, which may lead to preignition and backfire. A too delayed injection may cause an increase in residual hydrogen, increasing the possibility of backfire.

Similarly, (Navale, Kulkarni, & Thipse, 2017) experimentally studied manifold injection of hydrogen under WOT conditions following lean hydrogen fueling. They observed that despite low power generation, the BTE of hydrogen was better than gasoline. HRR and peak CP were also reported better for hydrogen, while CoV was low and improved with increasing speed. However, NO_x increased with speed and reporter high for hydrogen for mid-speed range (1450-1650rpm).

NO_x emission is usually an issue of a PFI hydrogen engine, and the causes are attributed to relatively high adiabatic flame temperature and laminar flame speed. Besides, the electronic injection has better η_{vol} and guided hydrogen supply, increasing oxygen and promoting tumble flow. (J. Duan et al., 2017) had explained it through the combustion model; they noticed a rapid increase in OH concentration and temperature in the flame front with ϕ. The NO concentration increased mainly due to an increment in T_{max} and MGT. After rapid combustion, behind the flame front, MGT drops, and NO decomposes up to 2200K. They reported NO to be the largest constituent of NO_x with a 97% share.

2.2.3. Influence of CR and IT on HICE

CR and ITs are two prime drivers of fuel burning and operational results of SI engine; depending upon fuel, it decides performance and emission. Besides, fuel's auto-ignition temperature plays a vital role in limiting CR, while flame speed is decisive for ITs.

(Sadiq Al-Baghdadi, 2004) had studied the effect of CR on PFI hydrogen; they reported that the operational ϕ limit was reduced with increasing CR and speed. However, optimum IT was observed to advance, and its operational range of ϕ also increased with CR. For a very lean fuel, optimum IT was pretty advanced. Thermal efficiency was reported to reduce with ϕ; however, thermal efficiency at any ϕ was increased to peak with CR and then dropped. They proposed that the CR and ϕ must be carefully selected to observe the best performance.

On the contrary (Pal & Agarwal, 2015) had reported an improvement in engine performance by increasing CR. Increasing CR helped in the early combustion start and reduced combustion duration. BTE was improved, and EGT was reduced by increasing CR. However, NO emissions had been reported to increase.

(Ma et al., 2012) had analyzed the combined effect of changing CR and IT at a fixed λ; they observed a parallel increase in ITE, BTE, and brake torque with increasing CR. Advancing ignition first benefitted performance and then worsened gradually. P_{max} and HRR were increased and advanced with CR, while CA10, CA10-90, and CoV were reduced. IT had noticed profitability by advancing from 10ºCA to 28ºCA bTDC at CR10. Increasing CR has advanced this optimal IT.

In a similar study, (Maintenance et al., 2019) explained exergy and energy changes due to CR and IT in hydrogen SI engines under WOT conditions. They pointed out that the elevated CR increased CP, MGT, and HRR; peaks were also advanced. The EGT and EGP had increased by increasing CR while retarding ignition led to an increase in EGT rapidly. The EGP increased gradually at low CR but rapidly at high CR with ignition retard. Cylinder wall temperature increased by CR and reduced by ignition retard; molar concertation of water vapor and NO_x have increased with CR and ignition retard. However, BTE had increased with CR but improved by ignition retard up to 10ºCA bTDC only.

Though increasing CR is observed to be convincing for SI engines, outcomes depend on mixture strength too. (J. Zhao et al., 2013) had experimentally illustrated it as CA10 had reduced rapidly with CR for λ just over 1; with a further increase in λ, the CA10

drop rate had reduced. Similarly, CP and HRR started rising much faster at $\lambda=1.0$; peaks were advanced too. However, CA10-90 had a different story; the increasing λ had severe effects on higher CR, leading to increased CA10-90 for CR12 than CR10 for $\lambda>1.8$. A similar experience was reported for CoV and ITE. However, NO_x had increased rapidly with λ for all CR, while a range of increases with λ was reduced by increasing CR. A highly lean ($\lambda>1.7$) fuelling reported near 0 emissions.

(Bhasker & Porpatham, 2017) had similar research for the hydrogen-enriched engine. They reported an increase in BTE with ϕ to a specific limit depending on CR. However, increasing CR had increased BTE at all ϕ. The optimal ϕ was reported to fall in a leaner zone with increasing CR. The lean misfire limit was increased, CP and HRR were increased, while CA10 was reduced with increasing CR and ϕ. MBT IT was reported to retard with CR and ϕ. Though the cyclic variations improved with increasing CR, with ϕ, it was reported first to reduce and then increase slightly. NO emissions were increased with CR, but ϕ had noticed a considerable drop after 0.8.

A wide range of CR (up to 17:1) was studied by (Seungmook Oh et al., 2019); who reported improved lean operation, reduced residual gas, and increased power with increasing CR. They also indicated very high NO_x emissions at a slight lean feeding. CA10 had reduced continuously with CR while CoV_{IMEP} was reduced too, up to a certain CR. BTE was first improved with CR and then dropped. The backfire-limited λ was increased.

(Gong et al., 2019) had studied the IT effects of hydrogen PFI engine. HRR was increased first with advancing ignition, then decreased slightly. The peak HRR was reduced and shifting delayed with speed. At low speed, ignition delay was more, but it was increased continuously with spark advance for higher speed. The combustion duration and CoV_{IMEP} were reported to be reduced with spark advance. NO_x was reported to increase with spark advance.

(Dhyani & Subramanian, 2019a) had tested water injection strategies of NO_X and backfire control. They reported that the knocking pressure and backfire were reduced to normal by water injection. The water injection rate (WHR) rapidly increased the

minimum ignition energy. WHR reduced the peak CP. Similarly, the peak cylinder temperature and EGT were reduced too by WHR. WHR elongated the combustion constituents, such as the start of combustion and flame periods. The η_{vol} has slightly decreased with WHR for small injections till 2, increased till 8, and then decreased rapidly. The η_{th} for WHR first slightly reduced and then gradually increased. The CoV of IMEP and P_{max} had no effects of WHR till a specific limit after that, WHR had reported to worse them. The NO_X emission with WHR implementation was reported as a sudden fall.

(Xu et al., 2019) had studied emissions during the cold start period of hydrogen-fueled engines. They reported that the engine speed rose rapidly with spark delayed during the first 5 seconds, but the CP was first increased from 25ºCA to 15ºCA and then decreased with further delay for the first cycles. The maximum rate of pressure rise was reported to increase with spark advance till 15ºCA. CA10 decreased with spark advance till 15ºCA, while CA10-90 was reported to decrease continuously with spark advance. The NO_x emission was found to increase with spark advance.

(Gao, Tian, Ma, Huang, et al., 2021) tested the effects of IT on an opposed rotary piston engine at three-manifold pressures. They observed a continuous increase in P_{max} with ignition advanced till 17.31ºCA bTDC and then a slight drop. The manifold pressure changes had negligible effects; however, wall heat losses were reduced with increasing manifold pressure and retarding ignition after 17.31ºCA. The exhaust pressure was increased with manifold pressure while ignition retard first reduced it and then increased. The NO_x emissions were increased with ignition advanced and reduced with manifold pressure increased.

(Sechul Oh et al., 2021) observed the idle characteristics of a hydrogen engine that the retarded IT had less CoV under rich conditions (λ near 1). However, misfire-backfire ignition limits were shortened, which was increased with increasing λ at the cost of increased CoV. The CoV increased to a very high range at extremely lean conditions, diminishing the combustion chances. Similarly, the BTE increases with λ, and the ignition angle corresponding to the maximum was advanced. NO_x emissions were increased with ignition advanced at low λ, while with λ increased after 1.5, NO_x

dropped rapidly. A retarded ignition after peak BTE was observed to reduce NO_x efficiently. They also noticed an increasing combustion efficiency with increasing λ.

2.3. NO_x control by EGR in HICE

NO_x emission is a significant drawback of HICE; since a high-temperature flame travels rapidly and reaches closer to the cylinder wall, it ensures a rapid rise in-cylinder temperature. Therefore, the MGT reaches the NO_x formation threshold, where a moderately lean mixture supplies sufficient oxygen and nitrogen to form NO_x. NO_x formation depends largely on peak temperature and ϕ and slightly on residence time. In SI, engine combustion duration is short; hence, residence time has no significance; therefore, controlling oxygen level is the option that also governs MGT.

EGR affects flame kernel growth, leading to impact combustion significantly. (Salvi & Subramanian, 2016b) had analyzed it on a hydrogen PFI engine. Their study observed a significant drop in flame kernel growth by EGR. In addition, they reported an increased probability of engine knock when ϕ is increased above 0.8. They concluded that flame kernel growth is a function of ϕ and EGR rates.

(Nande, Szwaja, & Naber, 2008) has experimentally studied EGR impacts on combustion; they noticed that CA10 had increased by 4.5ºCA, while CA10-90 had increased by 10ºCA for 35% EGR. However, increasing CR had reduced combustion duration. They also reported improvement in CoV up to 20% EGR irrespective of CR, but the pumping loss had reduced continuously. Though P_{max} was observed to reduce continuously with EGR, ITE first increased with EGR and then dropped at all CR; at low CR, it occurred for a larger EGR rate. The position of CA50 was observed to advance with CR, while with EGR, it first advanced and then retarded.

EGR strategy in HICE was numerically studied by (Eitel, Kramer, & Lutz, 2007); they suggested that the EGR ratio could be treated as a function of oxygen content in intake and exhaust. Their observation states that the frequency of CP fluctuations is reduced with the EGR ratio, indicating a reduction in knock probability under stoichiometric fueling.

In another study, (Ivanič, Ayala, Goldwitz, & Heywood, 2005) had studied the NO_x emissions mechanism in HICE during EGR. They observed a sharp reduction in NO_x with EGR, and at a fixed EGR, the reduction is steep for lean fueling. However, it depends on the thermal dilution parameter (TDP); the reduction rate increases with an increase in TDP after 1.2. the consequences on efficiency were quite interesting; at initial TDP, there is a sharp increase in BTE; after achieving maximum, it dropped. The rate of drop increased with TDP. TDP is a measure of EGR dilution.

The effect of hydrogen enrichment with EGR was studied by (Alger, Gingrich, & Mangold, 2007) at various CR; they reported a slight drop in CoV at the initial EGR rate; afterward, a sudden increase was noticed. The impact got reduced with increasing CR and enrichment of hydrogen. CA10-90 was reported to increase intensively with EGR irrespective of hydrogen fraction, and the combustion efficiency dropped rapidly after achieving slight modification at low EGR.

Determining the EGR rate is always a matter of discussion; researchers have different theories and methods to measure it. Since engine combustion depends mainly on composition, the dilution ratio affects it. Some researchers consider the mass flow of air and recirculate, while some consider oxygen availability. (S Verhelst et al., 2012) reviewed these techniques and proposed that relative error rises sharply with reducing EGR rates in all methods. They concluded that the method based on the molar mass of oxygen has the least error, while they ruled out the method based on relative humidity.

(Subramanian, Mallikarjuna, & Ramesh, 2007) has studied mass-based EGR rate and dilution effects; they reported a large drop in NO_x irrespective of ϕ with increasing EGR. There was a large drop in ITE and oxygen in the exhaust, while EGT was first increased gradually with EGR and then dropped sharply. The MBT ignition timing was advanced, while P_{max} dropped with EGR. However, CA10 and CoV were first reduced for low EGR and then increased, while overall combustion duration increased gradually with EGR.

(S. Lee et al., 2013) had studied EGR impacts during lean burning; there was a sudden drop in NO_x with increasing EGR; however, with an increasing amount of hydrogen,

there is a slight increase in NO_x. Combustion duration was observed to increase, and thermal efficiency dropped by EGR. Since methane was used as the primary fuel, HC emissions were reported to increase with the EGR rate.

EGR use reduces oxygen, leading to higher dilution, which prevents easy reach of fuel to oxygen despite high diffusivity. Therefore, combustion is elongated, and cooling losses increase, which results in a performance drop. (Yu, Guo, He, Dong, & Sun, 2019) had experimentally observed the consequences of EGR on engine combustion and performance. They noticed a slight initial rise in BMEP (up to 6-18% EGR, depending on hydrogen concentration) and then a sudden fall. CA10 was increased with EGR for all hydrogen concentrations, while CoV had increased. However, with the increase in hydrogen, it was settled down. NO_x was reported to reduce with EGR to a near 0 for EGR 30% irrespective of hydrogen or λ.

Ignition retard is also known to reduce NO_x and disturb performance slightly, while accompanied with EGR, it can control NO_x more efficiently. It was experimentally studied by (Jeeragal & Subramanian, 2019); they observed continuous reduction in HRR with ignition retard, and peaks moving away from TDC. Combustion duration was increased after achieving minimum with ignition retard, while NO_x was continuously dropped. Implementing EGR at that instance of the lowest NO_x EGR fraction had intensive suppression. The NO_x has reduced to near 5g/kWh from 16.5g/kWh. However, ignition lag had increased while MGT and BTE had dropped.

(Qiao, Li, Wang, Wang, & Liu, 2020) addressed the other-than NO_x issues associated with EGR; they noticed a continuous increase in ignition delay, CA10-90, CA50, and BSFC with increasing EGR. On the other hand, there was a loss of MGT and CP noticed, and peak ROPR and P_{max} were sunken, while their position was retarded with EGR rise. The energy efficiency ratio was dropped largely like friction losses. Though NO_x was limited to near 0 by EGR over 15%, HC emissions increased.

The two-way LP and HP of EGR were studied by (X. Duan, Liu, Liu, et al., 2019); They reported that peak combustion pressure decreased with increasing EGR either by HP EGR or LP EGR. HRR was retarded, and combustion was prolonged with EGR.

The P_{max} and HRR increased slightly with decreasing valve overlap. However, the increase rates were decreased with a reduction in valve overlap.

2.4. Recovering energy by manifold boost under EGR

Though EGR helps control NO_x, an effective rate drops power generation significantly; even combined with ignition retard, it has better control on NO_x at worse performance. Manifold boosting is a simple and most effective method among several available power regaining techniques. Manifold boost can be achieved by turbocharging or supercharging.

(S Verhelst, Maesschalck, Rombaut, & Sierens, 2009) in their study proposed to increase power by combining EGR with a supercharger. They observed that a supercharged engine delivers higher effectual power output than N/A; when EGR is employed at a low fraction, it improves further. They reported an improved backfire limit and increased torque with supercharging and combined strategy.

(Nguyen, Choi, Park, Kim, & Lee, 2020) investigated the supercharging impact on low load in a hydrogen SI engine compared with turbocharging. They noticed a better power improvement running on fixed ϕ by supercharging at high BTE and improved η_{vol}. NO_x is reported to be similar for both turbocharging and supercharging, while CP and CoV improve for supercharging.

(Qing-he he Luo et al., 2018) studied combustion and NO_x characteristics of hydrogen engines by boosting MAP through turbocharging. They observed that boost pressure increases with engine speed and BMEP. When the turbine cannot absorb enough exhaust gas energy, RGF increases, and combustion slows down. Turbo NO_x increases above normal but reduces faster with ignition retard.

(Natkin et al., 2003) have noticed a drop in intake temperature with MAP boost in their investigation of varying MAP in H_2 SI engine. The backfire limit and BTE were enhanced while NO_x was increased slightly with MAP.

(J. Lee, Park, Kim, et al., 2019) had reported a higher torque and power for a wide range of speed (≤ 5000rpm) for turbocharged H_2 engine than N/A, while BTE is improved for

a shorter range of speed($\leq$4000rpm). They also reported a reduction in CA10 for the entire speed range, while CA10-90 is reduced for a wide range of speeds. The CP and HRR were increased gradually, while exhaust pressure increased rapidly for the turbocharger with speed. EGT is reported consistently higher for turbocharged conditions.

(Gürbüz & Akçay, 2021) studied manifold boosting effects on combustion and emission at various IT. They observed that IMEP, P_{max}, and η_{vol} increase continuously with MAP boost and drop with ignition retard. P_{max} is retarded with MAP boost and ignition retard. They noticed an increase in CoV after achieving a minimum due to MAP boost, while CA10, CA10-90, and total combustion duration are increased. The intake air temperature is almost static while EGT is increased proportionally with MAP boost. NO_x is reported to increase gradually too.

(Oikawa et al., 2021) had experimentally analyzed the impact of manifold boosting in HICE. The reported reduction in cooling loss and increase in power by supercharging. They explained increased BTE due to weakened jet penetration due to supercharging injection in a high-pressure field. NO_x emissions were increased with MAP boost. This NO_x was suppressed by retarding ignition and carefully selecting λ without affecting BTE. They proposed that supercharging is an essential technology for improving BTE power output.

2.5. Summary of the literature survey

Hydrogen enhances combustion because of its high laminar burning velocity and high adiabatic flame temperature. The high diffusivity of hydrogen is responsible for the rapid mixing with air, but a higher specific volume replaces large amounts of air in the mixture. The coefficient of variation of BMEP and the knock probability also decreases with hydrogen induction. In the case of the premixing of hydrogen in the air before the inlet to the cylinder, hydrogen is supplied continuously to the intake manifold, which increases hydrogen concentration near the intake valve and inlet pipe, which increases the risk of backfire. This also reduces the inlet air, reducing the η_{vol} and the power output. However, a low amount of hydrogen by premixing is an efficient way to

increase η_{th}, decrease emissions, and reduce the chance of backfire. The hydrogen PFI has a better η_{th} for hydrogen percentage of 10%-30% by energy; however, an increase in the hydrogen percentage has a slight drop in η_{th}. The lean burning during PFI hydrogen at a higher speed has improved. NO_x emissions increase enormously with high hydrogen fraction, owing to a rapid rise in T_{max}. The NO_x emissions are worsened with a slight lean operation ($0.7<\phi<0.9$). Though increasing CR helps in improving combustion, it increases the probability of backfire and NO_x emissions. In addition, the safe operating range reduces with increasing CR.

Hydrogen is a fast-burning fuel with higher autoignition; a slightly retarded ignition helps keep the P_{max} near TDC in the expansion stroke, which improves η_{th}. However, a much-delayed ignition increases EGT and EGP and lowers P_{max} resulting in low η_{th} and increased CoV. The CA10 and CA10-90 improve with increasing CR; however, for a rich mixture, CA10 and CA10-90 are prolonged; further increased CR suppresses the flame propagation. However, a delayed ignition reduces CA10 to an extensive range, but CA10-90 improves for a shorter range. Since T_{max} is reduced by retarding ignition, NO_x emissions are significantly suppressed. Further, with increasing leanness, NO_x could be put down to 0 at the stake of large power loss. Hence, despite a significant reduction in NO_x, the influence is not enough to maintain a healthy limit. On the other hand, EGR is proven far better, reducing NO_x efficiently at the stake of a slight drop in performance. EGR basically controls oxygen flow and oxygen reach, increasing dilution; hence, combustion is prolonged. There is an improvement in combustion for a low EGR rate due to increased MGT. Higher EGR rates result in large dilution and stratification, leading to improper combustion, and increasing CoV. However, NO_x emissions drop to 0, but efficiency also falls drastically. The permittable limit NO_x can be achieved at a slight performance drop that can be regained by boosting MAP.

MAP boost is a technique to increase intake air pressure by either turbocharge or supercharge, which increases intake mass and hence improves combustion. MAP boost allows more fuel to supply, increasing η_{th} and BP. The CA10 increases due to extra cold air, while CA10-90 increases during maintaining of ϕ. While accompanied by EGR, MAP boosting helps regain the power loss, allows lean burn, and improves η_{th}. However, there is a significant NO_x for smaller EGR, but at a slightly high EGR (15%)

at moderately boosted MAP, NO_x is cut down to the emission corresponding to no boosting. In addition, power is also restored near to no EGR records.

2.6. Research gap

The research worked reviewed so far shows a limited work has been done on hydrogen as the primary fuel to any IC engine. Mostly, the character of hydrogen used is as a supplementary fuel or secondary fuel in addition to the primary fuel like gasoline, alcohol, or methane-based gases. There is limited amount of research is observed for higher CR, mostly CR is kept limited for hydrogen enriched fueling. Though thermal efficiencies and NO_x emission control through EGR during hydrogen operation involves large work but there is no sufficient research in mitigating the efficiency loss. Hence, these limitations in the research work are helping to set objectives for further research to assess the research gap.

2.7. Objectives of research

The research study focuses on using hydrogen as a primary fuel for the SI engine, including an analysis of fuel-air mixture formation, performance, combustion, and emission. This study also includes the EGR application to control excessive NO_x emissions. The objectives of the research work are;

- The study of hydrogen port injection (HPI) in SI engine.

  - Effects of compression ratio on the HPI engine.
  - Effects of equivalence ratio on the HPI engine
  - Effects of ignition timing on the HPI engine.
- Application of EGR to control NO_x emission.
  - Effects of EGR on NO_x, performance, and combustion.
  - Effects of applying MAP boosting technique to enhance performance.

CHAPTER 3

RESEARCH METHODOLOGY AND WORKBENCH

The experimental study is designed to carry out in two stages depending on the goals set through objectives. The first stage involves the study of variable CR, ϕ, and IT. However, considering the nature of hydrogen, as a prerequisite, parallel injection of a fraction of hydrogen with low calorific value fuel methanol is studied at variable CR. The motives were to know the manifold injection consequences of hydrogen; after getting assured of smooth operation, the quantity of hydrogen injection gradually shifted to 100%. The CR range was kept from below gasoline to equal to gasoline; the energy supplied by pure methanol was considered for shifting methanol to pure hydrogen. No abnormality was noticed; the experimental scheme was designed for the first stage.

All the experiments were conducted under WOT conditions for three engine speeds, 1400rpm, 1600rpm, and 1800rpm. The first stage of the experiments was designed in two phases, targeting two objectives simultaneously; in the first phase keeping ignition fixed, variable CR was studied with variable ϕ. Figure 3.1 provides the flow chart of the experimental scheme. CR is varied from 10 to 15, and ϕ from 0.4 to 1.0. Here, the experiments are designed to start at CR10, where ϕ would be varied from 0.4 to 1.0; since abnormal combustion such as backfire is suspected, the probable cause of hotspot/engine heating must be eliminated. Therefore, the cooling water flow rate is also increased with increasing ϕ. Once experiments are completed on CR10, the engine is set to attain CR11, and the same method is adopted. Similarly, experiments are conducted to complete the first two objectives. After comparing results, a set of optimal CR and ϕ are decided by considering a trade-off between BTE and NO_x emissions. In the second phase, at the optimal CR, IT is varied along with ϕ; here, ϕ is varied for a small range keeping optimal of the first phase in the center ($\phi_{optimal} \pm 0.05$). The IT range of study is varied from 24ºCA bTDC of gasoline to 14ºCA bTDC. Experiments are designed as at a fixed ϕ, IT is varied, once experiments are completed, next ϕ would be set. The effects are analyzed to set the grounds for the next stage of experiments to be carried out by comparing results, and the optimized condition is determined.
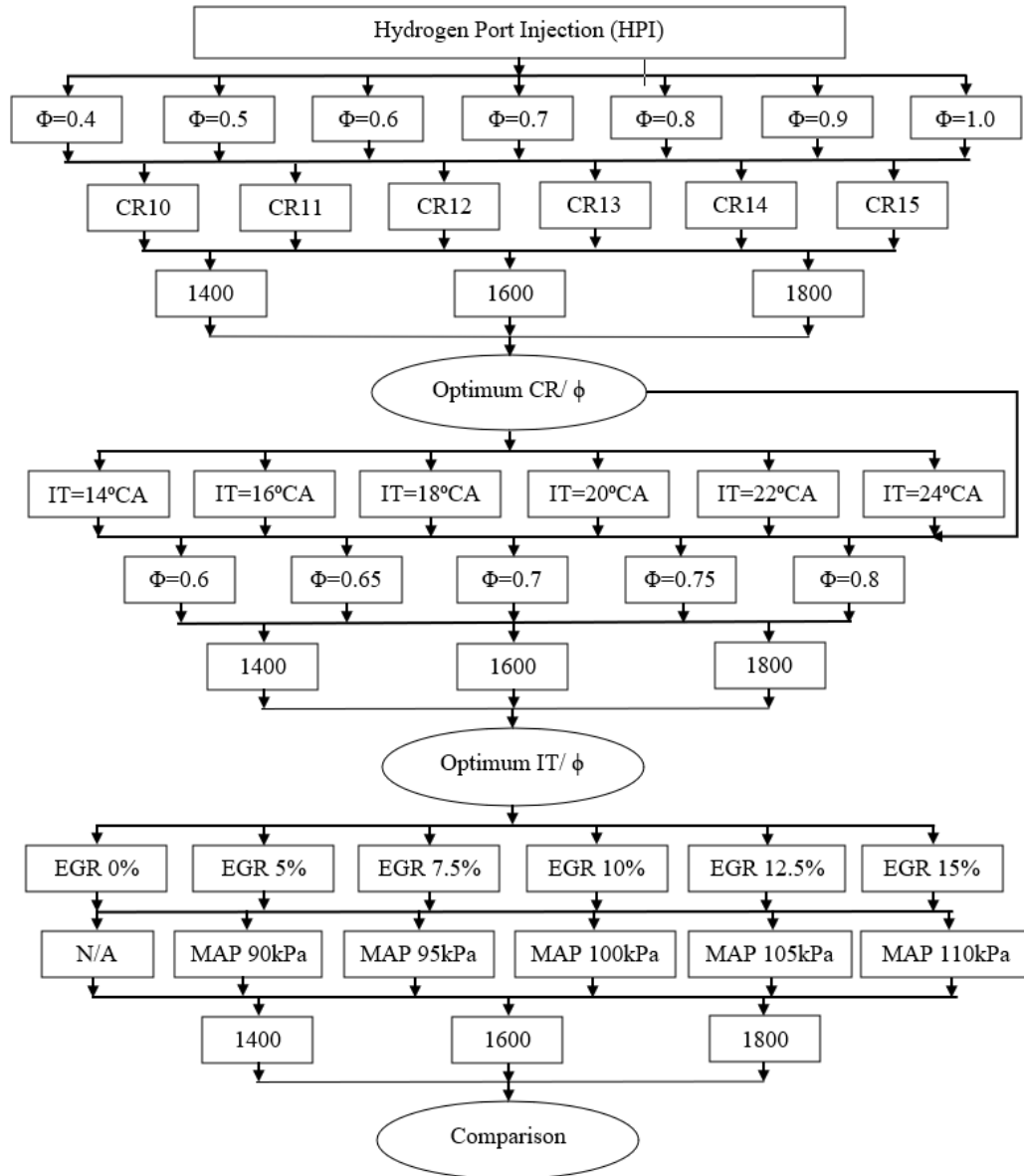
Figure 3.1.Experimental scheme

The second stage of the experiments targets the objectives of group 2. Here, NO_x emissions from the second phase of stage 1 are considered for NO_x control by EGR. The EGR is varied from 5% to 15% at an interval of 2.5%. However, as the literature suggests, the power drop could be noticed, and MAP boosting is performed simultaneously. MAP is varied from N/A to 110kPa. To measure MAP at N/A conditions, MAP sensor readings are considered for the entire range of speed; the average was set as MAP against N/A condition. after that 5kPa boost per experiment is considered, keeping an eye on a trade-off between NO_x and power. Experiments are

designed in such a way that at a fixed MAP, EGR would be varied from 5% to 15%. However, the hydrogen supply rate is fixed according to ϕ at no EGR and is not varied under EGR implementations. Since increasing MAP, gas induction has increased; hence, hydrogen flow is maintained to meet ϕ at no EGR.

3.1. Calculation

3.1.1. Calculation of EGR rate

The EGR flow rate is calculated using the mass of fresh air, the mass of EGR, and the mass of fuel supplied. Here, the data are collected from the two differential pressure sensors, providing output in mm of the water column.

Equations 1 and 2 are used to calculate the EGR ratio;

$$EGR \% = \dot{m}_{EGR} \Big/ (\dot{m}_{EGR} + \dot{m}_{exhaust}) \qquad \text{(eq. 1)}$$

Here,

$$\dot{m}_{exhaust} = \dot{m}_{air} + \dot{m}_{H_2} \qquad \text{(eq. 2)}$$

Here, $\dot{m}_{EGR}$ is EGR mass flow rate (g/s), $\dot{m}_{exhaust}$ is exhaust mass flow rate (g/s), $\dot{m}_{air}$ is intake air mass flow rate, and $\dot{m}_{H_2}$ is hydrogen mass flow rate (g/s).

$\dot{m}_{EGR}$ and $\dot{m}_{air}$ are calculated from the differential air pressure sensor from equation 3, assuming exhaust gas as air,

$$\dot{m}_{air} = \sqrt{(2g \times \rho_{air} \times \rho_{water} \times h_{water})} \times A_m \times C_d / 10^3 \qquad \text{(eq. 3)}$$

Here, g is the gravitational acceleration (m/s^2), ρ_{air} is the density of air (kg/m^3), ρ_{water} is the density of water (kg/m^3), h_{water} is the differential pressure reading of the air pressure sensor in mm of the water column, A_m is orifice area (3.142×10^{-4} m^2 for both airbox and EGR throat), and C_d is coefficient of discharge (0.6 for both airbox and EGR throat).

An excel program is used to feed the sensor output during EGR control; according to the EGR rate requirement, the control valve position is maintained.

3.1.2. Conversion of volumetric emissions to specific emissions

The exhaust gas analyzer provides data on a volumetric basis, such as CO_2 in % of volume while NO_x in ppm. Since the fuel and conditions vary in the study, an absolute comparison would be contradictory considering emissions in such a format. Hence, these volumetric basis emission data are converted into specific emissions (g/kWh). However, two kinds of such calculation are proposed: dry-based or we-based. Here, the specific calculation is done on a dry basis using equation 4 proposed by (Ağbulut, Sarıdemir, & Albayrak, 2019);

$$SE_i = VE_i \left\{ \frac{M_i}{M_{ex}} \times \frac{\dot{m}_{ex}}{BP} \right\} \qquad \text{(eq. 4)}$$

Here, $\dot{m}_{ex}$ is the mass flow rate of the exhaust ($\dot{m}_f + \dot{m}_{air}$) in g/min, M_{ex} is the molecular weight of exhaust (kg/kmol), SE_i is the specific emission of any entity (g/kWh), VE_i is emission data recorded by the analyzer of the entity, and M_i is the molecular weight of the entity (kg/kmol).

However, the experimental emission results are shown no significant deflection in CO, CO_2, and HC emissions; the NO_x emissions are only considered.

3.1.3. Manual calculations through excel programming

The sensor data are collected through DAQ, while some manual readings such as fuel flow rate, engine speed, load, airflow rate, temperatures, and water flow rates are collected manually. From these data, the excel program is prepared to calculate all the performance parameters, including BP, BTE, BSEC, ϕ, and energy flow. BP is calculated using equation 5, which is further used to find BTE by using equation 6.

$$BP = \frac{2\pi NPgl}{60000} \qquad \text{(eq. 5)}$$

$$BTE = \frac{BP}{(\dot{m}_{H_2} \times lhv)} \qquad \text{(eq. 6)}$$

Here, N is engine speed (rpm), P is the load applied (kg), g is gravitation acceleration (m/s^2), and l is armlength at which load is applied; the armlength of the dynamometer is fixed as 0.185m.

Similarly, $\dot{m}_{air}$ and $\dot{m}_{H_2}$ are used to calculate the A/F ratio and ϕ by using equation 7.

$$\phi = \frac{\text{A/F}_{sto}}{\text{A/F}_{actual}} = \frac{34.2}{\dot{m}_a / \dot{m}_{H_2}} \qquad \text{(eq. 7)}$$

Here, A/F_{sto} is the stoichiometric air-fuel ratio, and A/F_{actual} is the actual air-fuel ratio.

The energy flow in fluids like cooling water and exhaust gas is calculated using equation 8 and the temperature reading recorded by sensors.

$$h_{exhaust/cooling\ water} = \dot{m}_{exhaust/water} \times C_{p_{exhaust/water}} \times \Delta T \qquad \text{(eq. 8)}$$

Here, h is the energy flow of exhaust air or cooling water, C_p is the specific heat capacity of exhaust air or water, and ΔT is the inlet and outlet temperature difference. The C_p of exhaust air can be calculated using temperature data from the calorimeter and water flow rate by equation 9.

$$C_{p_{exhaust}} = \frac{\dot{m}_{water} \times C_{p_{water}} \times (T_{w\,out} - T_{w\,in})}{(\dot{m}_{air} + \dot{m}_{H_2}) \times (T_{exhaust\,out} - T_{exhaust\,in})} \qquad \text{(eq. 9)}$$

Here, $T_{w\,in}$ and $T_{w\,out}$ are cooling water temperatures at the inlet and outlet to the calorimeters, respectively, while $T_{exhaust\,in}$ and $T_{exhaust\,out}$ are exhausted air temperatures at the inlet and outlet to the calorimeter, respectively. $\dot{m}_{water}$ is the mass flow rate of cooling water in the calorimeter.

3.2. Workbench Preparation

The primary test setup has been developed modifying a direct injection single cylinder CI engine in SI engine to operate on different compression ratios. The original cylinder head is replaced with a modified one, which has housing to accommodate a piezo sensor and spark plug. A mechanically liftable cylinder block replaces the existing cylinder block to change the CR. The intake manifold is modified to accommodate a throttle body and electronically controlled hydrogen port injection (HPI) system. A capacitive discharge ignition (CDI) system is installed. Like the intake manifold, the exhaust manifold is modified to house a K-type thermocouple to measure EGT and is connected to a shell and tube type calorimeter. The existing flywheel is replaced with a spur-geared end flywheel to support self-starting through an electric motor. The crankshaft is connected to an eddy-current dynamometer for loading, which is installed with an S-beam type load sensor and a crank encoder. A circular precision disk with a trigger

mark is also installed on the crankshaft, which helps measure the crank revolutions but the help of a photoelectric sensor (rpm sensor). The engine specifications are mentioned in Table 3.1. The schematic diagram of the test rig is presented in Figure 3.2.
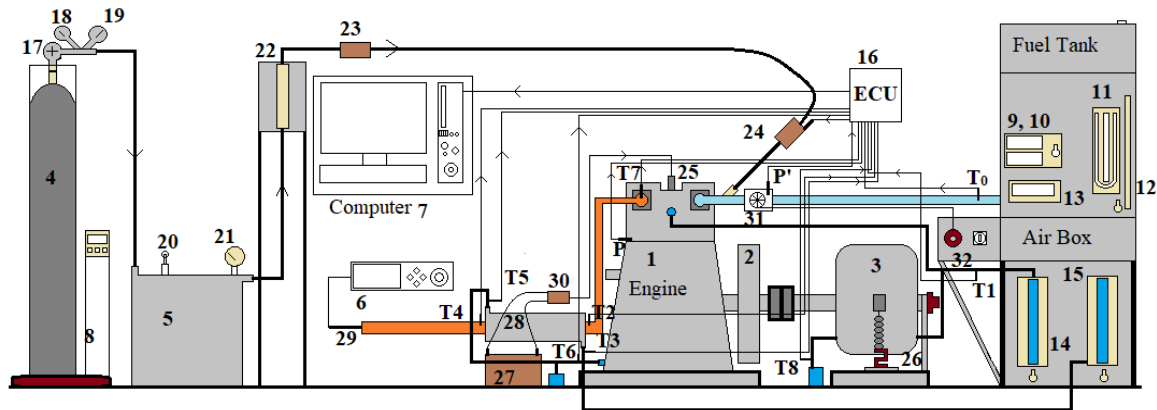

Figure 3.2.Experimental Test Rig (HPI)

1- Engine, 2 – Flywheel, 3 – Dynamometer, 4 - Hydrogen Cylinder, 5 - Wet Type Flame Trap, 6 - Exhaust Gas Analyzer, 7 – Computer, 8 - Weighing Machine, 9 - Temperature Display, 10 - Load Display, 11 – Manometer, 12 - Fuel Burette, 13 - rpm Display, 14 - Engine Rotameter, 15 - Calorimeter Rotameter, 16 - Engine Control Unit, 17 - Control Valve, 18 - Line Pressure Gauge, 19- Delivery Pressure Gauge, 20 - Safety Valve, 21 - Pressure Gauge, 22 - H2 Rotameter (LPM), 23 - Dry Flame Trap, 24 - Non-return Valve & Hydrogen injector, 25 - Spark Plug, 26 - Load Cell, 27 - Battery, 28 - Calorimeter, 29 - EGA Probe, 30 - Capacitor, 31 - Throttle Body & Regulator, 32 - Throttle Control Knob, T0 - Ambient Air Temperature, T_1 - Cooling Water Temperature at Engine & Dynamometer Inlet, T_2 - Exhaust Gas Temperature at Calorimeter Inlet, T_3 - Cooling Water Temperature at Calorimeter Inlet, T_4 - Exhaust Gas Temperature at Calorimeter Outlet, T_5 - Cooling Water Temperature at Calorimeter Outlet, T_6 - Cooling Water Temperature at the Outlet, T_7 - Exhaust Gas Temperature at Exhaust Manifold, T_8 - Cooling Water Temperature at Dynamometer Outlet, P - Engine Cylinder Pressure Piezo Sensor, P' - Inlet Manifold Pressure Sensor at Throttle body

The hydrogen supply unit consists of a hydrogen cylinder where 99.99% pure hydrogen is stored at 220bar, connected to a wet-type flame arrester through a 12mm high-pressure hose. Further, the supply line connects with a hydrogen mass flow rotameter coupled with a flow regulator. The rotameter supplies fuel to the fuel injector by bypassing a non-return valve. On the other hand, since the engine is water-cooled, the water supply is maintained with the help of an electric pump, where two rotameters measure the flow to the engine and calorimeter. These rotameters are installed in the

panel box, which also houses an airbox coupled with an airflow meter and a U-tube manometer. Similarly, the loading unit, display unit, throttle knob, and fuel metering unit are housed in the panel box. A five-gas analyzer is used to measure exhaust emissions. An open ECU is used to control the IT and injection duration. Signals from all the sensors are collected by an I/O type data acquisition system (DAQ), which sends these to the computer with the help of a USB interface, where a Lab-View-based program reads the signals and analyses the results. The specifications of the sensors and DAQ are mentioned in Table 3.2.

Table 3.1.Engine Specifications

Make/Model	Kirloskar/TV1
Capacity	0.661 liter (87.5mm $\times$ 110mm)
No. of cylinders	One (water-cooled)
Compression ratio	Variable (08-15)
Ignition timing	Variable (36ºCA bTDC-0ºCA bTDC)
Power output	5.8kW@1800rpm at CR11 with gasoline

3.2.1. Modification in test set-up for stage II

The experimental setup is slightly modified for stage 2 experiments, in which a manually operated EGR system is attached, as shown in the schematic diagram in Figure 3.3. The EGR system involves an insulated EGR supply line made up of mild steel and covered by glass wool. After the exhaust cooler, a T section is installed in the exhaust section to house the ball valve working as an EGR valve. A T-type exhaust gas mixing section is attached to the intake line between HPI, and the throttle body connects the EGR line. Another air flowmeter is installed at the EGR valve to measure EGR mass flow rates. The air supply box is connected to the surge tank of the compressor with the help of a pressure regulator fitted with a dial-type pressure gauge. The specifications of the compressor are listed in Table 3.3.

Table 3.2.Sensors and measuring units Specifications

Dynamometer	Eddy-current (water-cooled, Make- Technomech, Model- TMEC10)
ECU	PE3 Series ECU, Model PE3-8400P
Piezo sensor	PCB Piezotronics, Model SM111A22
Crank encoder	Make Kubler, Model 8.KIS40.1361.0360, Resolution 1 Deg, Speed 5500 rpm with TDC pulse
Gas ECU	Stag AC300
Gas Injector	Stag IG 01, single hole, 0.5-2.5bar
Gas flowmeter	Make- Tansa Equipment, HS-90261090, 0-200 LPM, LC 0.1 lpm
DAQ	16-bit, 250kS/s, NI-USB-6210
Load Sensor	Make Sensotronics Sanmar Ltd., Model 60001, S beam, 0-50 kg.
Air Flowmeter	Make WIKA, Model SL-1-A-MQA-ND-ZA4Z-ZZZ, output 4-20 mA, supply 10-30 Vdc, conn. 1/2"NPT(M), Range (-)25 - 0 mbar
Water rotameters	Make Eureka Model PG 5 & PG 6, Range 25-250 lph/40-400lph, Connection ¾" BSP vertical, screwed, packing neoprene.
Temperature sensors	Type RTD, PT100: - 1
	K-type thermocouple: - 8

Table 3.3.Compressor Specifications

Model	CPA 10 TMD
Type	Scroll
Serial No.	PNE630622
Max Pressure	7.2bar
Capacity	42CFM
Motor Power	10HP
Tank Volume	300 Litres
Dehumidifier Model	CPX 40
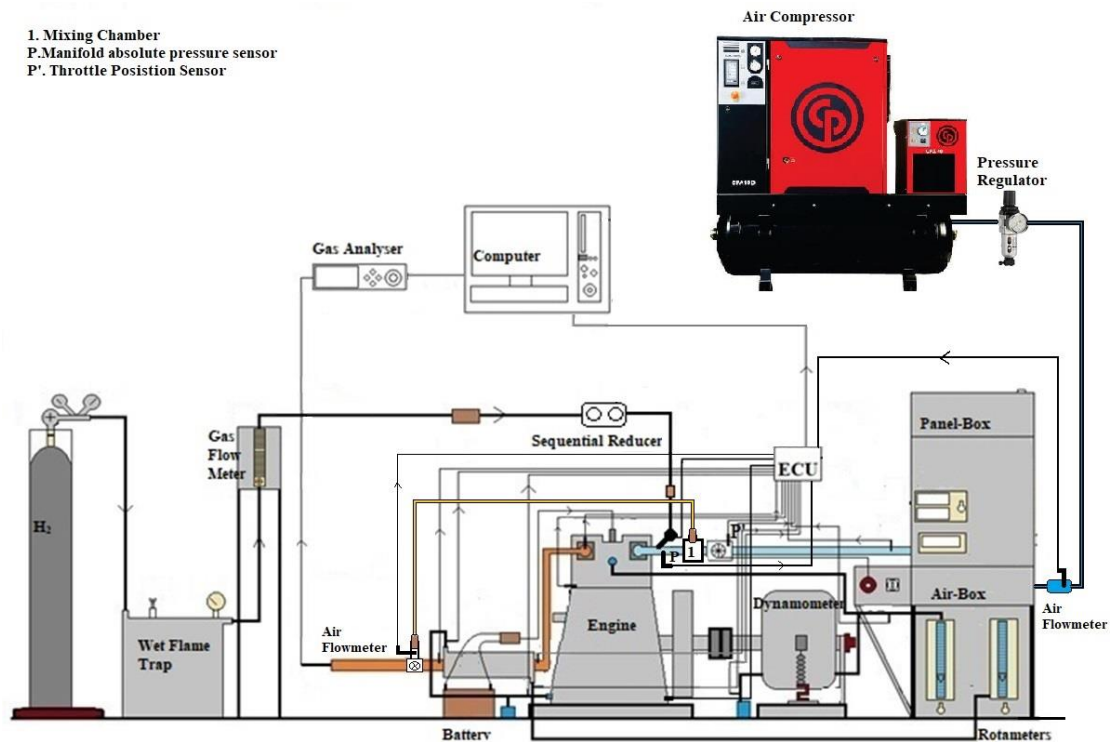
Figure 3.3.Experimental Test Rig (with EGR and MAP boost arrangement)

3.3. Uncertainty Analysis

The uncertainty analysis is performed in two phases where the first phase involves analyzing independent variables such as speed, CP, temperature, etc. Each experiment is designed to record data of 100 cycles, and there are two repeats; in this way, 300 cycles are there. Hence, error analysis is performed for 300 cycles by considering mean, standard deviation, and variance using reference equations (Senturk Acar & Arslan, 2017). A similar analysis is performed for emission parameters, where 100 continuous readings are considered. In the same way, dependent parameters like BP and BTE uncertainty are analyzed for the same 100cycles calculated from BMEP and engine speed. Table 3.4 enlists uncertainty for independent parameters.

Table 3.4.Uncertainty for different parameters

Parameter	Uncertainty (%)
Engine Speed	±0.113%
P_{max}	±0.242%
Angle of P_{max}	±0.925%
IMEP	±01.1%
EGT	±1.02%
T_{max}	±1.235%
NHR_{max}	±0.327%
CA10	±3.55%
CA10-90	±7.118%
Total Combustion Duration	±8.521%
CA50	±5.291%
NO_x	±1.152%
BP/BTE	±5.415%/±5.286%
η_{vol}	±2.138%

CHAPTER 4

RESULTS AND DISCUSSION

To achieve listed objectives the exhaustive experiments are conducted as mentioned in the previous chapter, the experiments are conducted under WOT condition for three speeds, 1400rpm, 1600rpm, and 1800rpm. The base reading with gasoline is also conducted under WOT conditions, however, CR is set to 11 and IT is kept 24⁰CA bTDC as designed. This IT corresponds to the maximum BTE for gasoline. The fuel injection duration for gasoline is set to meet ϕ 0.95, which corresponds to better fuel economy, and the fuel table is prepared based on throttle opening and speed combination. The results recorded for hydrogen operation are grouped based on speed and compared with the gasoline operation. The present investigation is to achieve the feasibility study of hydrogen in SI engine by varying CR, IT, ϕ, EGR, and MAP, and graphs are prepared. However, the results are compared in three sections according to the experimental scheme. Hence, explanations with a probable cause are discussed in three sections afterward; the first section discusses the influence of CR and ϕ, the second section discusses the impacts of IT and ϕ, and the last section explains the combined strategy of EGR and MAP boosting.

4.1. Influence of CR and ϕ

4.1.1. Brake power (BP)

BP is largely depend on the energy supplied; since, it increases with increasing ϕ, BP also increases (Porpatham, Ramesh, & Nagalingam, 2012). While an elevated CR helps the engine breathe by efficiently scavenging exhaust gases that results in a longer suction (Ravi et al., 2017). Therefore, to maintain constant ϕ, the required fuel supply increases. Hence, the energy supply is increased too. However, higher hydrogen replaces a large amount of intake air, limiting the average volume and BP. Figure 4.1 shows that with increasing ϕ, the effect of CR reduces, as at $\phi<0.6$, there is a continuous increase in BP for the entire range of CR. While at $\phi=0.6$, there is a negligible increment in BP at CR15. A further increase in ϕ worsens BP as a large drop in BP is noticed after

CR 14. Probably at high CR, the increased exhaust pressure reduces effective suction length at larger ϕ, also, there is a large amount of fuel burnt before TDC. The maximum increment is observed for CR14. However, with increasing speed, the rate of increase in BP/CR reduces, reducing further with increasing ϕ. Also, BP is dropped at CR14 at ϕ 1.0. BP of hydrogen fueling is less than gasoline at low CR and ϕ due to less energy supply by hydrogen. At CR>13 and 1400rpm, it is higher than gasoline at ϕ≥0.9, which improves with increasing speed. At 1600rpm, even at CR 12 for ϕ≥0.9, BP is higher, while at 1800rpm and ϕ≥0.9 BP is higher than gasoline at all the CR.
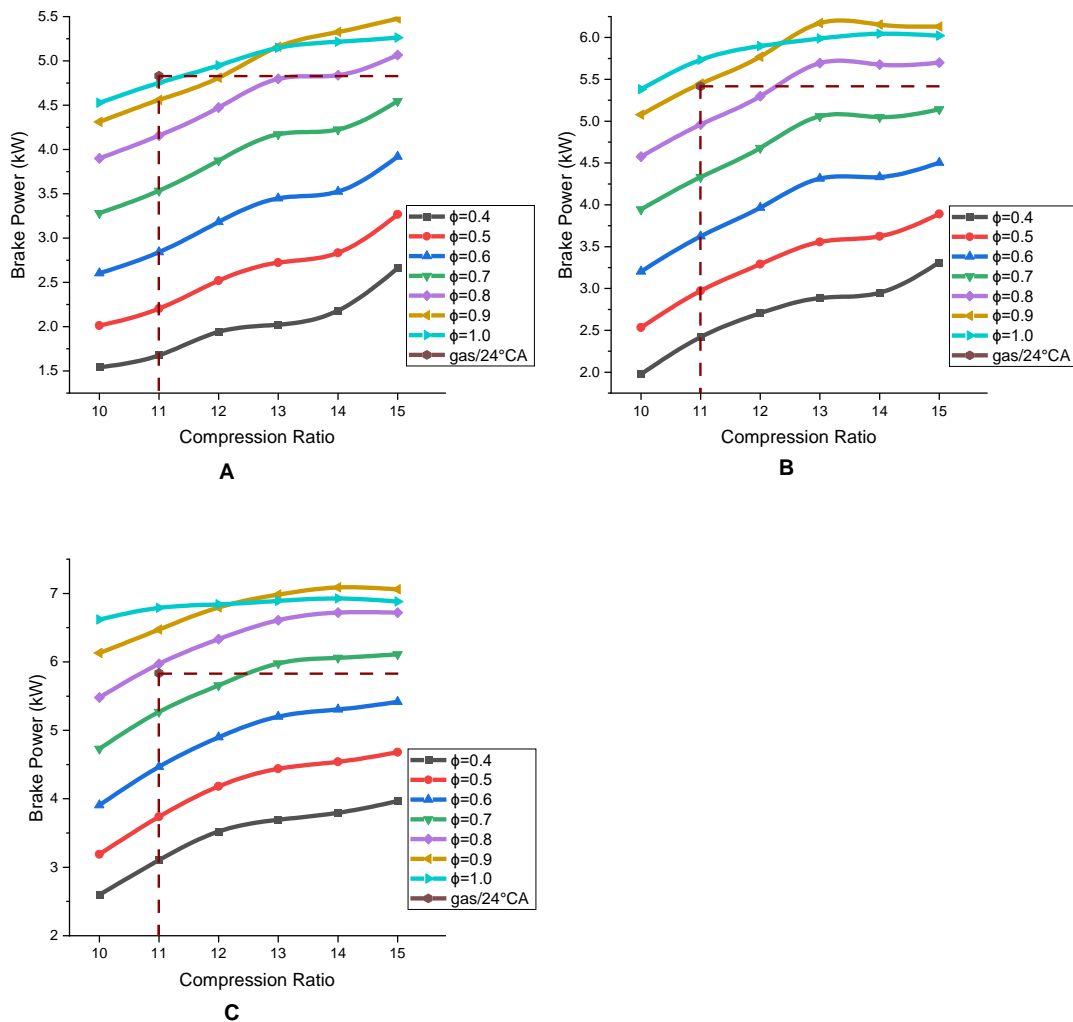
Figure 4.1.BP varies with CR at different ϕ (A-1400rpm, B-1600rpm, C-1800rpm)

4.1.2. Brake thermal efficiency (BTE)
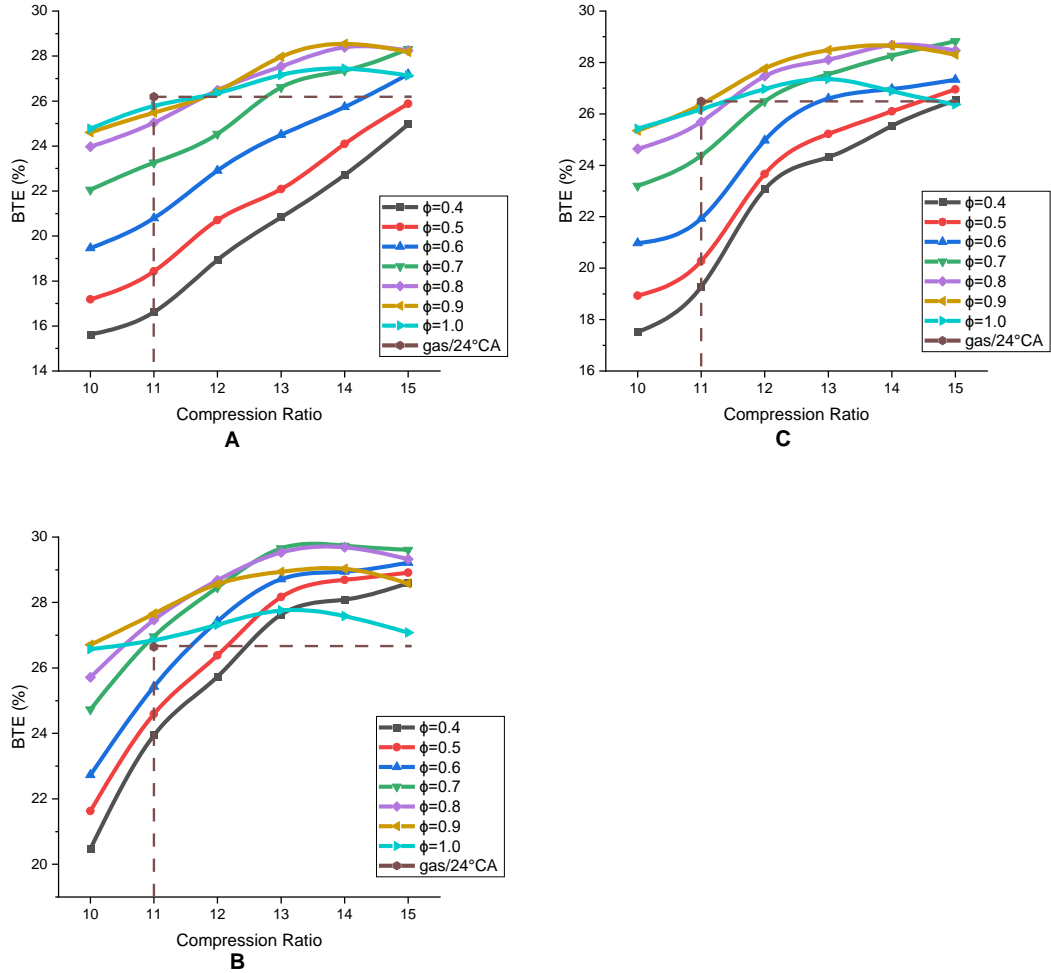
Figure 4.2.BTE varies with CR at different φ (A-1400rpm, B-1600rpm, C-1800rpm)

From Figure 4.2, BTE increases continuously for lean fueling (φ≤0.7) with CR, while at φ>0.7, it increases to a maximum. CR corresponding to the maximum BTE depends on φ and speed, as φ=0.8 exhibits the maximum BTE at CR 14 at 1400rpm and 1600rpm, while at 1800rpm, it is CR 13. Similarly, increasing φ observes a lower CR corresponding to maximum BTE, as at φ=0.9 and φ=1.0, CR14 exhibits maximum BTE at 1400rpm, while CR13 observes maximum at 1600rpm and 1800rpm. Since, increasing CR results in higher air inflow, hydrogen supply also increases to maintain φ, hence, larger energy added helps higher operating pressure and BTE improves.

However, after certain CR, increased hydrogen supply to maintain a fixed ϕ compensates suction benefits of CR, resulting in low BTE. In addition, increasing flame speed with ϕ allows larger mass to burn before TDC. Also, the flame compression takes place at high CR with increasing ϕ, reducing BTE (J. Zhao et al., 2013). Though increasing ϕ observes an increase in BTE continuously at CR10 while increasing CR favors lean burning, BTE is always lower at ϕ<0.7. Since laminar flame speed depends on the mixture strength, the combustion speed drops for low ϕ, leading to prolonged burning. Therefore, a large part of the heat produced is used to heat the excess air, reduce the work/cycle, and hence, BTE. Increasing ϕ helps improve the combustion speed and reduces the sensible losses. However, after a certain ϕ, the available air and the time available for combustion reduce with speed, leading to incomplete combustion, and BTE drops (S. Wang et al., 2014). It intensifies with increasing CR. Rich fueling at higher CR proves better than gasoline at low speed due to better combustion quality. However, with increasing speed beneficial ϕ over gasoline shifts to lean, and CR to a low value.

4.1.3. Volumetric efficiency (η_{vol})

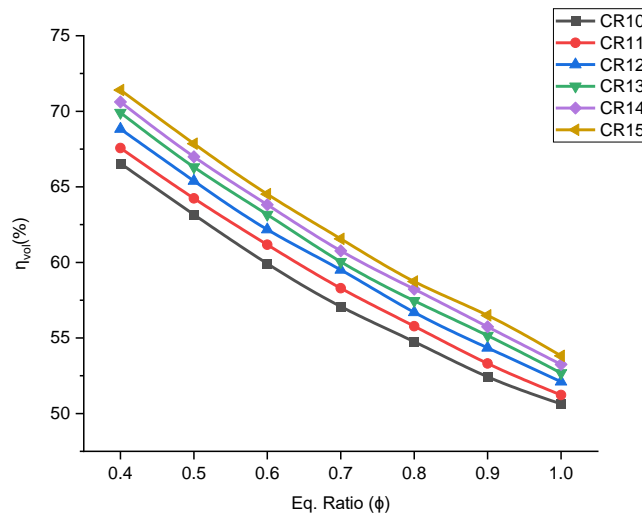

Figure 4.3.η_{vol} varying with CR and ϕ

The η_{vol}, at particular ϕ, is almost static irrespective of speed; hence, Figure 4.3 represents average η_{vol} over the entire speed range. The η_{vol} increases with increasing

CR due to reduced pumping losses; however, with increasing ϕ, a parallel drop in η_{vol} can be traced. This clearly shows the extent of air being replaced by the increased hydrogen quantity, which is also a prominent cause of a slight drop in BP and a BTE at higher values of ϕ. Increasing ϕ observes an almost 18% drop averaged over all CRs while increasing CR from 10 to 15 results in an 8.67% boost averaged over all the ϕ.

4.1.4. Combustion duration (in ºCA)
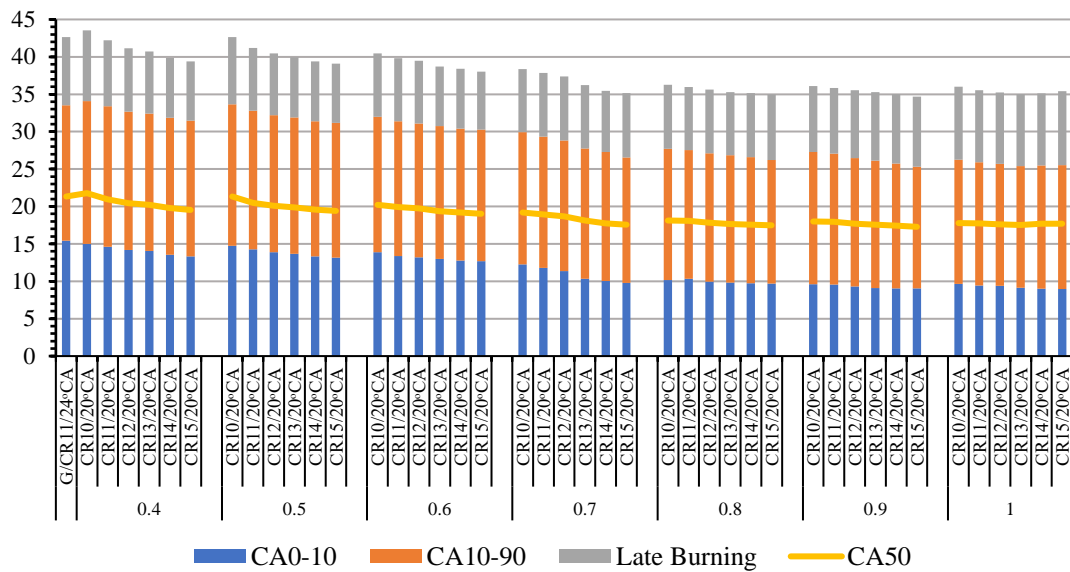
Figure 4.4.Combustion duration at various CR and ϕ at 1400rpm

In Figure 4.4-Figure 4.6 combustion duration is plotted against CR for each variation of ϕ. CA100 reduces by increasing CR at lean conditions while increasing speed boosts it too. Similarly, increasing ϕ also helps quick combustion, reducing it to a minimum and then increasing slightly (Qing he Luo et al., 2019). However, compared to gasoline CA100 for $\phi \leq 0.5$ is higher at low CR, increasing CR improves combustion and reduces it below gasoline. For $\phi > 0.5$, it is always below gasoline but observed to increase with CR at $\phi > 0.8$ after achieving a minimum. Despite increasing CA100 at $\phi > 0.8$, CA10 is observed to reduce continuously with increasing CR at any ϕ. However, the reduction rate decreases with increasing ϕ and CR. Since the increasing CR increases instantons pressure and temperature at the time of ignition, the flame stabilization gets easier, and cooling of flame due to charge ahead of flame front reduces the CA10 (X. Duan, Liu,

Lai, et al., 2019). Similarly, increasing φ reduces the specific heat of charge, helps rapid flame stabilization(Hagos, A. Aziz, Sulaiman, & Mamat, 2019) and reduces CA10. CA10-90 also reduces with CR continuously; however, at φ>0.9 and 1400rpm, there is an increase in CA10-90 when CR is increased after 13. With the increase in speed, such effects get persistent even at φ=0.9. Similarly, increasing φ increases flame velocity, resulting in rapid combustion and reducing the CA10-90(Qing-he et al., 2019). At rich conditions (φ>0.8), increasing CR helps in reducing CA10-90 by increasing flame speed up to a certain CR. A further increase in CR results in compression of the flame front to a greater extent, increasing CA10-90 infinitesimally(Valiev et al., 2013; S. Wang, Ji, & Zhang, 2010).
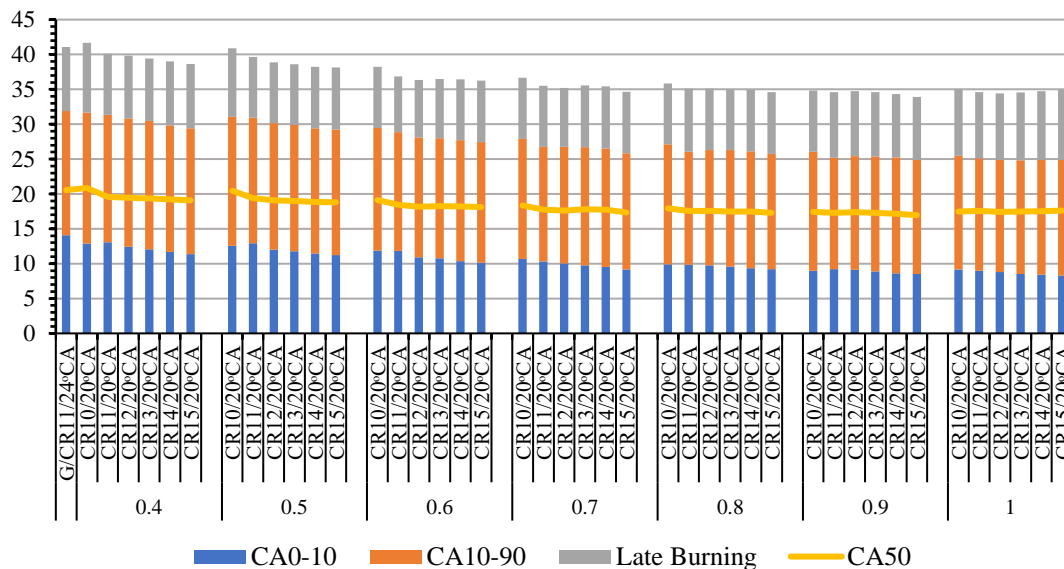
Figure 4.5.Combustion duration at various CR and φ at 1600rpm

The CR limit of a minimum CA90-100 at φ≥0.9 depends on speed, as minimum CA90-100 is observed at CR14 for φ=0.9 and CR13 for φ=1.0 at 1400rpm, while CR13 observes minimum at 1800rpm for both φ. Since CA90-100 falls in expansion stroke where pressure drops rapidly, a longer CA10-90 compels it to a delayed angle where pressure is lower. Therefore, the combustion speed reduces; hence CA90-100 increases(Dinesh, Pandey, & Kumar, 2022). Apart from φ=0.4 at CR10 and 11, the CA10, CA10-90, and CA90-100 of hydrogen fueling are less than gasoline, which

indicates why BTE is improved. The CA50 also follows CA10-90 and behaves in the same fashion.
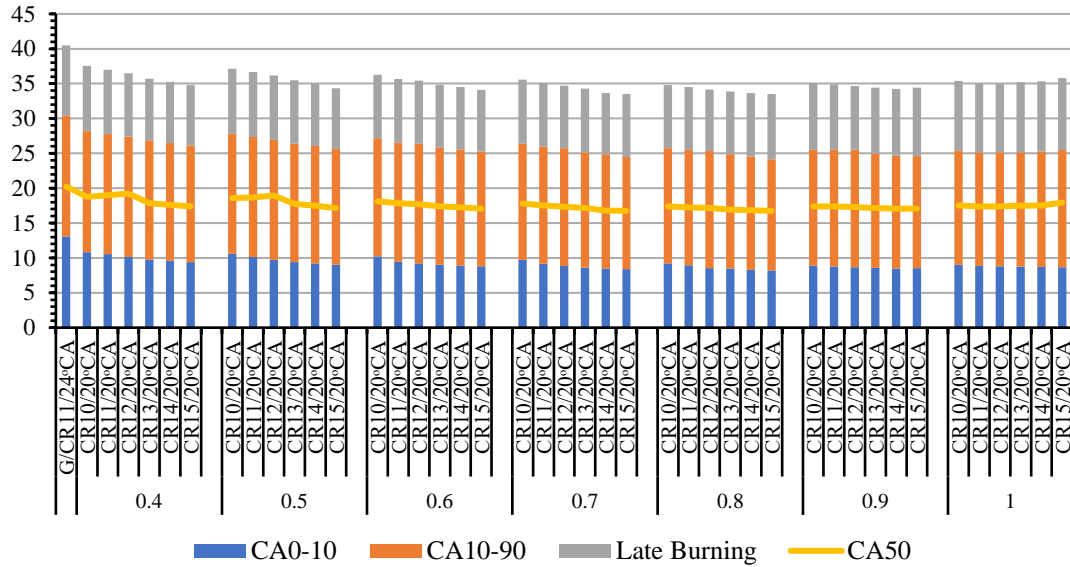
Figure 4.6.Combustion duration at various CR and ϕ at 1800rpm

4.1.5. Cylinder pressure (CP)

CP variations near TDC from 260ºCA to 460ºCA are considered for analyzing combustion behavior. Since a similar trend for all speed are noticed, 1800rpm adopted here, Figure 4.7 represent the same, while Figure 4.8 represents the variations in P_{max} with CR and ϕ. From observations, increasing CR increases P_{max}, and increasing ϕ increases it too (Diéguez et al., 2014). However, P_{max} drops insignificantly for ϕ>0.9 at CR>13. The hydrogen supplied is relatively high in such conditions, reducing the η_{vol}, and flame compression leads to a slight drop in P_{max}. The increasing CR advances the position of P_{max} towards TDC, and increasing ϕ too helps in advancing P_{max} position. At a particular speed and CR, increasing ϕ is responsible for the rapid rise of the pressure near TDC; that is, RPR increases with ϕ in the late compression stroke (Catapano, Iorio, Sementa, & Vaglieco, 2016). The same trend follows for increasing CR too for a particular ϕ. At 1800rpm, an average 2.78% increment at ϕ=0.4 reduces to 1.56% at ϕ=1.
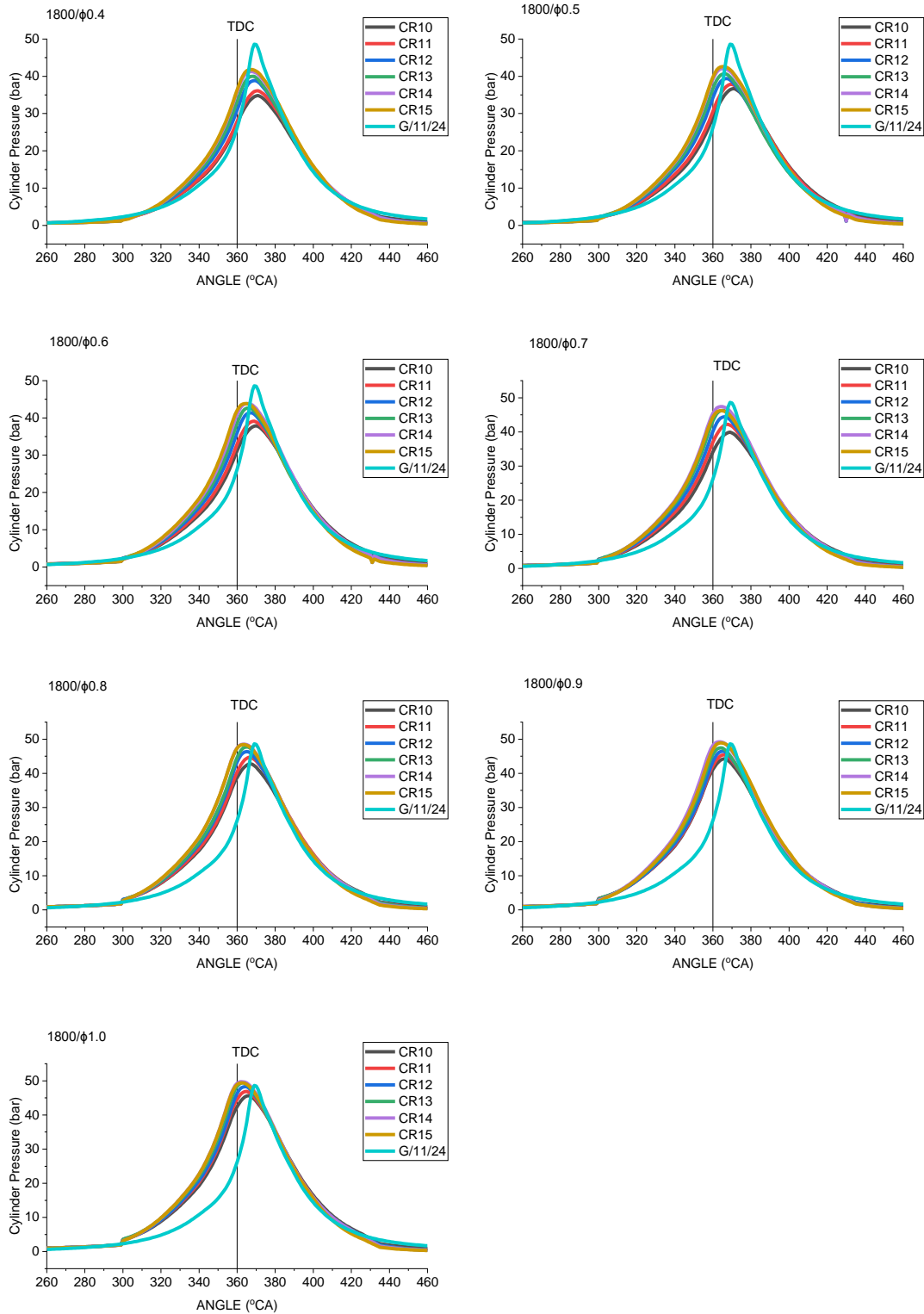
Figure 4.7.CP varying with crank angle and CR at various ϕ at 1800rpm

56

Similarly, at CR10, an average increase of 5.62% at ϕ=0.4 reduces to 0.79% ϕ=1. Similarly, at CR 10, P_{max} reduces to 3.3%, and at CR15, to -0.56%. Compared with CR10 and ϕ 0.4, the P_{max} is almost double for ϕ 1.0 at 1400rpm, which reduces to merely 26.33% at 1800rpm. However, there is a 19.15% average increase from CR10, ϕ 0.4 to CR15, ϕ 1.0 at 1400rpm, which reduces to 13.3% only at 1800rpm.
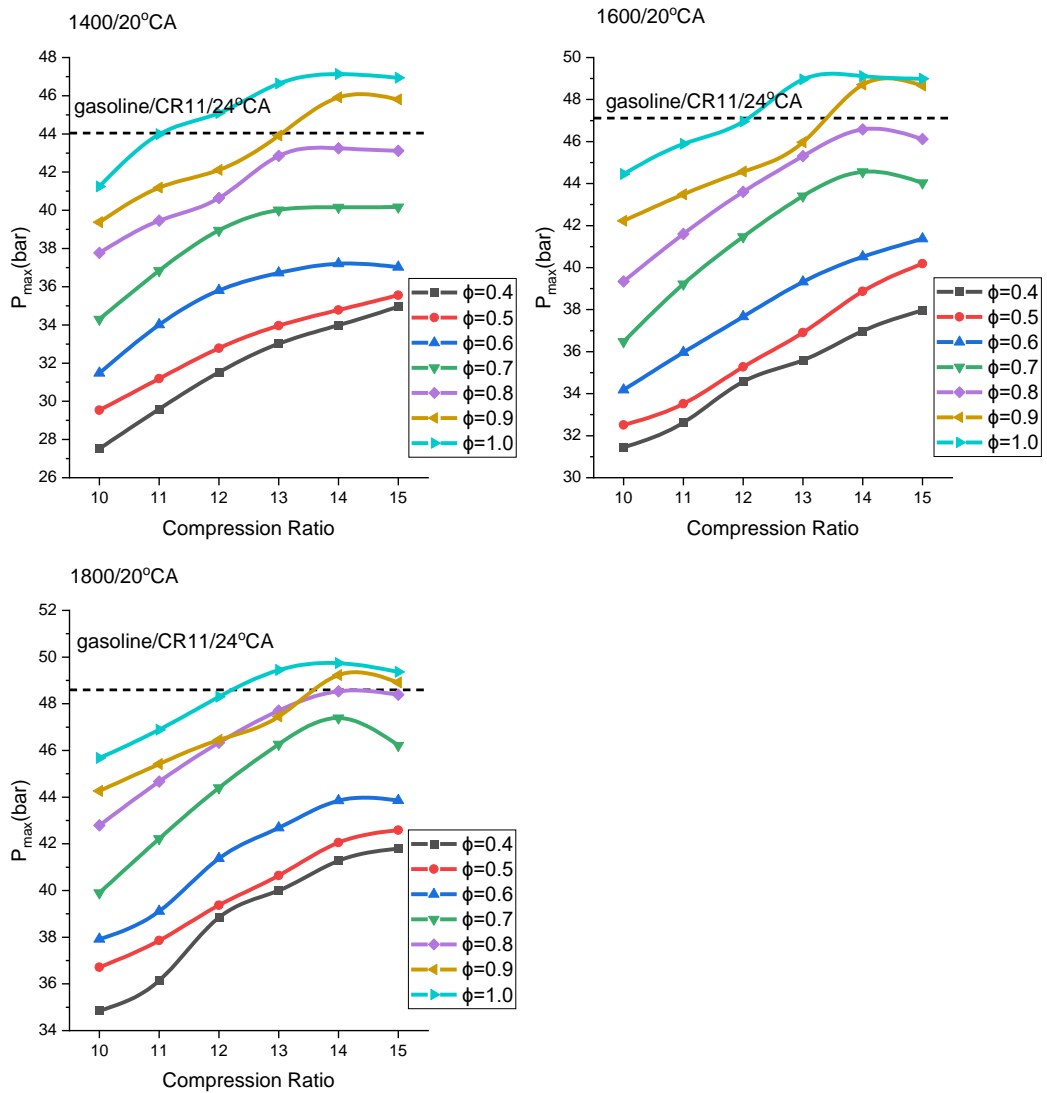
Figure 4.8.P_{max} varying with CR and ϕ at various speeds

4.1.6. Heat release rate (HRR)

HRR variations are depicted in Figure 4.9-Figure 4.11. Since the HRR depends upon combustion, curves are shown for a short range of 260ºCA to 460ºCA, drawing a relation with CP.
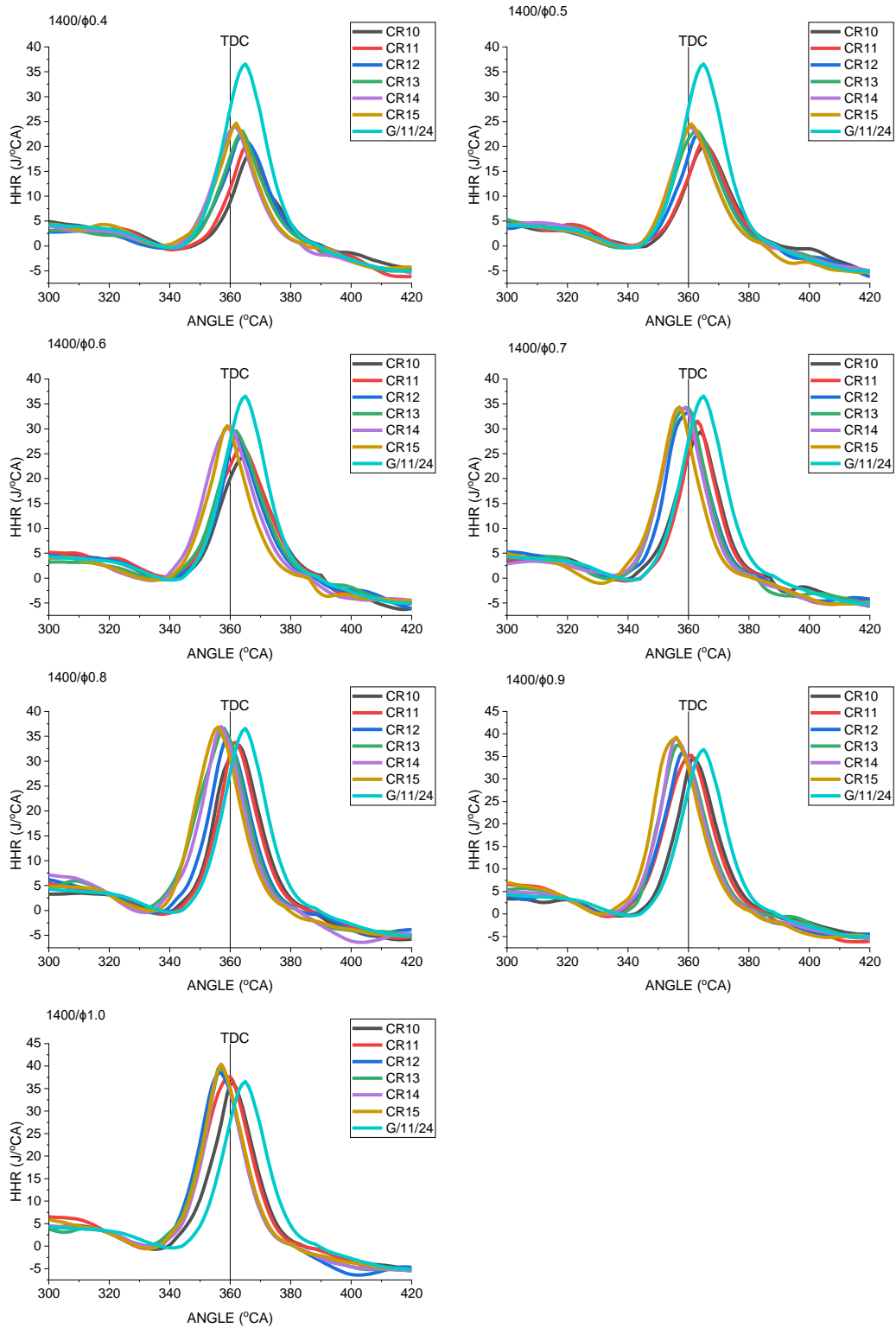
Figure 4.9.HRR varying with crank angle and CR at various φ at 1400rpm
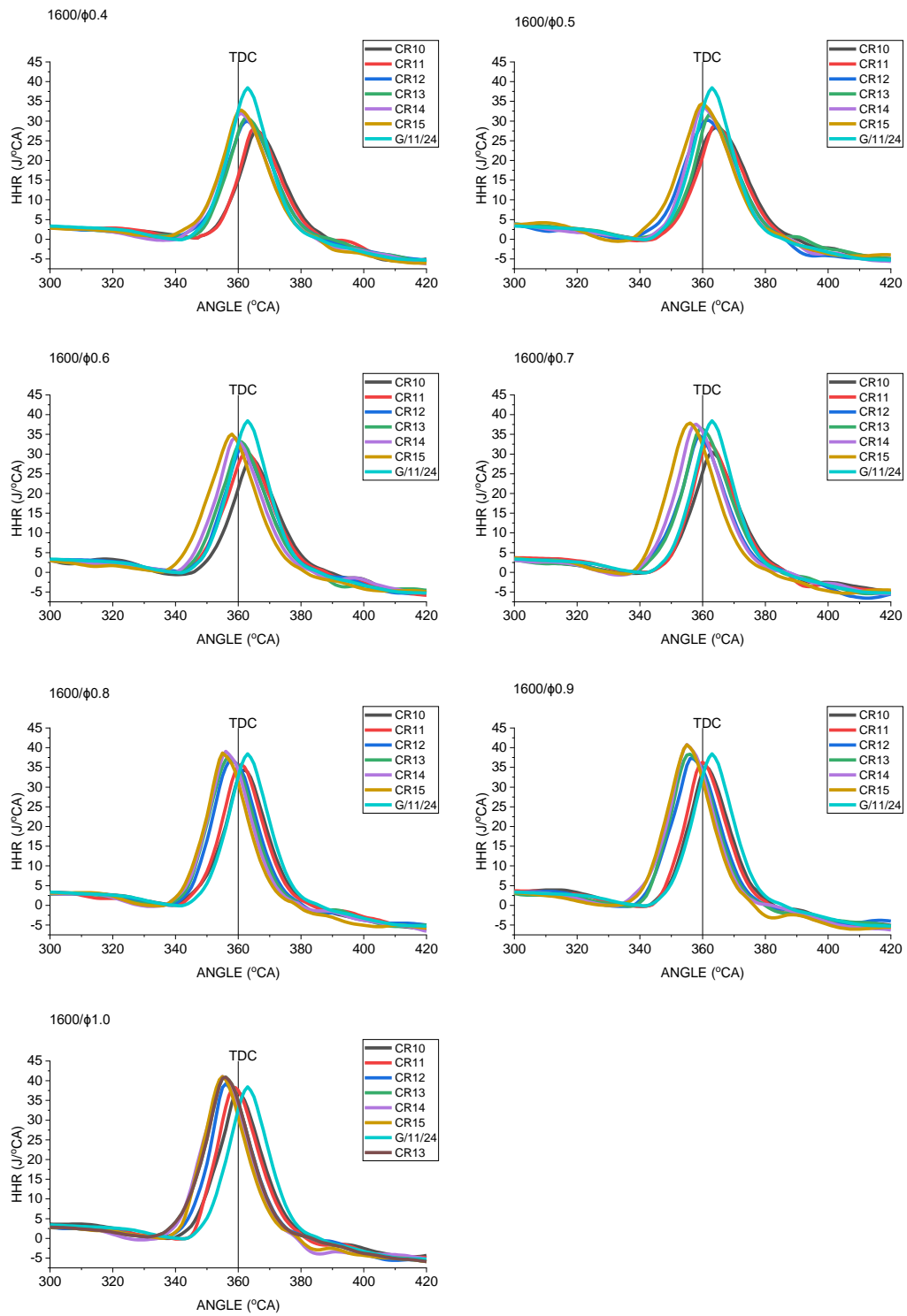
Figure 4.10.HRR varying with crank angle and CR at various ϕ at 1600rpm
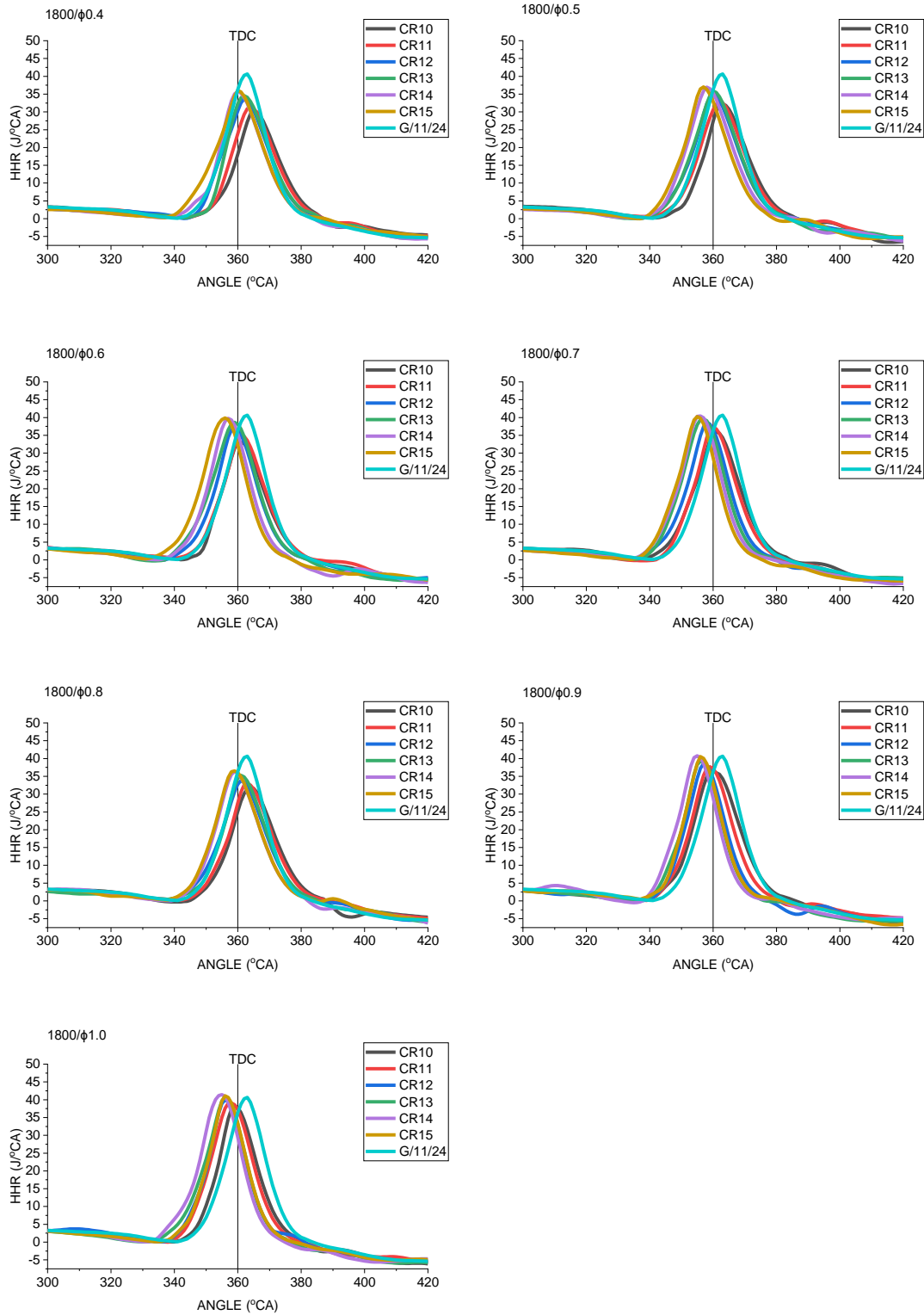
Figure 4.11.HRR varying with crank angle and CR at various ϕ at 1800rpm

The increasing CR increases enthalpy of the working fluid which reduce the ignition delay and promotes fast burning. Also it reduces the RGF, which improves suction(Ma et al.). Hence, the combustion process speeds up, leading to high HRR. It advances the peak HRR (HRR_{max}) too. At a low speed (1400rpm) and low hydrogen content ($\phi<0.7$), the rate of increase in HRR gets enhanced with increasing CR, while for $\phi\geq0.7$, the rate of increase in HRR increases with CR up to CR14 and falls slightly at CR15. It can be observed from the width of the parabola, which gets narrowed, representing a higher rate of HRR rise. Similarly, peak HRR gets advanced continuously with an increase in CR at $\phi<1.0$, while at $\phi=1.0$, the peak advances till CR13 and then remains static. With increasing speed, the effect of CR increases at lean conditions ($\phi<08$ at 1600rpm and $\phi<0.7$ at 1800rpm) and reduces at rich conditions. It is also observed that the HRR_{max} for $\phi=1.0$ finds nearly identical value that of $\phi=0.9$. The peak is also retard at $\phi=1.0$ for CR15 at high speeds. As described earlier in the section on CP and combustion duration, flame compression is one of the major causes behind the retard (Z. Y. Sun & Li, 2016). Due to the availability of cooling time at low speeds, this effect is insignificant, which is very effective at high speeds. The scarcity of available oxygen at stoichiometric conditions at higher CR may be the reason for the drop in HRR_{max}.

4.1.7. Peak cylinder temperature (T_{max})

T_{max} represents combustion efficiency and the quality of energy produced. It depends upon the type of fuel, ϕ, CR, IT, etc. T_{max} is reduced continuously by reducing ϕ due to reduced energy supply, and an increased combustion period allowing efficient cooling of working fluid(Su, Ji, Wang, Cong, & Shi, 2018). Besides, the increased amount of air increases the specific heat capacity of the incoming charge, which results in cooling of the cylinder wall and restricting the T_{max}(B. Zhang, Ji, & Wang, 2015). CR is an essential factor in deciding MGT; the more is the CR, the more is MGT, helps combustion and increases T_{max}(Lattimore, Herreros, Xu, & Shuai, 2016). Figure 4.12 T_{max} variations; it is observed to increase with CR continuously for lean conditions ($\phi\leq0.7$). For $\phi>0.7$, T_{max} increases with CR till CR14 and then drops, and the rate of drop/CR increases with ϕ. The increasing ϕ increases combustion speed, increasing T_{max}, further boosted by CR. However, at higher ϕ, elevated CR increases flame compression probability, which reduces combustion efficiency and so the T_{max}(Curry,

1963). At low CR, the increment rate increases with ϕ as at 1400rpm and CR10; it increases from 3.3% to 5.43%. It gets reversed at high CR, as at 1400rpm and CR15, T_{max} increment rate reduces from 5.42% to 2.34%. The increasing speed also reduces T_{max} increment rate with ϕ, which intensifies with CR, as at 1800rpm and CR15, it varies from 4.1% to 1.83%. However, T_{max} of hydrogen witnesses benefit over gasoline for $\phi=1.0$ at any CR. With increasing CR, this limit broadens, leading to higher T_{max} for $\phi \geq 0.7$ than gasoline due to the combustion qualities of hydrogen (Balki & Sayin, 2014).
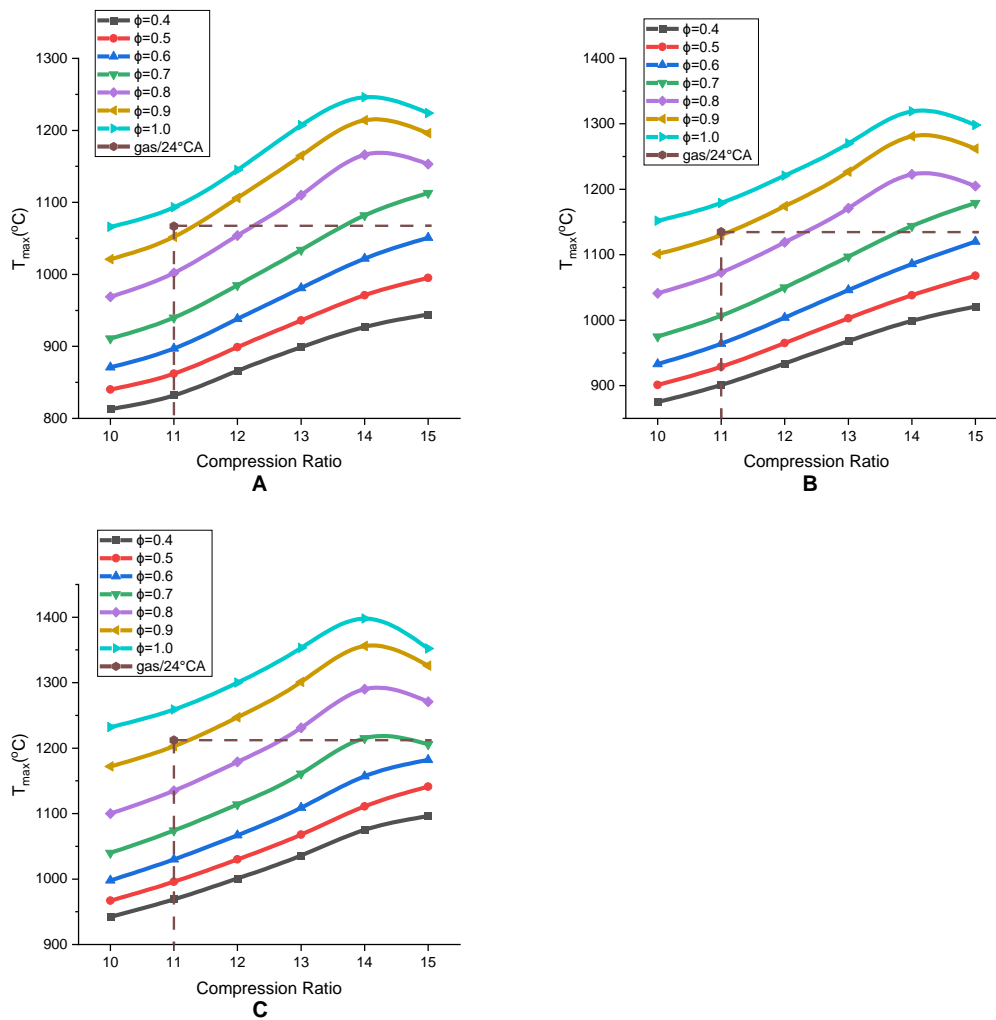
Figure 4.12. T_{max} varying with CR and ϕ (A-1400rpm, B-1600rpm, C-1800rpm)

4.1.8. Coefficient of variations of IMEP (CoV$_{imep}$)
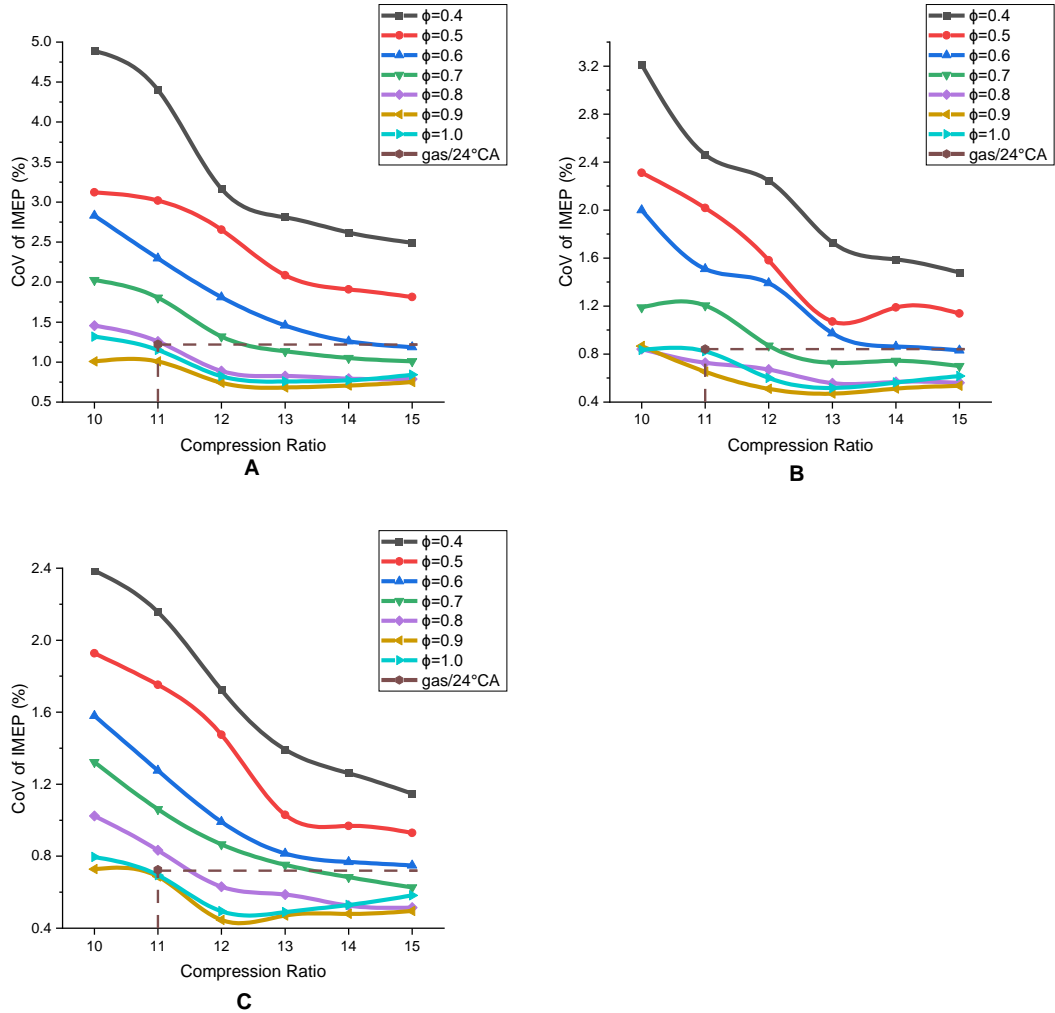
Figure 4.13.CoV$_{imep}$ varies with CR and ϕ (A-1400rpm, B-1600rpm, C-1800rpm)

The CoV$_{imep}$ indicates the extent of cycle-by-cycle variations and depends upon the smoothness of combustion. Since, increasing CR favors combustion and also hydrogen has an impressive combustion quality, CoV$_{imep}$ reduces. However, low ignition energy, and a relatively large pressure at the end of compression due to increased CR, promote knock for rich fueling (Gómez Montoya, Amador Diaz, & Amell Arrieta, 2018). Hence, CoV$_{imep}$ increases. Figure 4.13 depicts a similar trend; here, at any ϕ<0.8 at 1400rpm, CoV$_{imep}$ reduces with increasing CR. The rate of reduction per CR change reduces with increasing ϕ. When ϕ increases above 0.7, the CoV$_{imep}$ first reduces with CR up to CR13

and remains nearly constant. While observing the effect of ϕ, CoV$_{imep}$ reduces with increasing ϕ at any CR. However, at low CR, the continuous reduction persists till $\phi=1.0$, which after CR11 faces a slight increase due to a large amount of fuel concentrating as end charge at the end of the compression stroke (Zheng et al., 2009). The increasing speed favors combustion by increasing MGT and MGP. However, increasing ϕ also tries to concentrate large fuel mass and increase cylinder wall heating. Therefore, despite reducing CoV$_{imep}$ with speed, minimum CoV$_{imep}$ limits to an early ϕ. The reduction rate also decreases with increasing speed due to less time available for cooling and exhaust (Ma & Wang, 2008; Z. Wang, Liu, & Reitz, 2017). However, rich fuelling is better than gasoline, improving stable combustion and cycle-by-cycle variations(Akif Ceviz et al., 2012).

4.1.9. Exhaust Gas Temperature (EGT)

Figure 4.14 indicates that EGT increases continuously with CR at a fixed ϕ. Since increasing CR demands a higher fuel flow rate to maintain fixed ϕ, increasing the amount of heat supplied. Moreover, it also improves combustion, leading to higher T$_{max}$ and higher EGT(Pal & Agarwal, 2015). In the same way, increasing ϕ at any CR demands a higher fuel flow rate, and also the increased laminar flame velocity improves combustion leading to increase EGT as a result of increased T$_{max}$. There is no definite relation in EGT variation except that the increment/CR reduces with ϕ; however, $\phi=0.9$ at 1400rpm faces a rapid rise in EGT with CR, probably due to the higher relative increase in hydrogen supply rate. The increasing speed also motivates EGT leading to a higher rate of increase. At 1400rpm, EGT increases by 10% at CR10 moving from ϕ 0.4 to 0.5, which reduces to 3.89% from 0.9 to 1.0. However, at 1800rpm, at the same CR10, EGT increases by 25.27%, moving from ϕ 0.4 to 0.5, which reduces to 2% moving from 0.9 to 1.0. At low speed, the high CR with higher ϕ produces EGT higher than gasoline, while at high speed, the same CR EGT is greater than gasoline even at slightly lean conditions.
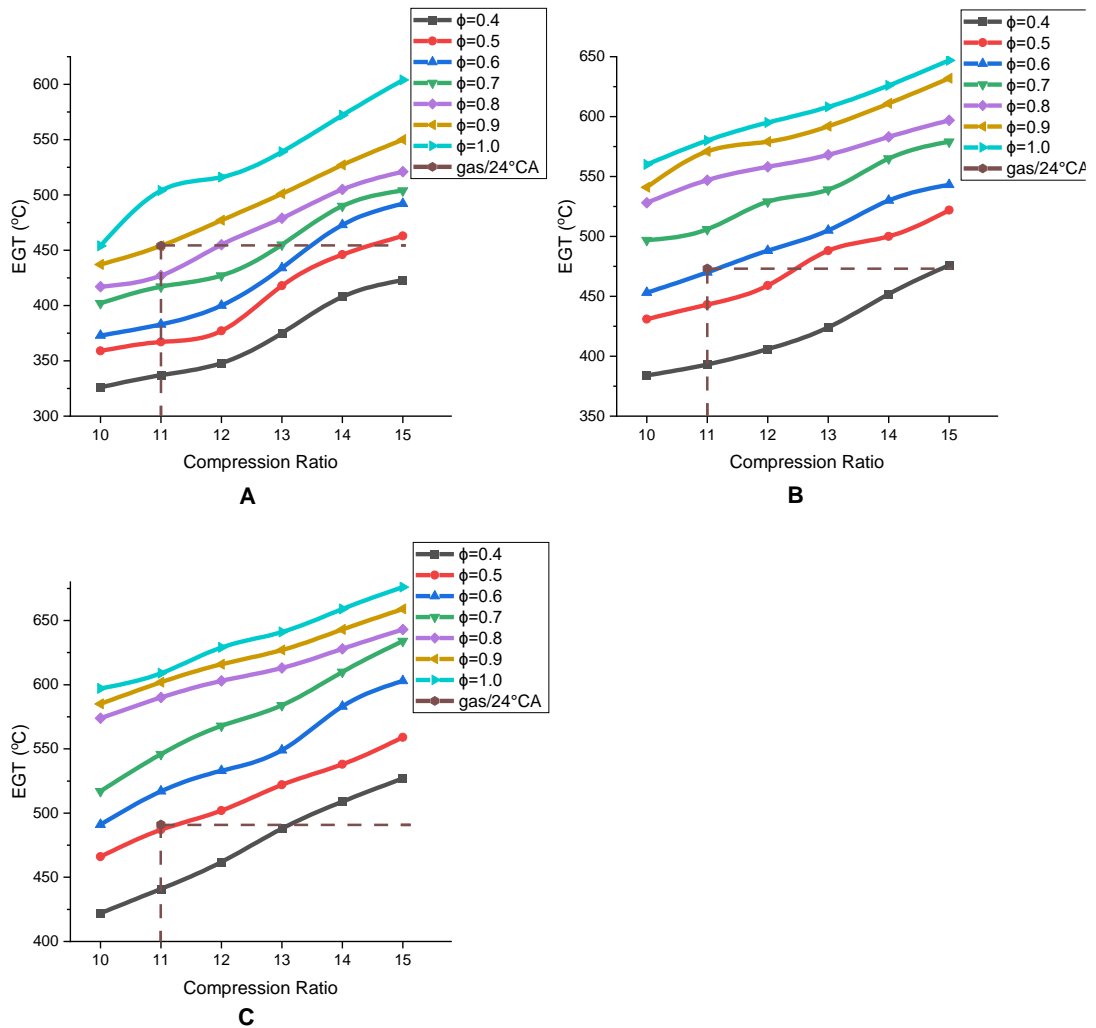
Figure 4.14.EGT varies with CR and φ (A-1400rpm, B-1600rpm, C-1800rpm)

4.1.10. NO$_x$ Emissions

A very high adiabatic flame temperature and laminar flame speed of hydrogen results in relatively high T$_{max}$, therefore motivating the NO$_x$ formation. In addition, better BTE results in good power conversion; hence, the specific emissions get reduced. The trade-off between these two factors decides the specific emissions (X. Duan, Li, et al., 2019). From Figure 4.15 shows that increasing CR continuously increases NO$_x$ at any φ; however, the increment rate first increases with CR up to CR13 at 1400rpm and 1600rpm, while at 1800rpm remains almost constant after CR13.
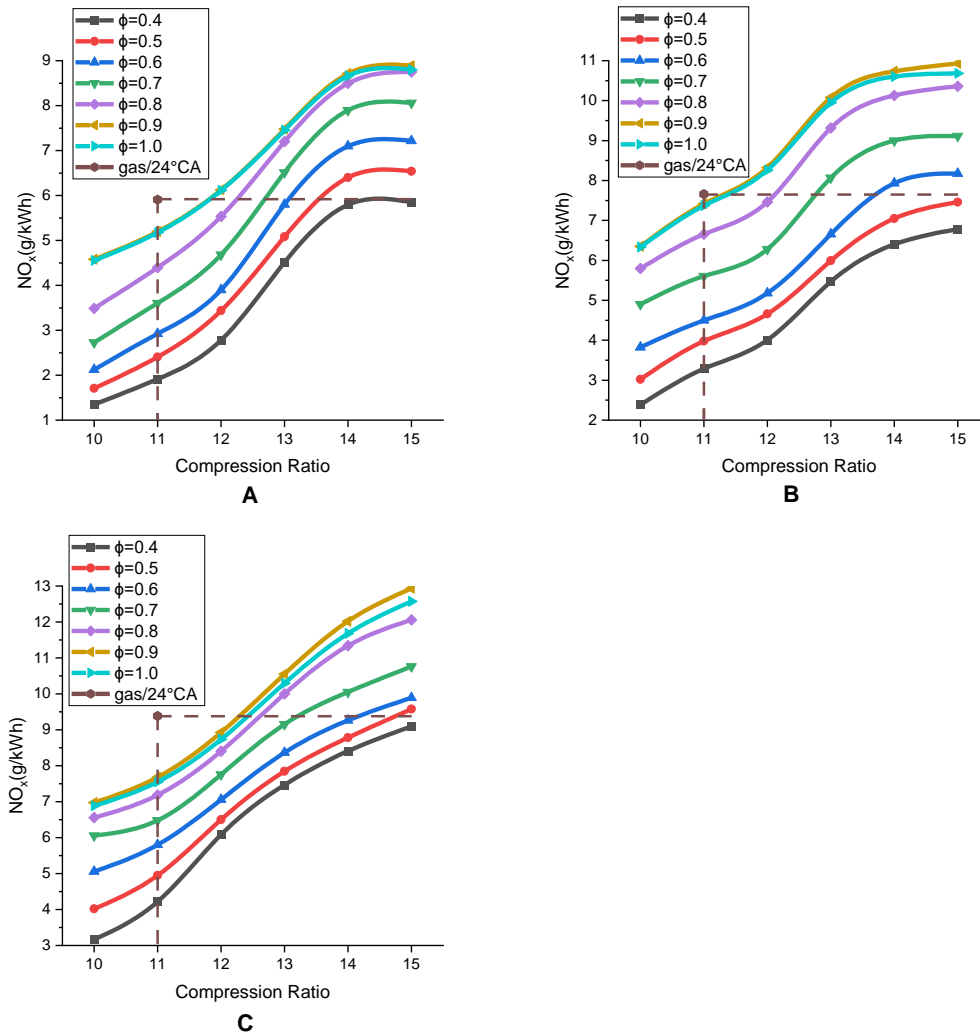
Figure 4.15.NOₓ varying with CR and φ (A-1400rpm, B-1600rpm, C-1800rpm)

On the other hand, increasing ϕ sees a continuous increase in NO_x up to $\phi=0.9$, and then it decreases. The increment rate increases till $\phi=0.7$ and then drops. Since the laminar flame speed increases with ϕ as well as total energy content, it boosts the T_{max}, leading to an increase in NO_x. Besides increasing ϕ after 0.7, BTE decreases, increasing the specific NO_x. However, at $\phi \geq 0.9$, the available oxygen reduces; therefore, the increment rate drops, leading to a slight drop in NO_x emissions at $\phi=1.0$. Similarly, for CR15, the flame compression creates a hurdle in combustion with reduces T_{max} and BTE; therefore, the NO_x increases slightly (Bhasker & Porpatham, 2017). At low CR, energy supply by hydrogen is less than gasoline, reducing the T_{max} and, hence, NO_x is below

66

gasoline. However, with increasing CR, MGT increases, increasing T_{max}; hence, NO_x increases rapidly.

4.1.11. Conclusion of section 4.1

The experimental results of phase 1 of stage 1 are compiled and discussed above in brief; the outcomes are concluded as follows;

- Hydrogen under a high CR (CR≥13) and a moderate equivalence ratio (ϕ=0.7-0.8) has improved performance, increasing the BP and BTE above gasoline. The fast-burning quality reduces cooling losses and provides better energy conversion.
- Under high CR (CR≥13) and equivalence ratio of 0.9, the CA10 and CA10-90 exhibit minimum values leading to fast combustion and high peak pressure.
- Hydrogen is also found responsible for drastically reducing the volumetric efficiency, which gets overcome by a significant margin by increasing CR.
- The CP and HRR are also increased with increasing CR, and the peak gets advanced, gets intensified further with increasing ϕ.
- The rich fueling has shown a drop in performance, P_{max}, peak HRR, and increased combustion durations at higher CR, probably due to the flame compression and over-increased MGT.
- Increasing the compression ratio reduces the CoV_{imep}, which gets boosted by increasing ϕ up to ϕ=0.8; the CoV_{imep} then starts climbing. However, the EGT increases continuously with CR and ϕ.
- The NO_x emission increases rapidly with increasing ϕ and CR due to a rapid increase in T_{max}. At CR15 and ϕ 1.0, NO_x is recorded above gasoline.
- At high CR, there is an additional allowance to use more fuel to overcome the limited energy density of hydrogen.

4.2. Influence of ignition timing (IT)

The experimental outcomes of phase 1 of stage 1 indicate a significant improvement in performance by increasing CR to 14 for a range of ϕ between 0.6 to 0.8. Therefore,

phase 2 experiments are conducted at CR14 for 0.6≤ϕ≤0.8 at different ITs. The results obtained are compiled and discussed below;

4.2.1. Brake power (BP)
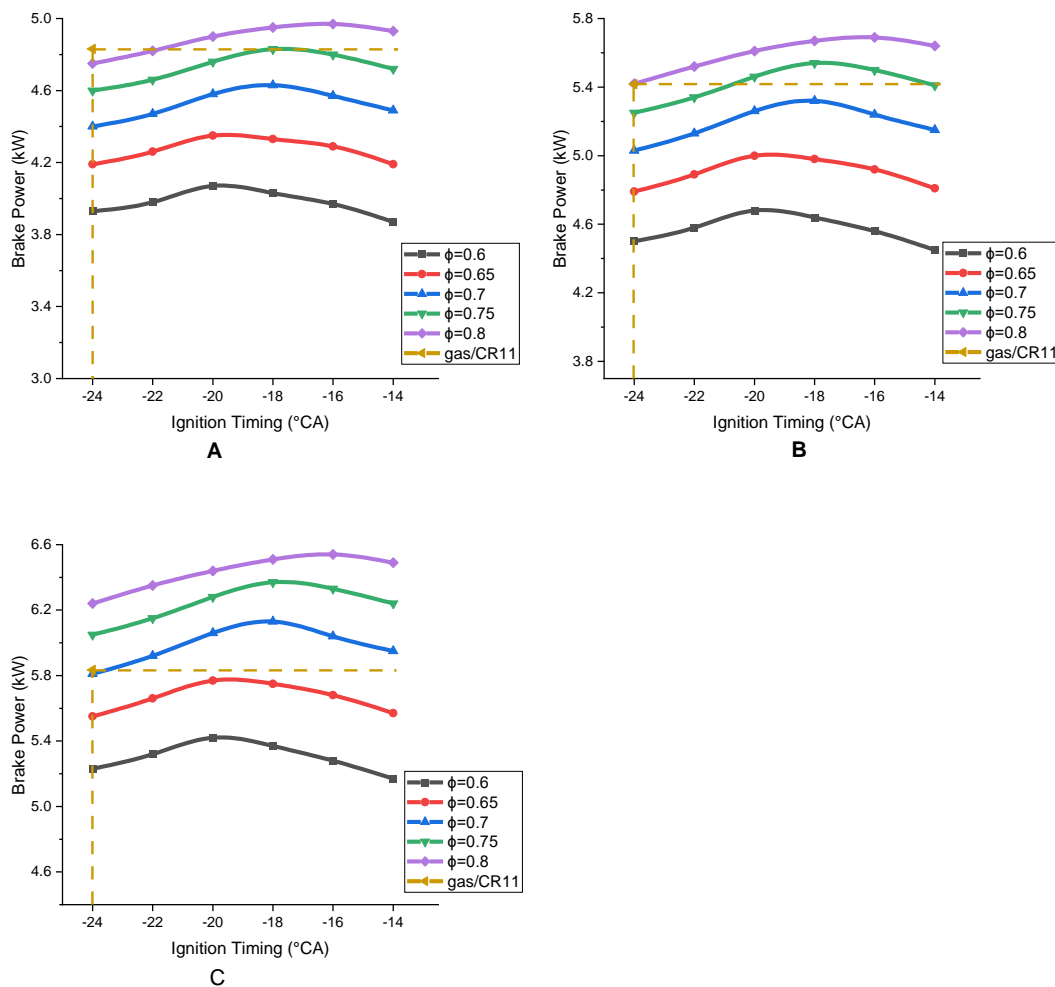
Figure 4.16.BP varying with IT and ϕ (A-1400rpm, B-1600rpm, C-1800rpm)

Figure 4.16 represents IT effects on BP at all three speeds separately. However, it affects BP in the same fashion irrespective of the speeds. Retarding IT from gasoline (24⁰CA bTDC) improves BP to a maximum, after which it drops. At lean conditions (at ϕ 0.6-0.65), IT corresponding to maximum BP falls earlier than in rich conditions (at ϕ 0.8). The increment rate reduces with ignition-retard; however, after maximum BP, the

drop rate increases with ignition-retard. Since hydrogen has a higher autoignition temperature and high laminar flame velocity, a delayed ignition helps the rapid combustion zone fall near TDC, increasing the conversion efficiency(Lee et al.). However, the combustion speed depends on the strength of hydrogen in the mixture; the reducing ϕ reduces the speed and hence, the best IT advances (Ma & Wang, 2008; Yousufuddin & Masood, 2009). Compared to gasoline, ϕ=0.8 exhibits comparable BP at low and mid-engine speeds and better at high speed. The BP at 1800rpm and ϕ=0.8 is higher than gasoline even at advanced ignition.

4.2.2. Brake thermal efficiency (BTE)
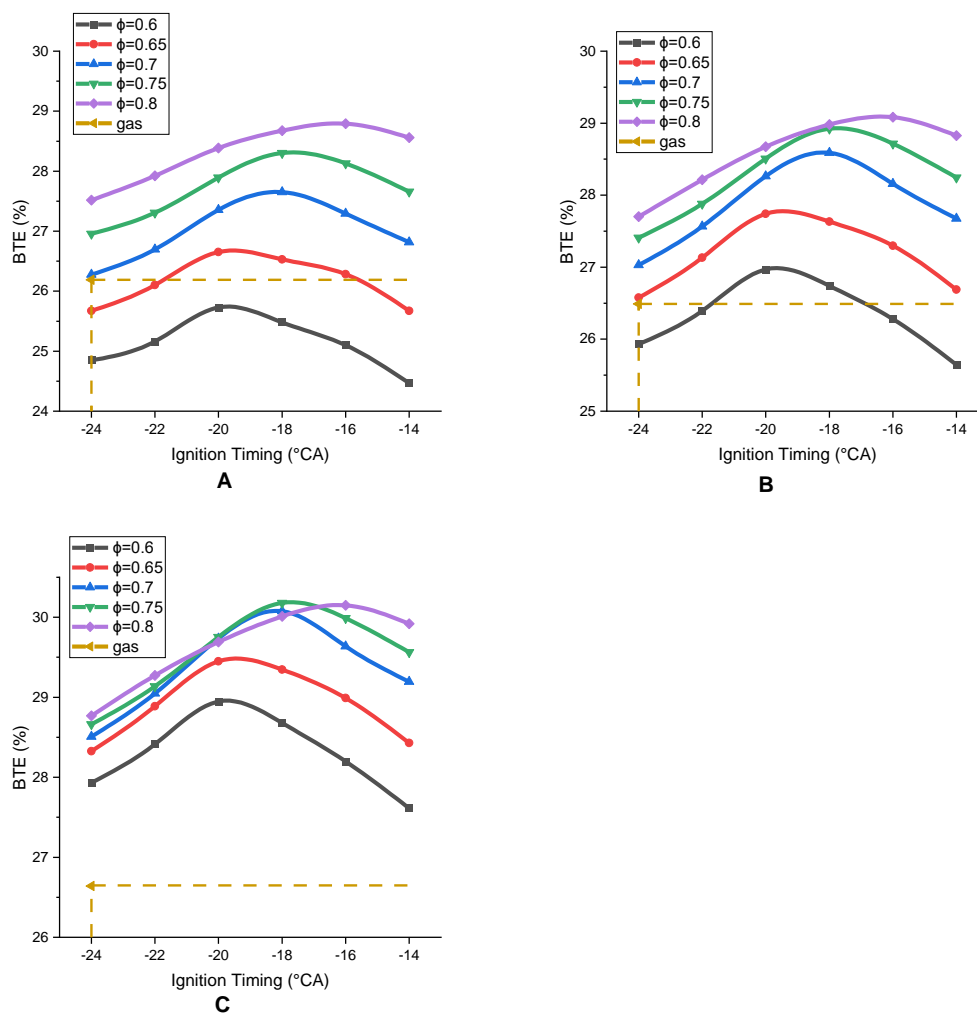
Figure 4.17.BTE varies with IT and ϕ (A-1400rpm, B-1600rpm, C-1800rpm)

Figure 4.17 shows BTE at CR14 is greater than gasoline at 1800rpm for $\phi \geq 0.6$ irrespective of IT. However, with reducing speed, BTE drops, as mentioned earlier, below gasoline for $\phi = 0.6$ at 1600rpm and $\phi < 0.7$ at 1400rpm. Probably, the effect of reducing combustion speed due to reduction in MGT with decreasing speed. However, delaying the ignition from gasoline (24ºCA bTDC), BTE increases to a maximum and then drops. At low ϕ, IT corresponding to maximum BTE is observed to fall at an advanced position, while with increasing ϕ, it retards. At small ϕ, combustion is slow; therefore, delaying ignition moves rapid combustion zone to expansion stroke, leading to a drop in P_{max} and MGP. Therefore, the work/cycle drops, reducing the BTE(Boggio, Lacava, Merola, Pe, & Irimescu, 2018). Similarly, at rich ϕ, an advanced ignition burns a larger mass before TDC, increasing compression negative work. Hence, the work per/ cycle reduces, leading to BTE drop (Ji, Wang, & Zhang, 2010).

4.2.3. Combustion duration

CA100 at any ϕ reduces to a minimum by delaying the ignition from 24ºCA and then increases (Figure 4.18-Figure 4.20). At low speed and lean ϕ, IT corresponding to the minimum is achieved earlier than at high speed.
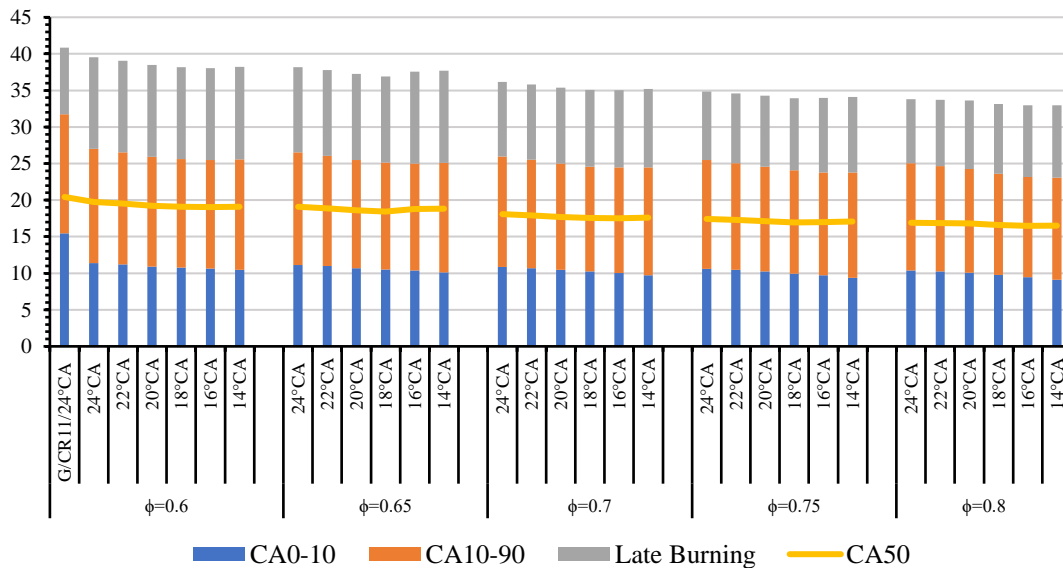
Figure 4.18.Combustion duration at various IT and ϕ at 1400rpm

However, CA10 reduces continuously by delaying IT at any ϕ and speed. There is an average 5.27% reduction/2ºCA IT retard noticed at any speed. Retarded IT results in a

higher temperature at the time of spark, which increases the flame speed and reduces sensible losses in heating the charge(Boggio et al., 2018). Hence, CA10 reduces continuously, and the effect intensifies with increasing speed. A large portion of CA10-90 falls in the expansion stroke. Initially pressure drop is less (expansion stroke), which is compensated by energy liberated due to combustion. The pressure drop rises with the extent of expansion, hence, after some certain angle an uncontrollable pressure drop deteriorates combustion. For lean mixture, low flame speed causes longer CA10-90 at retarded ignition, but for rich mixture, fast flame travelling prevents major combustion zones to fall in rapid-pressure-drop zone(Chen et al., 2019). Hence, for lean conditions ($\phi<0.7$), IT corresponding to minimum CA10-90 is more advanced than in rich conditions. There is an overall 1.23% drop per 2ºCA ignition retard in CA10-90 till minimum.
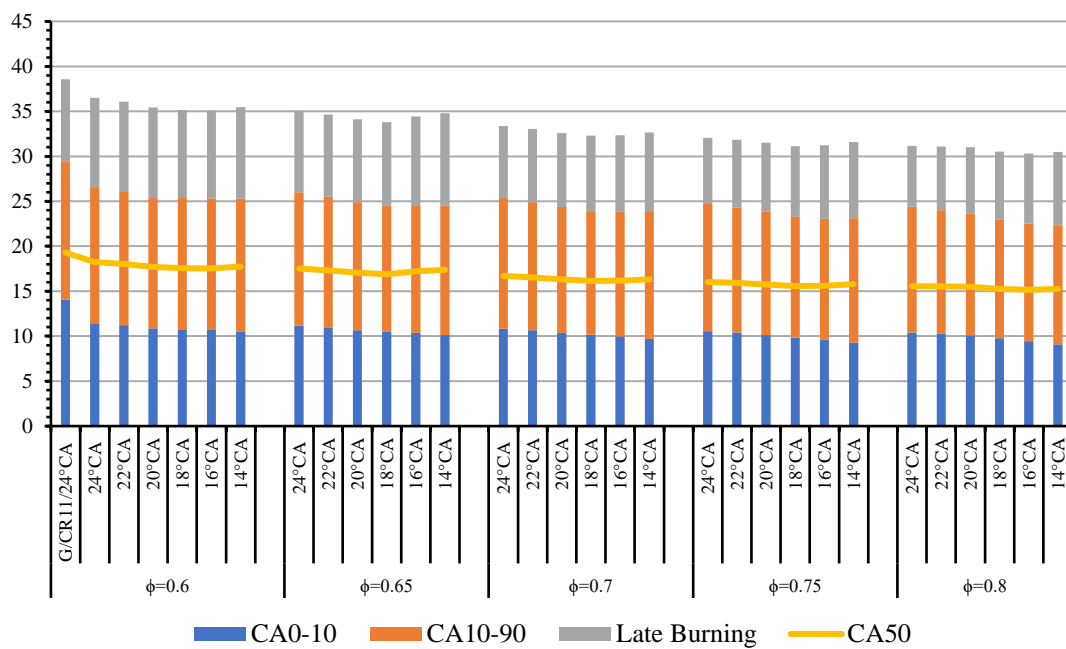
Figure 4.19.Combustion duration at various IT and ϕ at 1600rpm

CA50 follows CA10 closely; as with ignition retard, CA50 reduces continuously at any ϕ. At extremely retarded ignition (18ºCA to 16ºCA bTDC) at rich conditions, CA50 is nearly static. The CA50 represents peak combustion speed, which getting shorter signifies better combustion quality (Gong, Li, Yi, & Liu, 2020). A shorter CA50, ending before or at TDC, signifies the power utilized to overcome negative compression work,

indicating the low BTE. A significant drop in CA50 is noticed compared to gasoline, thanks to the impressive combustion qualities of hydrogen (Ji et al., 2010).
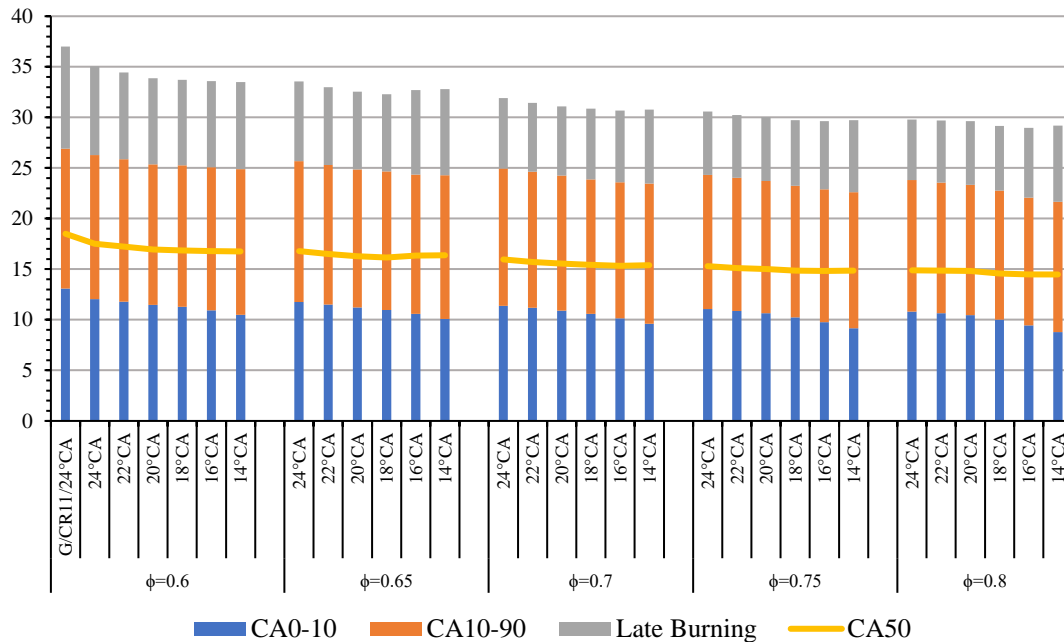
Figure 4.20.Combustion duration at various IT and ϕ at 1800rpm

4.2.4. Cylinder pressure (CP)

Figure 4.21depict instantaneous CP at 1800rpm, while Figure 4.22 represents variations in P_{max} at various speeds. P_{max} increases with an increase in ϕ; since the strength of hydrogen increases with ϕ in the mixture, the laminar flame speed increases, leading to fast combustion. Which increases the amount of energy liberated per unit volume of working fluid, increasing CP (Xu et al., 2020). The angle corresponding to the P_{max} advances too. Compared to gasoline, P_{max} is lower for most of the increase in ϕ because of low energy addition and retarded ignition. However, the gap reduces with increasing ϕ and speed; at 1800rpm, P_{max} at an increased ϕ=0.8 is 0.4% higher than gasoline. For ϕ <0.8, the energy supplied by hydrogen is lower than gasoline, hence, P_{max} is far below gasoline. On the other hand, P_{max} is increased and advanced continuously with advancing IT(Diéguez et al., 2014). P_{max} occurs very close to TDC for a much-advanced IT, leading to increase compression negative work, reflected in low BP. P_{max} reduces continuously with retarding IT at all the speeds. Since retarding ignition moves the

72

rapid combustion zone to expansion stroke, CA10-90 falls in the expansion stroke. Hence, continuous pressure drop does not allow P_{max} to increase. However, RPR before TDC rises with delayed IT due to high temperature resulted from higher extent of compression.
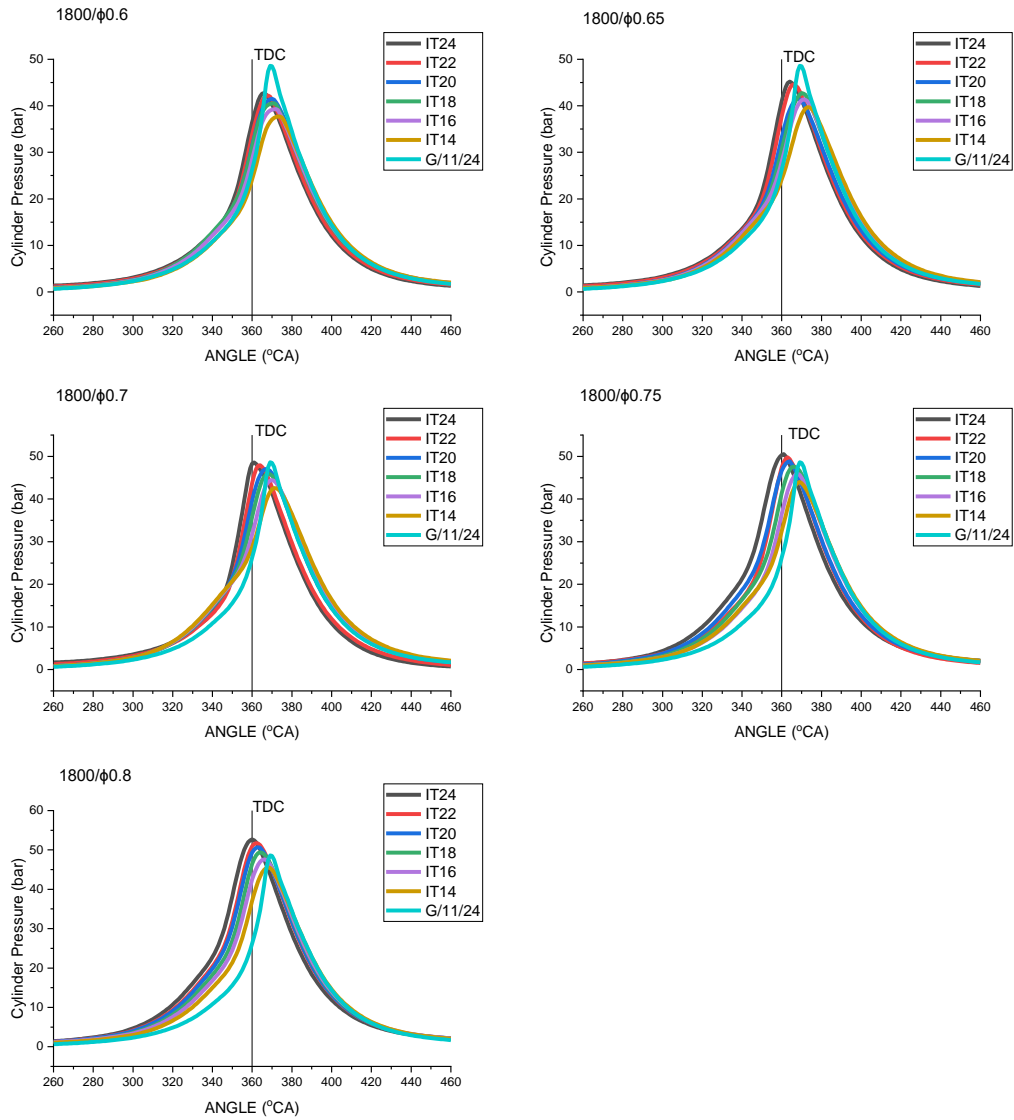
Figure 4.21.CP varying with crank angle and IT at various ϕ at 1800rpm
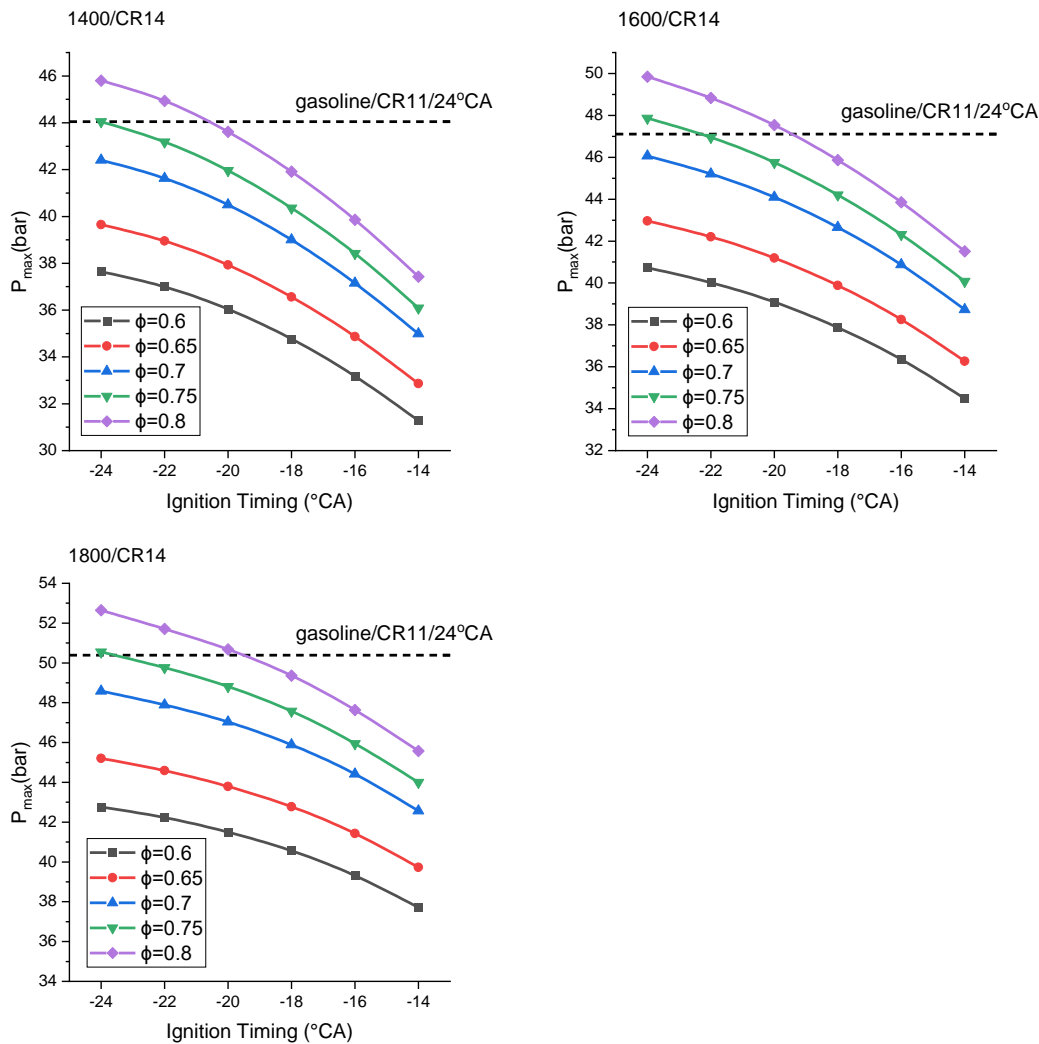
Figure 4.22.P_{max} varying with IT and ϕ at various speeds

4.2.5. Heat release rate (HRR)

HRR_{max} of hydrogen at $\phi=0.8$ is higher than gasoline due to excellent combustion qualities. The increasing hydrogen strength in the charge motivates fast combustion, resulting in higher HHR (J. Lee, Park, Bae, et al., 2019) as depicted in Figure 4.23- Figure 4.25. Simultaneously, HRR_{max} advances with ϕ, reflecting a shorter combustion period. While, advancing IT increases HRR as an early ignition of fast burning hydrogen results in large fuel burnt before TDC, increasing the cylinder temperature with the course of compression stroke. Hence, increasing flame velocity further increases HRR and peak advances too(Zhen et al., 2021).
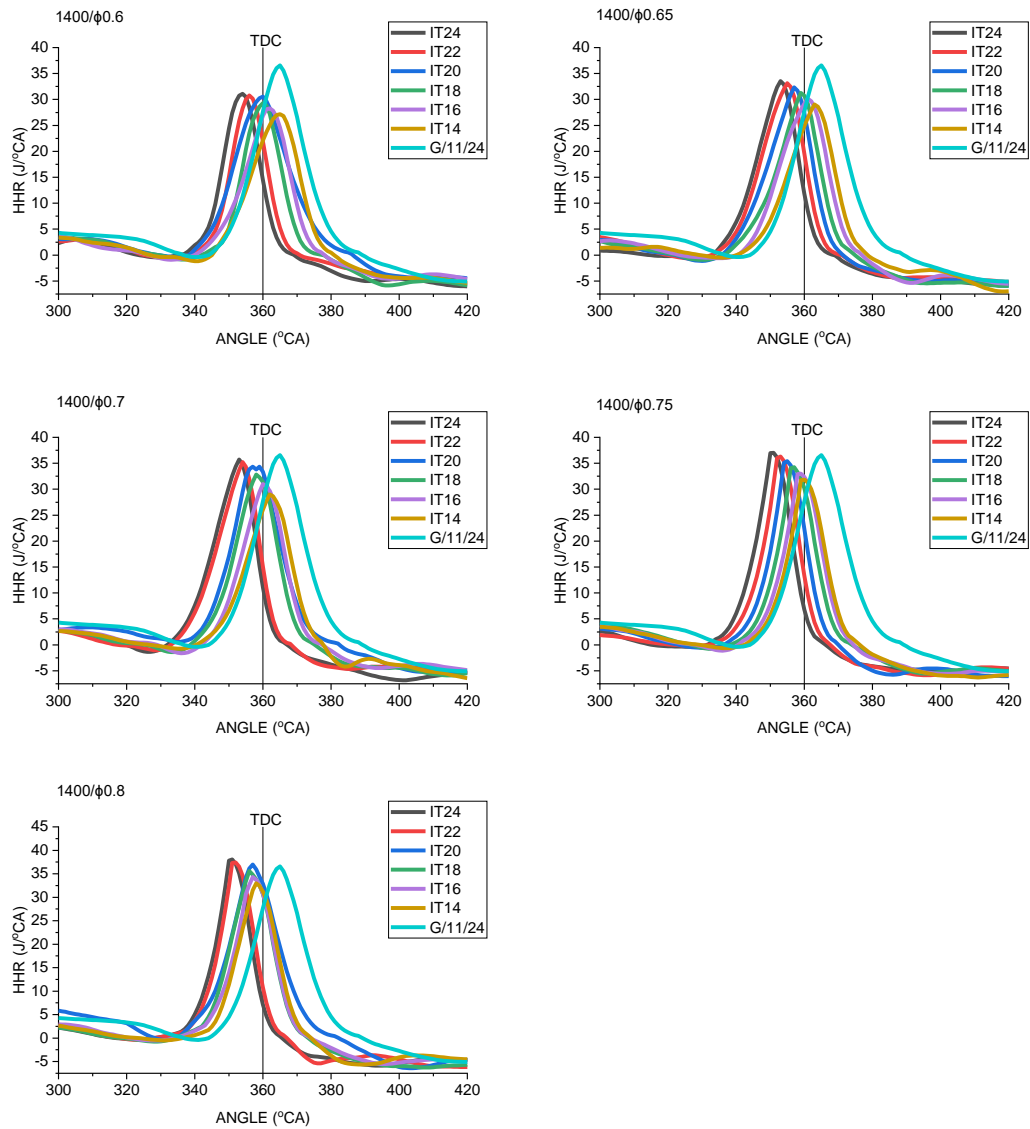
Figure 4.23.HRR varying with crank angle and IT at various ϕ at 1400rpm

However, the increment rate of HRR$_{max}$ reduces due to flame compression with advancing IT(Dhyani & Subramanian, 2018). As a result, the advancing angle of HRR$_{max}$ is less than the 2ºCA change in IT. IT retard shifts CA10-90 after TDC, hence, a sudden drop in pressure and temperature leads to reduced flame velocity, reducing HRR(Heywood, 2018). Due to combustion favouring conditions, this drop in HRR$_{max}$ decreases at higher speeds than low speeds. It can be related to the combustion duration from Figure 4.18-Figure 4.20. There is an average 5.2% increase in HRR$_{max}$ with ϕ noticed at 24ºCA bTDC and 1400rpm, which reduces to 4.9% at 14ºCA bTDC. While

at 1800rpm, it reduces to 2% to 2.7%. On the other hand, an average 2.7% reduction in $HRR_{max}/2°CA$ IT retard is noticed at 1400rpm irrespective of ϕ, which reduces to 1.87% at 1800rpm.
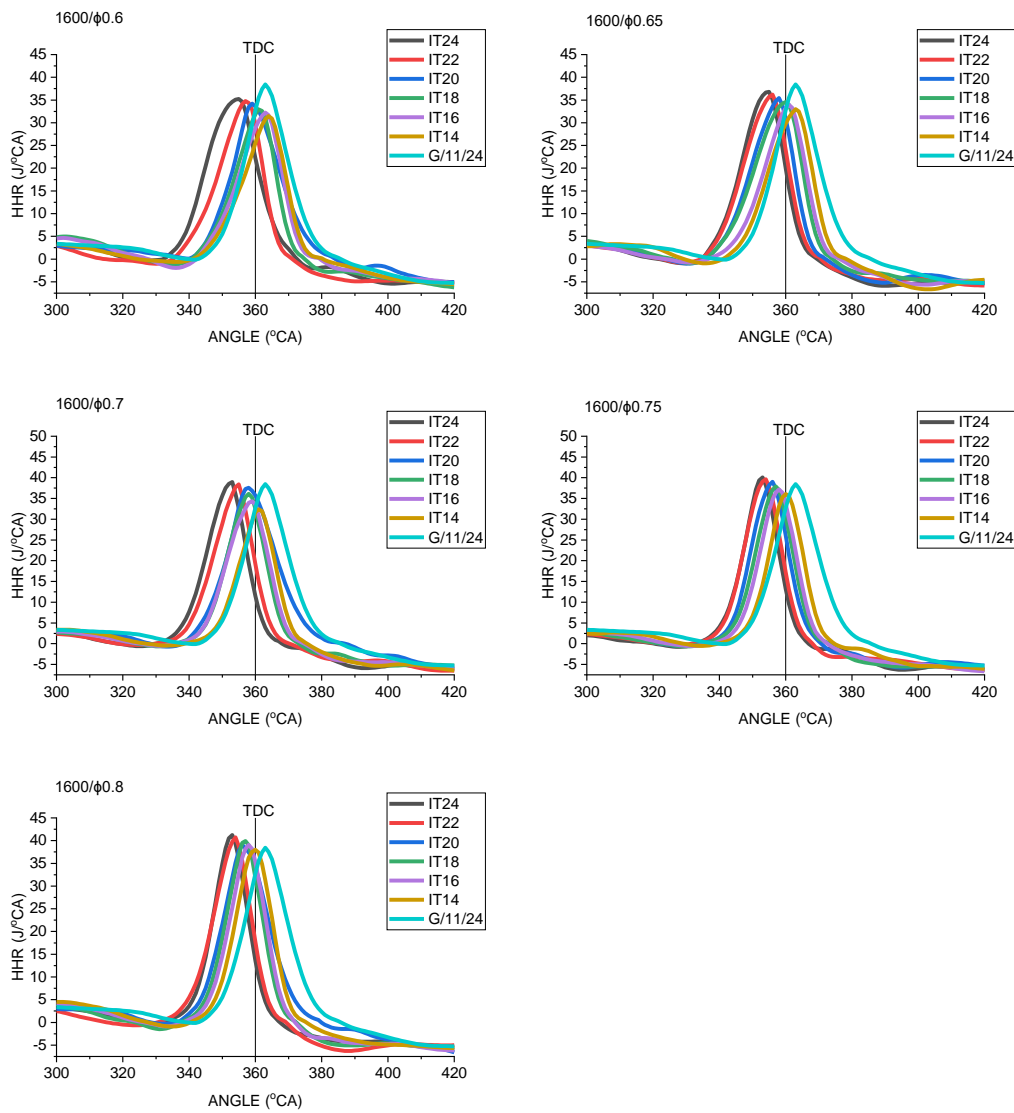
Figure 4.24.HRR varying with crank angle and IT at various ϕ at 1600rpm
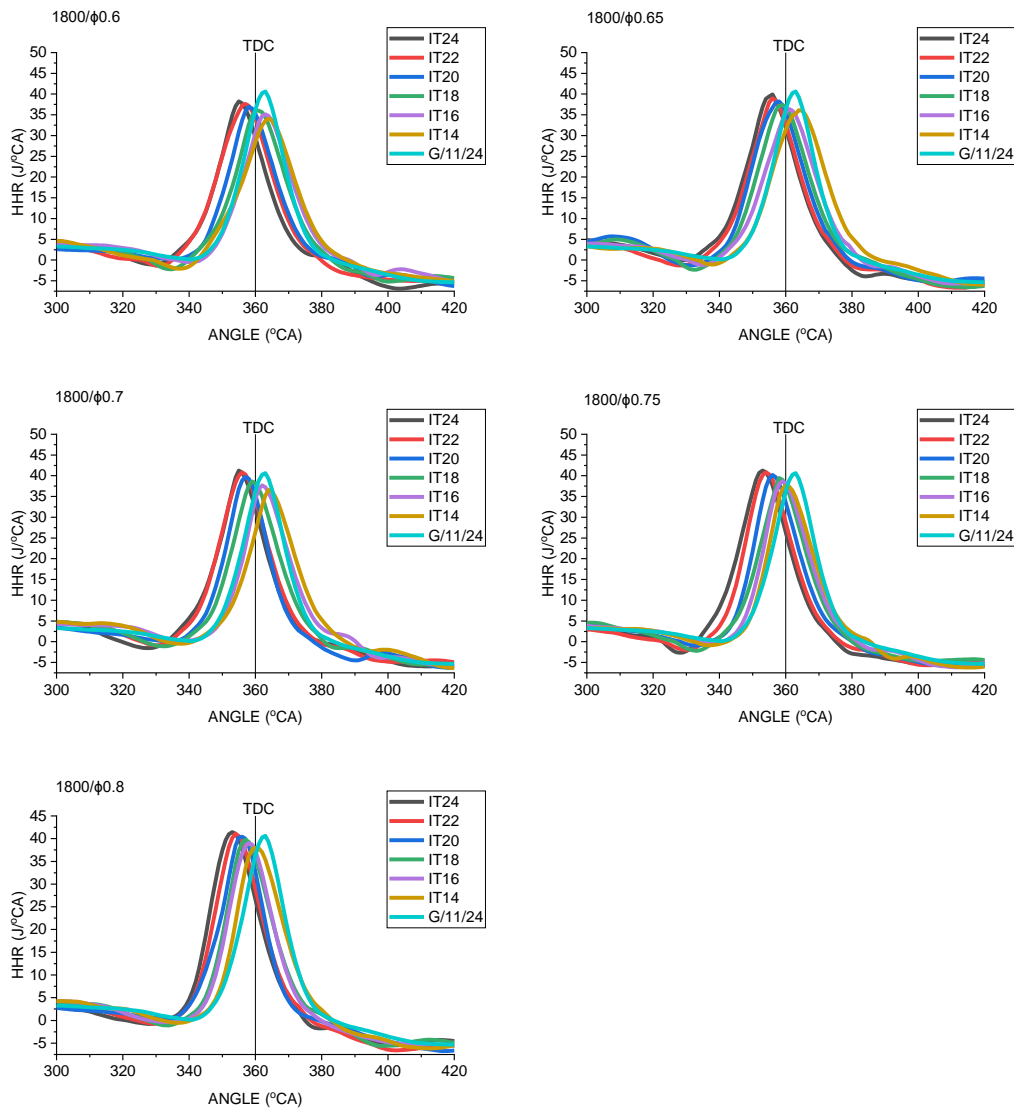
Figure 4.25.HRR varying with crank angle and IT at various φ at at 1800rpm

4.2.6. Peak cylinder temperature (T_max)

Retarding IT reduces the effects of ϕ on T_{max} which decreases continuously. It can be noticed from Figure 4.26 that the drop rate in T_{max} is almost unchanged at any speed, as at 1400rpm 3.56% increment in T_{max} with ϕ at 24ºCA bTDC reduces to 3% at 14ºCA bTDC. Though IT retard helps reduce ignition lag, it pushes P_{max} away from TDC, which means a large part of the rapid combustion zone shifts towards expansion stroke, which reduces P_{max} and T_{max} (Ji & Wang, 2010). However, with increasing speed, this effect reduces as improved combustion speed compensates for the effect of IT retard.

77

Therefore, with increasing speed, the range of IT corresponding to T_{max} higher than gasoline widens, as $\phi=0.75$ has a higher than gasoline T_{max} at 18ºCA bTDC IT. Probably, MGT (Yang et al., 2017) and cylinder wall temperature(Manigandan et al., 2020) increases with speed, reducing the effect of reducing ϕ.
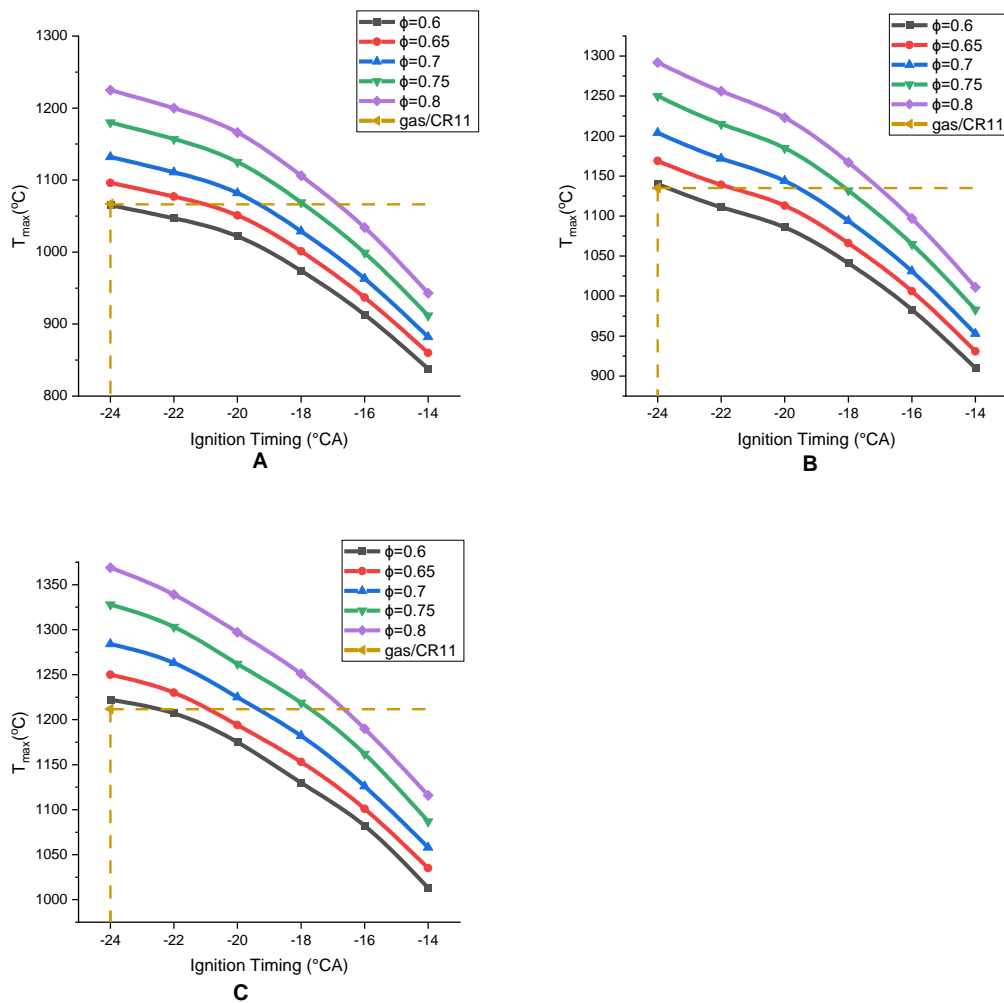
Figure 4.26.T_{max} varying with IT and ϕ (A-1400rpm, B-1600rpm, C-1800rpm)

4.2.7. Coefficient of variations in IMEP (CoV$_{imep}$)

From Figure 4.27, there is a common observation that IT retard from gasoline reduces CoV$_{imep}$ to a minimum and then increases. The IT corresponding to the minimum CoV$_{imep}$ gets retarded with increasing ϕ at any speed too as at $\phi=0.6$ it is 20ºCA bTDC at 1400rpm, which retards to 18ºCA bTDC at $\phi=0.8$ and 1800rpm. However, the drop

rate with IT retard reduces with speed, but the rate of increase after minima increases with it. Since CP and temperature are low at an early ignition, resulting in low laminar flame speed during CA10. Hence, it increases the cycle-by-cycle variations (Porpatham, Ramesh, & Nagalingam, 2007). On the other hand, a retarded ignition compels rapid combustion to fall in the expansion stroke, which reduces combustion efficiency due to rapidly dropping pressure and temperature. Therefore increasing the after-burning period, resulting in increased CoV_{imep} (Ma et al., 2008). However, due to high CR, hydrogen has lower CoV_{imep} than gasoline.
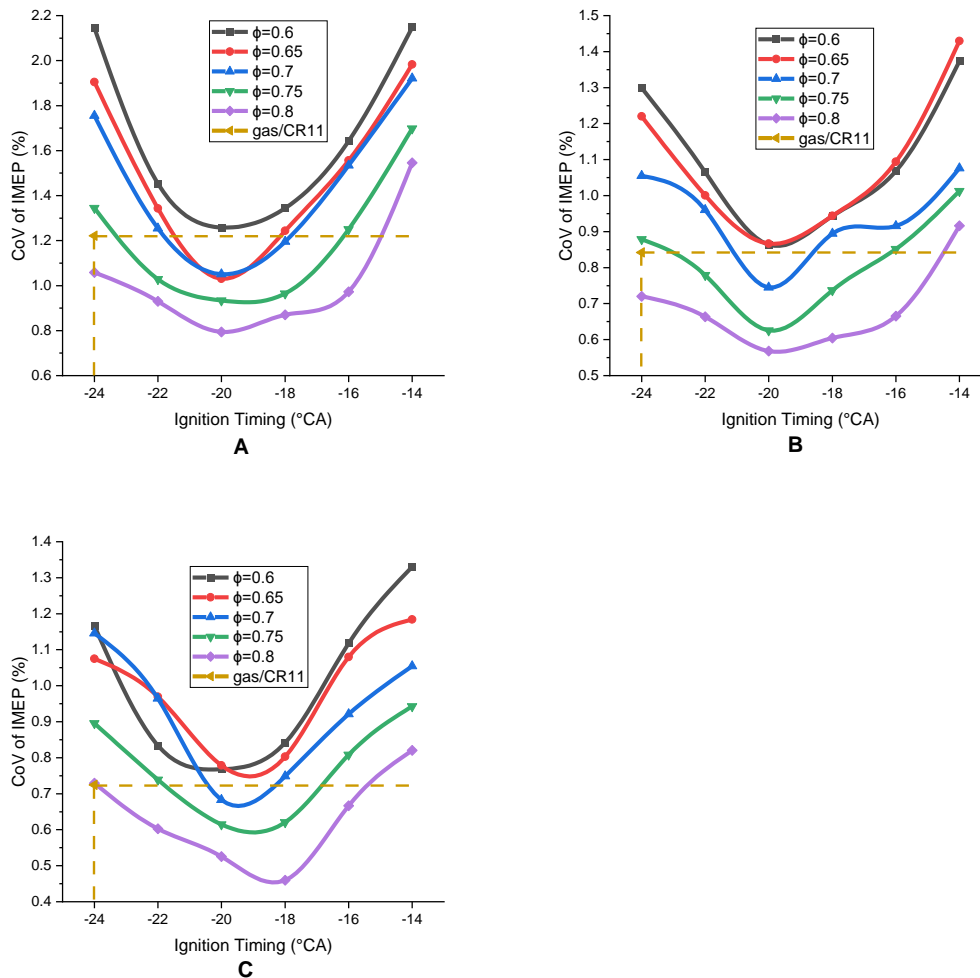
Figure 4.27.CoV$_{imep}$ varies with IT and ϕ (A-1400rpm, B-1600rpm, C-1800rpm)

4.2.8. Exhaust gas temperature (EGT)
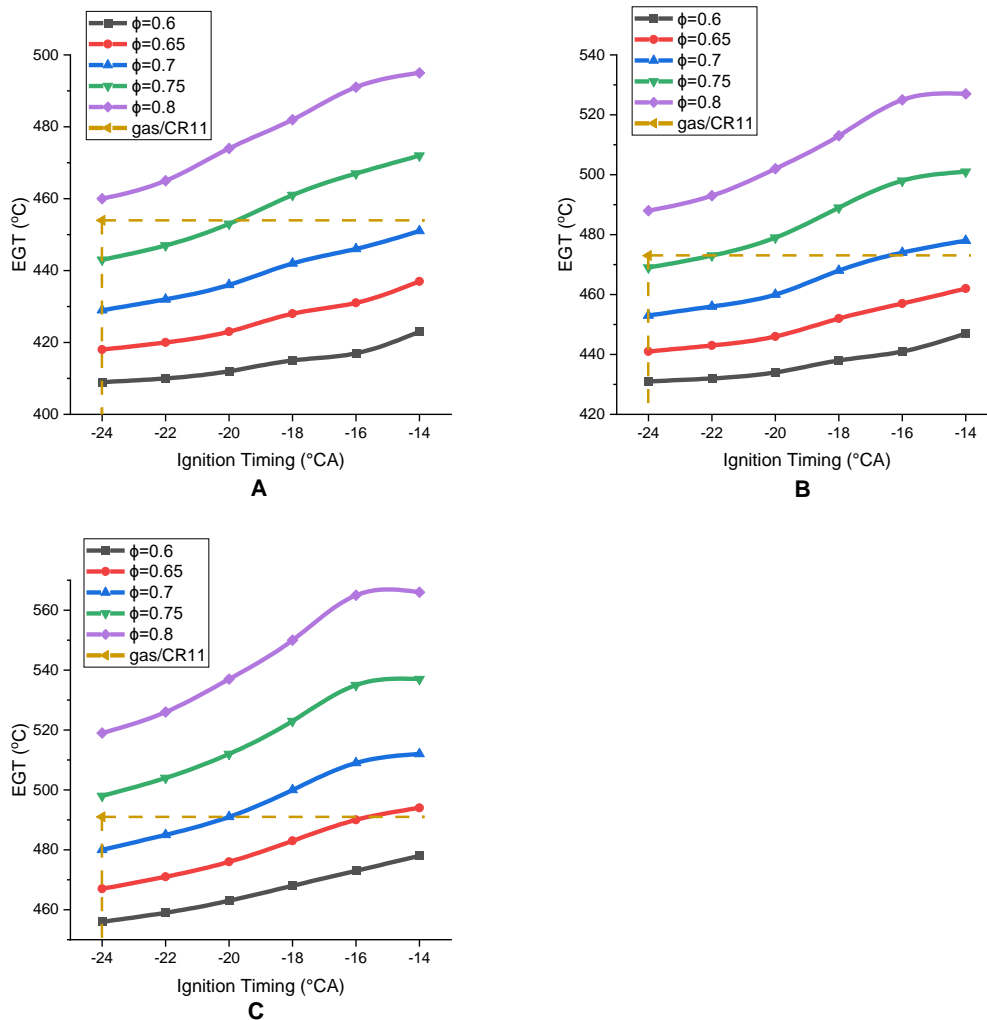
Figure 4.28.EGT varies with IT and φ (A-1400rpm, B-1600rpm, C-1800rpm)

The delayed ignition results in an extended after-burning period due reducing cylinder temperature and the flame speed in expansion stroke. Hence, high EGT is observed, as shown in Figure 4.28 (Lim, Lee, Park, Choi, & Kim, 2014). Figure 4.18-Figure 4.20 explains the combustion duration; the effect of IT can be noticed in the after-burning period. Initially, a small increment in the after-burning period leads to a gradually increased EGT. However, delaying IT after 18⁰CA bTDC elongates the combustion period, maintaining a relatively higher temperature at the end of the expansion stroke, leading to high EGT. There is an average 0.68% increase at 22⁰CA bTDC noticed,

which increased to 1.16% at 14°CA bTDC. The increasing ϕ increases the amount of fuel, which increases the effect of IT on EGT (Gao, Tian, Ma, Xing, & Huang, 2021). Also, the increased amount of fuel results in a slightly long after burning period despite the improved laminar flame speed, increasing the EGT, which gets severe with retarding IT. As, 2.98% increase/0.5 change in ϕ at 24°CA bTDC increases to 4.1% at 14°CA bTDC. However, with increasing speed, there is a slight drop in after burning period, but insufficient time for engine cooling increases MGT, leading to a further boost in EGT.

4.2.9. NOx emissions
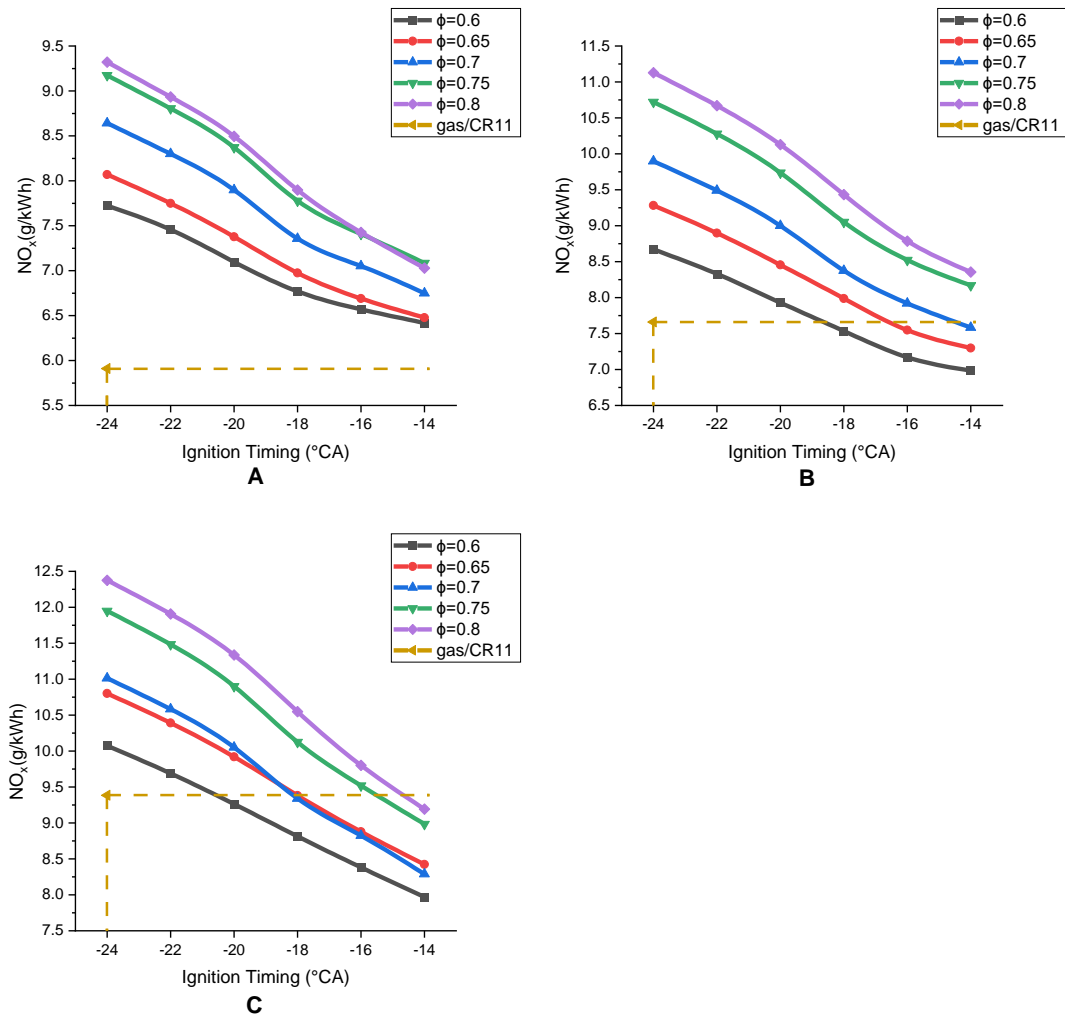
Figure 4.29.NOx varying with IT and ϕ (A-1400rpm, B-1600rpm, C-1800rpm)

IT retard reduces NO_x emissions due to a reduction in T_{max}, as depicted in Figure 4.29. The extent of the drop in NO_x emissions due to IT retard depends on ϕ. The drop rate is higher in the case of higher ϕ, where T_{max} drops significantly. There is 4.4% drop/2^oCA ignition retard is observed at $\phi=0.6$ at 1400rpm which increases to 6.4% at $\phi=0.8$ at the same speed. With the increasing speed the rate of drop increases to 5.4%/2^oCA ignition retard at $\phi=0.6$ and 6.7%/2^oCA ignition retard at $\phi=0.8$ at 1800rpm. The increasing ϕ at advanced IT faces an increasing rate of NO_x emissions, as 1.2% increase at $\phi=0.6$ increases to 12% at $\phi=0.8$ at 24^oCA bTDC and 1400rpm. Since the laminar flame velocity and energy addition increase with ϕ, an advanced IT burns a larger mass before TDC, leading to an increase in T_{max}. However, at a retarded IT, major combustion zone shifts in the expansion stroke, which witnesses rapid pressure drop, and hence, T_{max} is reduced, which reduces NO_x formation (Binjuwair & Alkudsi, 2016; Chen et al., 2019). Similarly, despite the increasing speed, which increases the NO_x emissions, the drop rate due to ignition retard increases. Which results in lower NO_x emissions than gasoline.

4.2.10. Conclusion of section 4.2

The experimental results of phase 2 of stage 1 are discussed above in brief, and the outcomes are concluded as follows;

- IT corresponding to optimum BTE/BP is observed retarding with increasing ϕ and speed.
- The CA10 reduces continuously with ignition retard due to higher temperature and pressure at the ignition time, while CA10-90 and CA100 first reduce and then increase due to the pushing of the rapid burning zone into expansion stroke. IT corresponding to optimum CA10-90 and CA100 retards with increasing ϕ.
- The CP and HRR are observed to decrease continuously with ignition retard; however, the increment rate in CP and HRR increases. The P_{max} and HRR are retarded due to the shifting of the rapid combustion zone away from TDC.
- The CoV_{IMEP} is observed to reduce with delayed ignition to a minimum and then increase. The reduction rate is low, while the increase rate increases with the extent of retarding the ignition. The increasing ϕ reduces the effect of IT on CoV_{IMEP}.

- The T_{max} reduces continuously with ignition retard, because of the elongated combustion in expansion stroke at rapidly reducing pressure.
- The EGT continuously increases with ignition retard, a major cause of which is the extended late burning period. The impact of IT intensifies with increasing ϕ.
- The NO_x emissions reduce with retarding the ignition; due to reduced T_{max}, the effect intensifies with increasing ϕ due to ample fuel volume.

4.3. Effect of EGR and MAP boost

The experimental results from stage 1 provide an optimal CR, ϕ, and IT condition concerning better performance at moderate NO_x emissions. CR14 at ϕ=0.8 is observed to have the best performance, while at IT of 16ºCA bTDC, it has slightly controlled NO_x without power deflection. Hence, in stage 2, experiments are conducted to control NO_x by EGR by not allowing a significant drop in η_{th}, for which MAP boosting is tested. The results are compared parallelly for EGR and MAP boosting, and the illustration of the results with probable cause is provided below;

4.3.1. Brake power (BP)

BP largely depends on the total energy supplied and combustion speed. The fuel requirement increases with boosting MAP due to improved engine breathing, as shown in Figure 4.32. Therefore, fuel supply is increased, leading to an increase in BP, as fromFigure 4.30. However, implanting EGR reduces available oxygen, increasing the ϕ (Figure 4.33). At low EGR, ϕ increases without significant scarcity of air, which increases combustion speed; hence, BP increases. An average 1.7% increment noticed at 5% EGR on all the speed at N/A condition and 1.97% at 110kPa. While EGR is increased further, large-scale dilution results in scarcity of oxygen and increasing heterogeneity. Therefore, BP drops rapidly. The reduction rate worsens with the extent of EGR, which intensifies further with the rate of boosting MAP. At low speed of 1400rpm, the BP drop rate due to EGR is very low as 1.7% averaged over all MAP. Also, BP improves vastly by MAP boost at low speed. EGR impacts BP to drop faster with speed while boosting MAP improves BP slightly to reduce EGR impact.
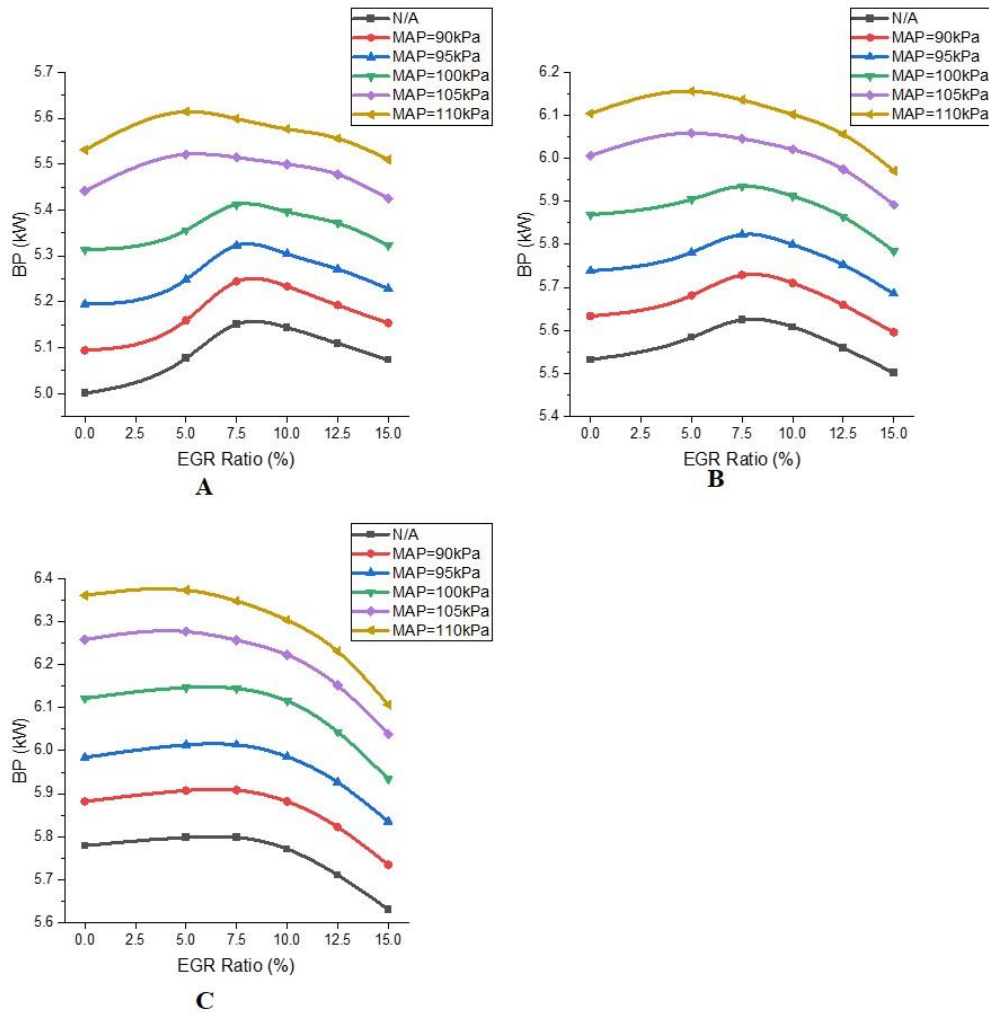
Figure 4.30.BP varies with EGR and MAP (A-1400rpm, B-1600rpm, C-1800rpm)

4.3.2. Brake thermal efficiency (BTE)

While super-diffusive hydrogen fuses into the air, some zone would result in a rich-mixture zone, and some zone would have lean; this increases with increasing EGR rate. Therefore, at high EGR rates, despite reducing λ, BTE drops rapidly(Kim et al., 2018). From Figure 4.31 initially CP increases at ignition when MAP is boosted, leading to better conversion efficiency shifting from 28.9% of N/A to 29.75% of 110kPa at 1800rpm. However, BTE increment with increasing MAP reduces after implementing EGR. At the initial EGR of 5%, the stratification is overtaken by increased λ, which increases the combustion speed, improving BTE. However, the increasing EGR rates increases heterogeneity and available oxygen; hence, BTE drops rapidly. It reduces the effects of MAP boosting. BTE, which was increased to 29.75% from 28.9% for MAP

110kPa from N/A at 0% EGR, is changed to 28.58% from 28.16% for MAP100kPa from N/A at 15% EGR. It is almost static at 28.58% for MAP boosted further.
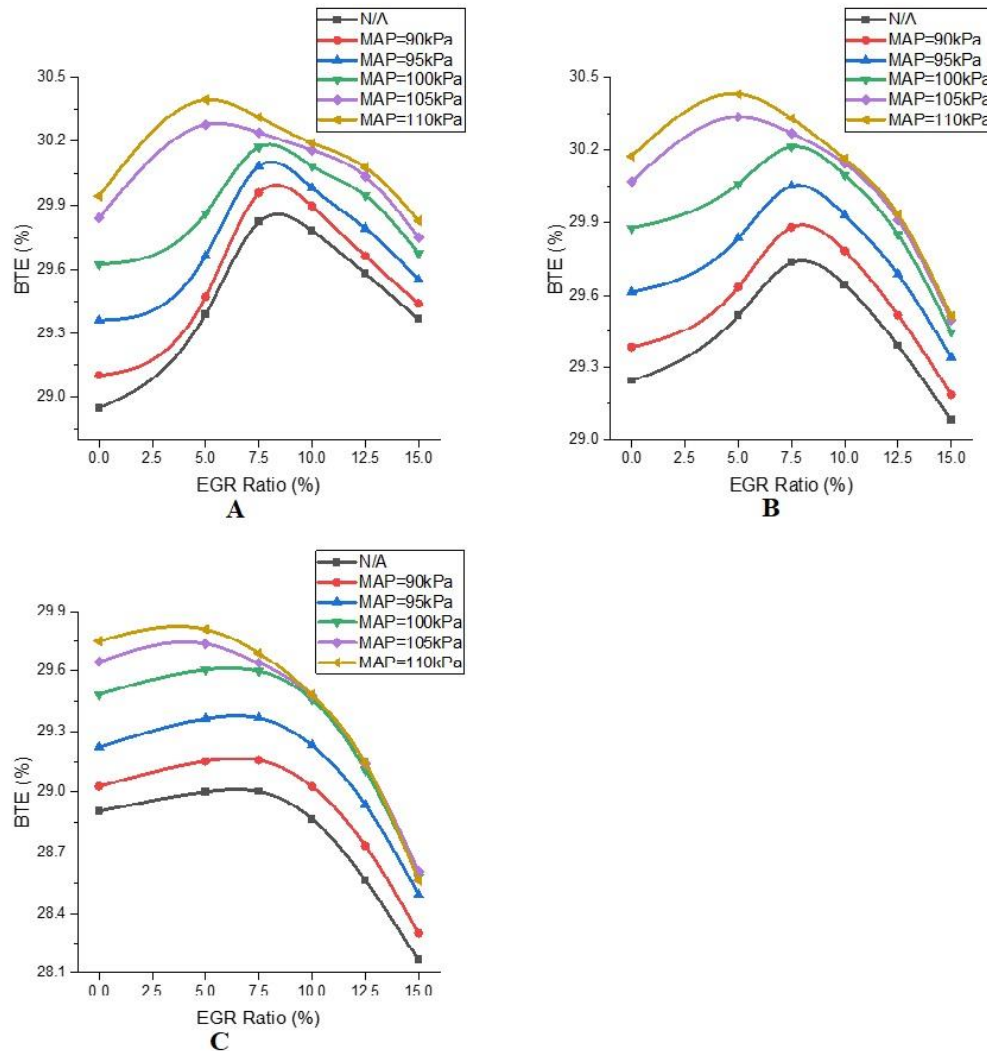
Figure 4.31.BTE varies with EGR and MAP (A-1400rpm, B-1600rpm, C-1800rpm)

4.3.3. Volumetric efficiency (η_{vol}) and Equivalence Ratio (ϕ)

Figure 4.32 depicts η_{vol}. At a N/A condition, when EGR is implemented, η_{vol} drops rapidly due to replacing low-pressure cold intake air with high pressure recirculates. The drop rate grows enormously with the rate of EGR because the two-way expansion of EGR. However, boosting MAP reduces the extent of EGR expansion towards the intake line; hence, η_{vol} improves. It increases the density of cold air too, compensating for the overheating due to EGR, resulting in increased η_{vol}. A nearly 12.6% improvement was noticed for 1800rpm at 0% EGR, which increased to 23.5% at 15%

EGR by boosting to 110 kPa. Though η_{vol} suffers little influence of speed at N/A condition, there is a small impact of speed at boosted MAP.
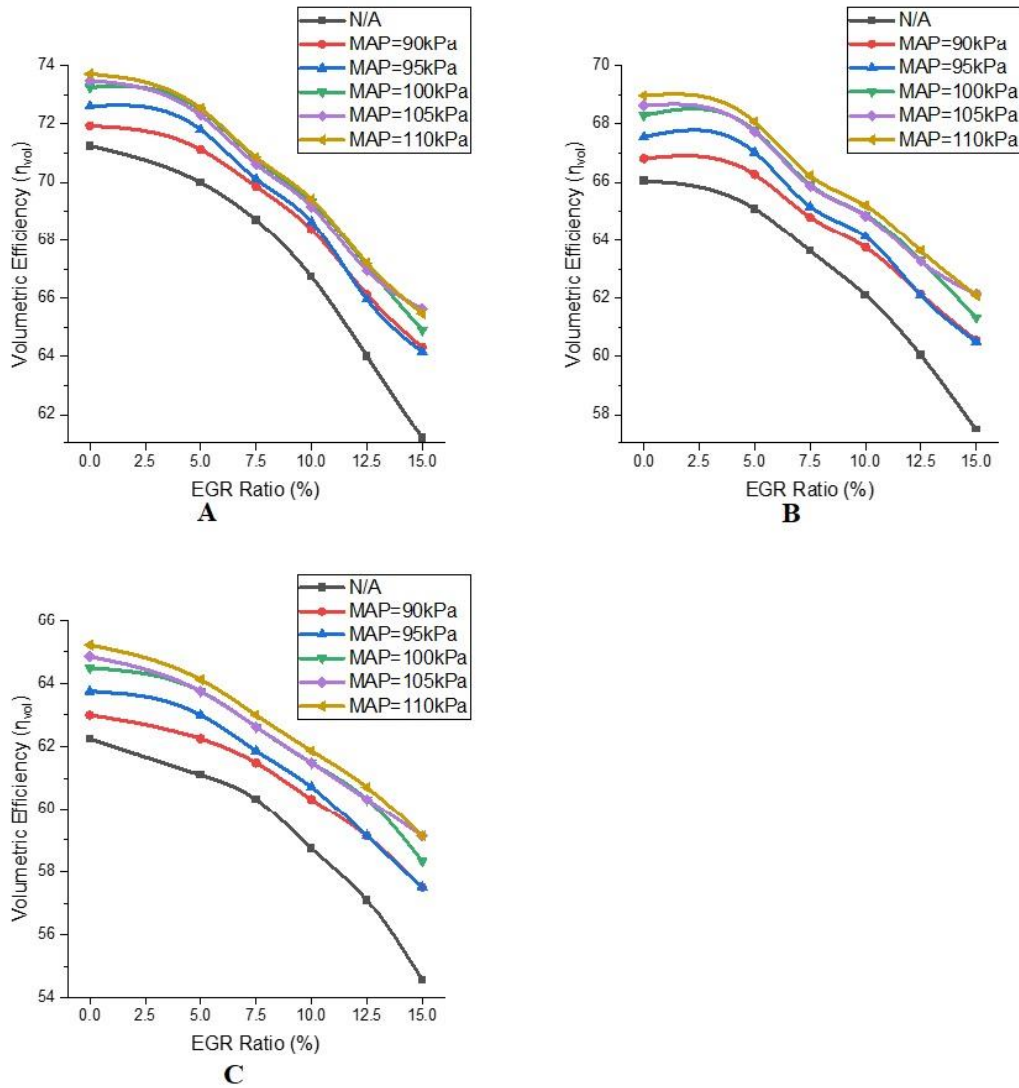
Figure 4.32.η_{vol} varies with EGR and MAP (A-1400rpm, B-1600rpm, C-1800rpm)

The consequences of η_{vol} are directly reflected in ϕ. Since ϕ is maintained at 0.8 at 0% EGR only, an increment in MAP requires more fuel to maintain it. However, with increasing EGR, η_{vol} reduces, leading to an increase ϕ as the fuel supply is fixed. As it is noticed in Figure 4.33, boosting MAP reduced the impact of EGR on η_{vol}, and the impacts on ϕ are similar. Figure 4.33 shows an increased ϕ with EGR; however, increment rate reduces with MAP; hence, even at 15% EGR, there is a significant drop in ϕ at 110kPa from N/A. On the other hand, the impact of speed is insignificant on ϕ.
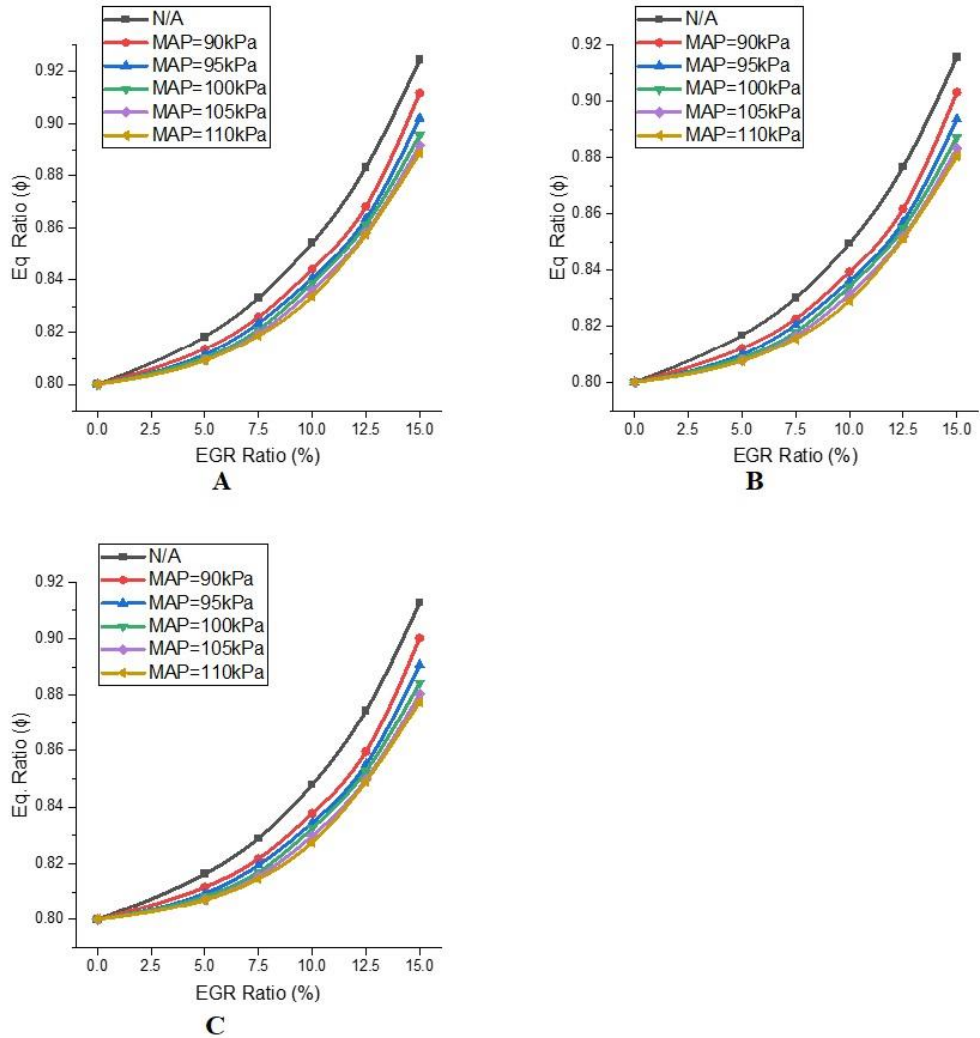
Figure 4.33.φ varies with EGR and MAP (A-1400rpm, B-1600rpm, C-1800rpm)

4.3.4. Combustion duration

All three sections of combustion duration are shown in Figure 4.34-Figure 4.36. The EGR reduces the combustion duration (CA10, CA10-90, and Late burning) at low rates. Probably, since at low EGR rates, the recirculates with high pressure and temperature increase the mixture temperature at the time of ignition, which helps in achieving fast combustion. In addition, φ also increases, leading to a relatively rich mixture. However, with the increasing EGR, oxygen reduces rapidly, and the increased mass of recirculates increases stratification, resulting in local zones of rich and lean mixtures. Hence, combustion duration increases.
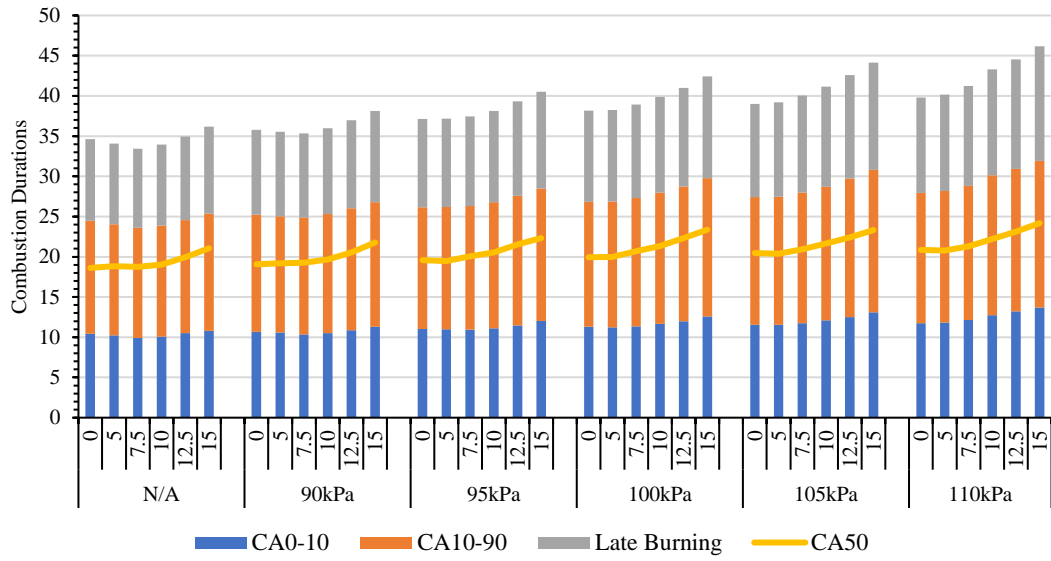
Figure 4.34.Combustion duration varying with EGR and MAP at 1400rpm
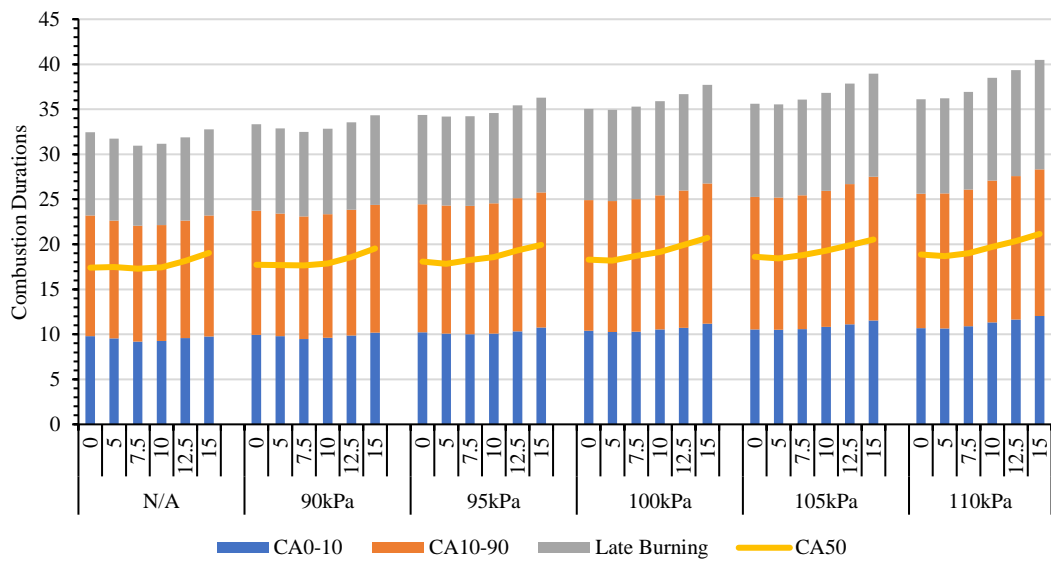
Figure 4.35.Combustion duration varies with EGR and MAP at 1600rpm
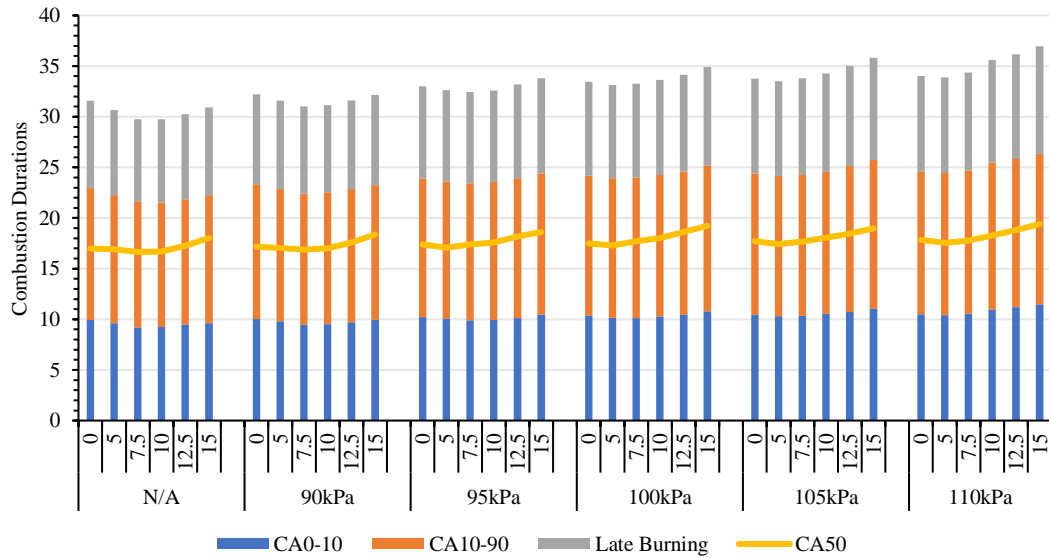
Figure 4.36.Combustion duration varying with EGR and MAP at 1800rpm

On the other hand, CA100 is observed to increase gradually with the extent of intake boosting. Since at boosted intake, engine breathing improves, allowing a larger mass of cold air, which elongates CA10(Gürbüz & Akçay, 2021). A high amount of fuel required to maintain ϕ compels for a longer time for CA10-90 and late burning. A similar trend is noticed in combustion durations at all the speeds; however, increased speed results in higher MGT, which increases combustion speed, leading to shorter combustion durations.

4.3.5. Cylinder pressure (CP)

A slight deflection is noticed for a longer length of compression stroke due to EGR; hence, curves are plotted for a shorter range, 310ºCA-410ºCA instead of 260ºCA-460ºCA. MAP boosting is known to increase the amount of intake; hence a large fuel mass is also supplied; therefore, despite elongated combustion, HRR increases. In addition, a higher pressure and temperature are obtained at the end of suction; hence, RPR is increased during compression, leading to a large CP at the time of ignition. Hence, a higher burning rate of larger mass is achieved. Therefore, P_{max} increases but retards. A 9.43% increment in P_{max} was noticed at 6ºCA retarded position at 10% EGR, from N/A to 110kPa MAP at 1800rpm. From Figure 4.37, CP observes to increase continuously with EGR at ignition due to the large mass of high pressure recirculates,

increasing initial pressure. At low EGR largely available oxygen helps combustion by reducing sensible heat loss to cold air, increasing RPR, larger P_{max} is observed at an advanced angle (Figure 4.38). At high EGR rates, though CP and MGT are high at ignition, the amount of recirculates is also increased, creating difficulties for combustion; therefore, the rate of CP rise reduces. At 1800rpm and 110kPa, P_{max} is observed to drop from 4.9×10^3 kPa to 4.483×10^3 kPa from 5% EGR to 15% EGR, and the peak retards by 5ºCA.
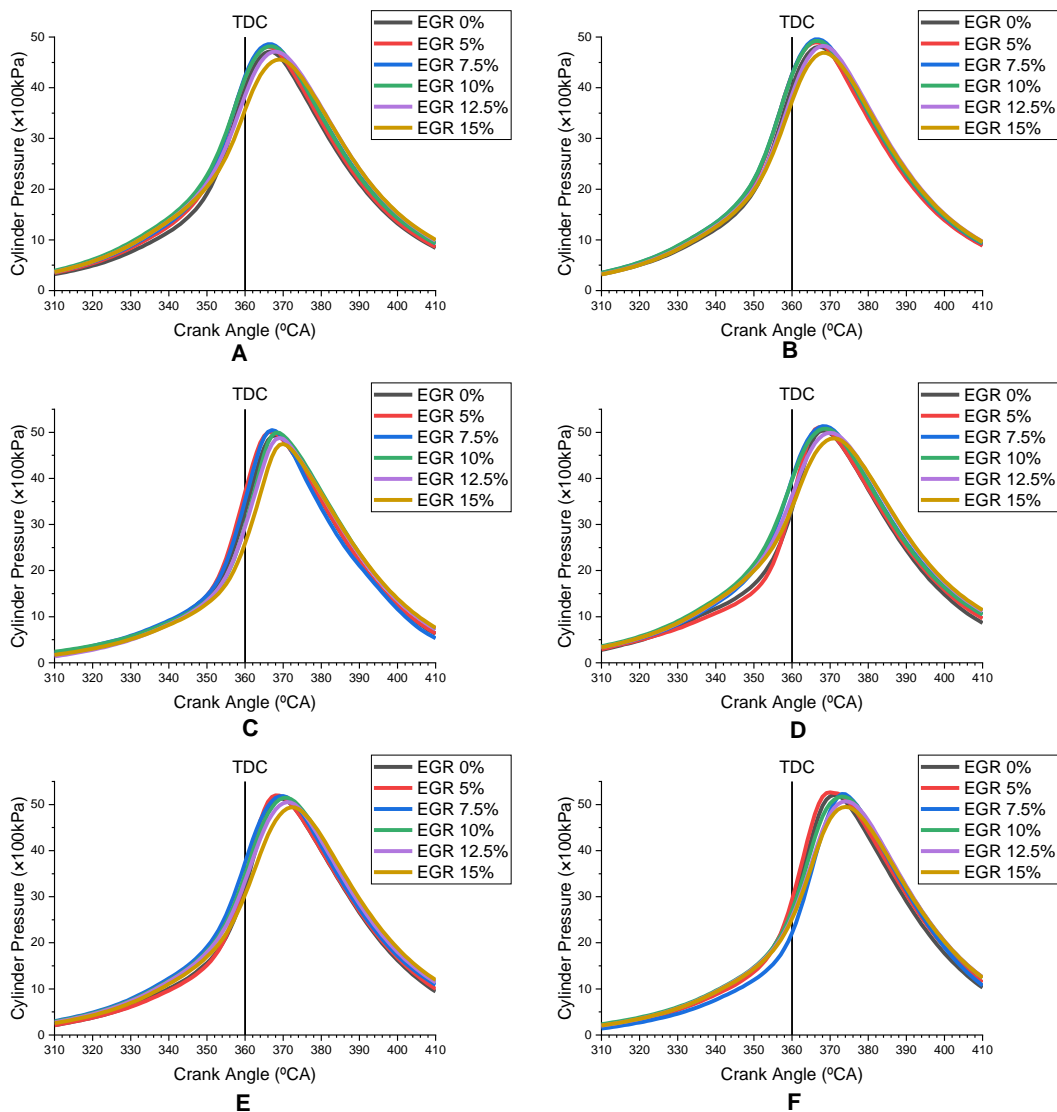
Figure 4.37.CP varying with crank angle and EGR at 1800rpm (A-N/A, B-90kPa, C-95kPa, D-100kPa, E-105kPa, F-110kPa)
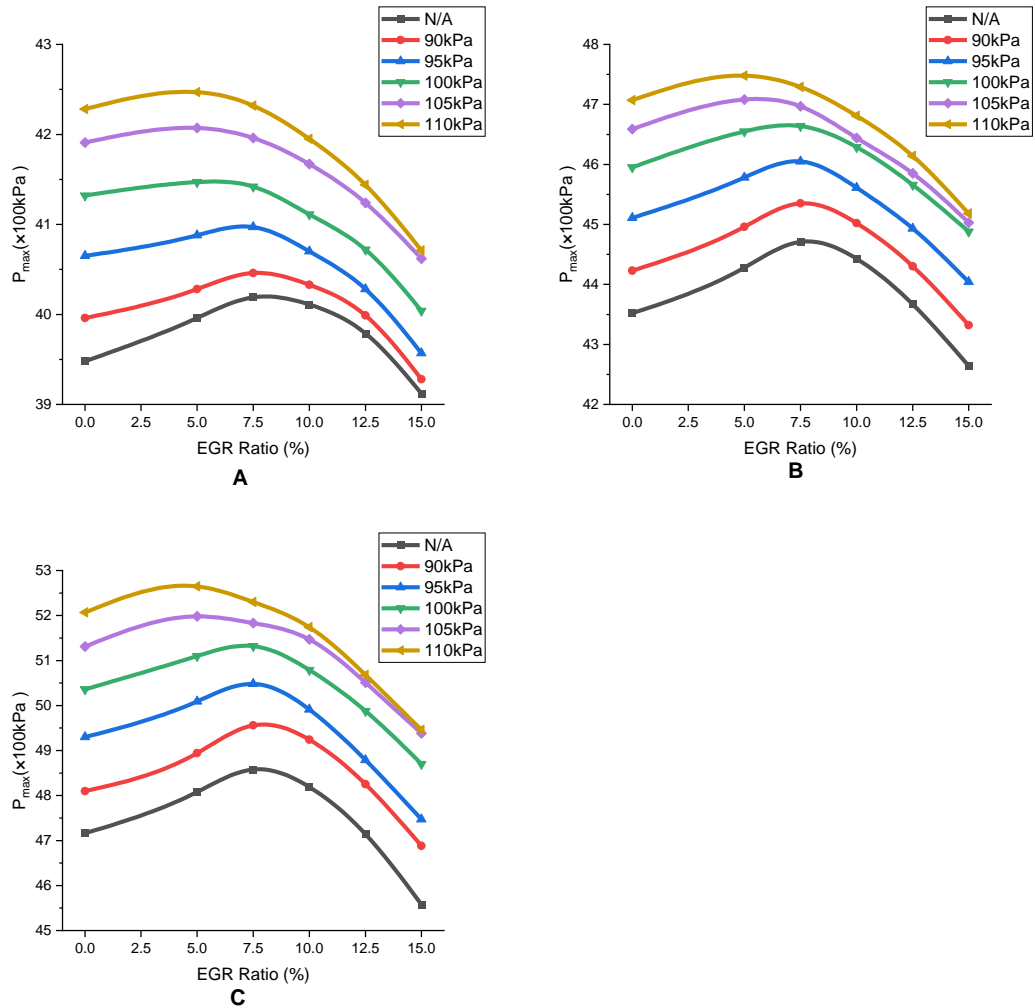
Figure 4.38.P_{max} varies with EGR and MAP (A-1400rpm, B-1600rpm, C-1800rpm)

4.3.6. Heat release rate (HRR)

The HRR curves are plotted for a shorter range of crank angles because combustion is the only cause behind it. Hence, a short period before ignition and post-combustion is considered as 320ºCA to 420ºCA. FromFigure 4.39Figure 4.41; as the EGR is implemented, HRR starts increasing initially due to increased CP at the time of ignition. HRR_{max} also tends to move near TDC because of a shorter combustion duration. However, the latter half of the curve shows a rapid drop in HRR since a larger mass is

already burnt, and a small amount of fuel at primarily occupied burnt gases faces slight difficulty in combustion. On the other hand, further increasing EGR increases the amount of recirculates, which reduces oxygen reach of fuel, and oxygen quantity in the mixture; hence, combustion elongates, which is further facing heat loss to the cylinder wall due to long combustion duration, which further reduces HRR and retards the peak. With the increase in engine speed, the η_{vol} drops, which allows improper engine breathing; hence, further implementation of EGR intensively hits the flame propagation. Therefore, fuel-burning slows down, and HRR reduces.
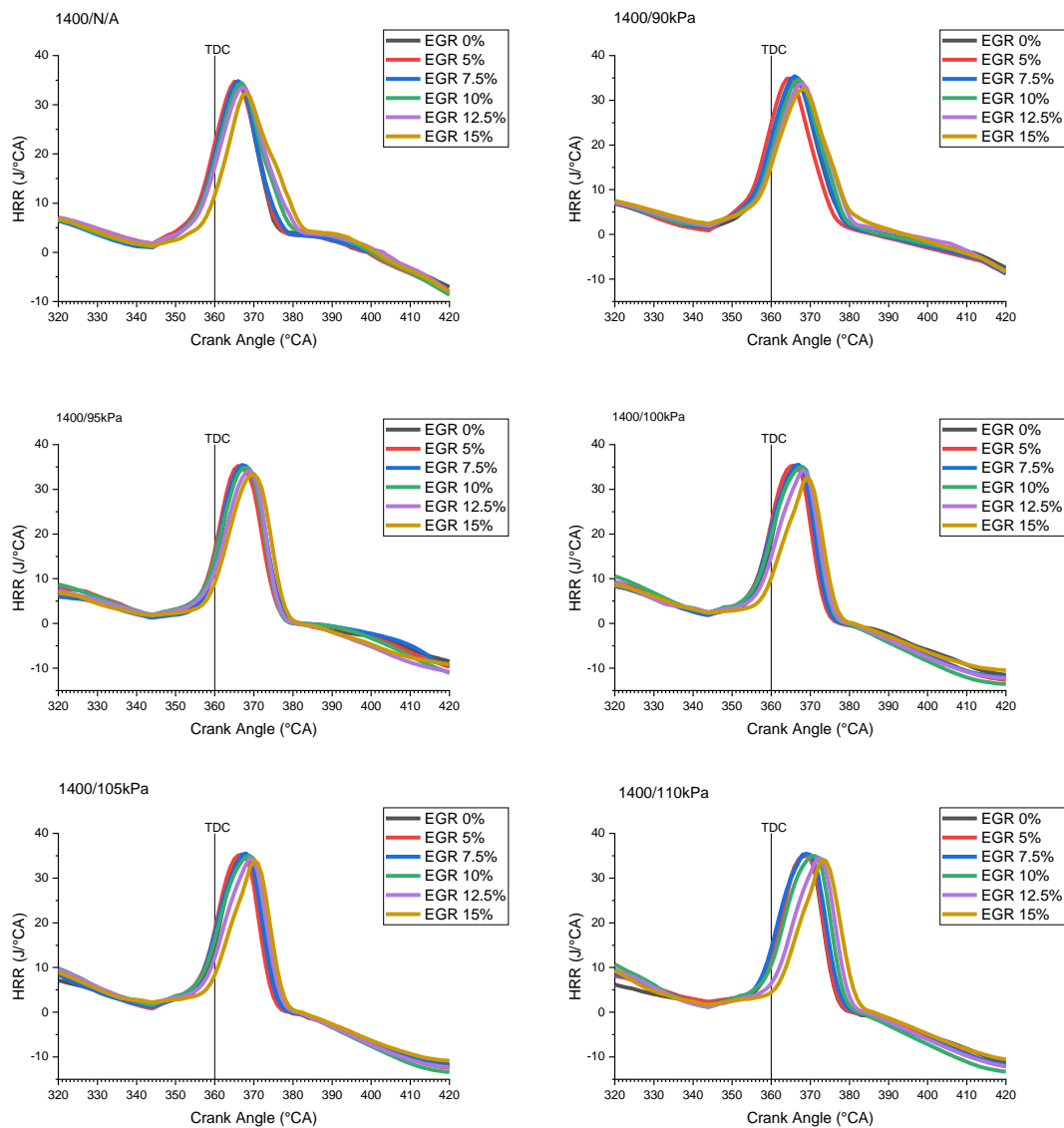
Figure 4.39.HRR varying with crank angle and EGR at various MAP at 1400rpm
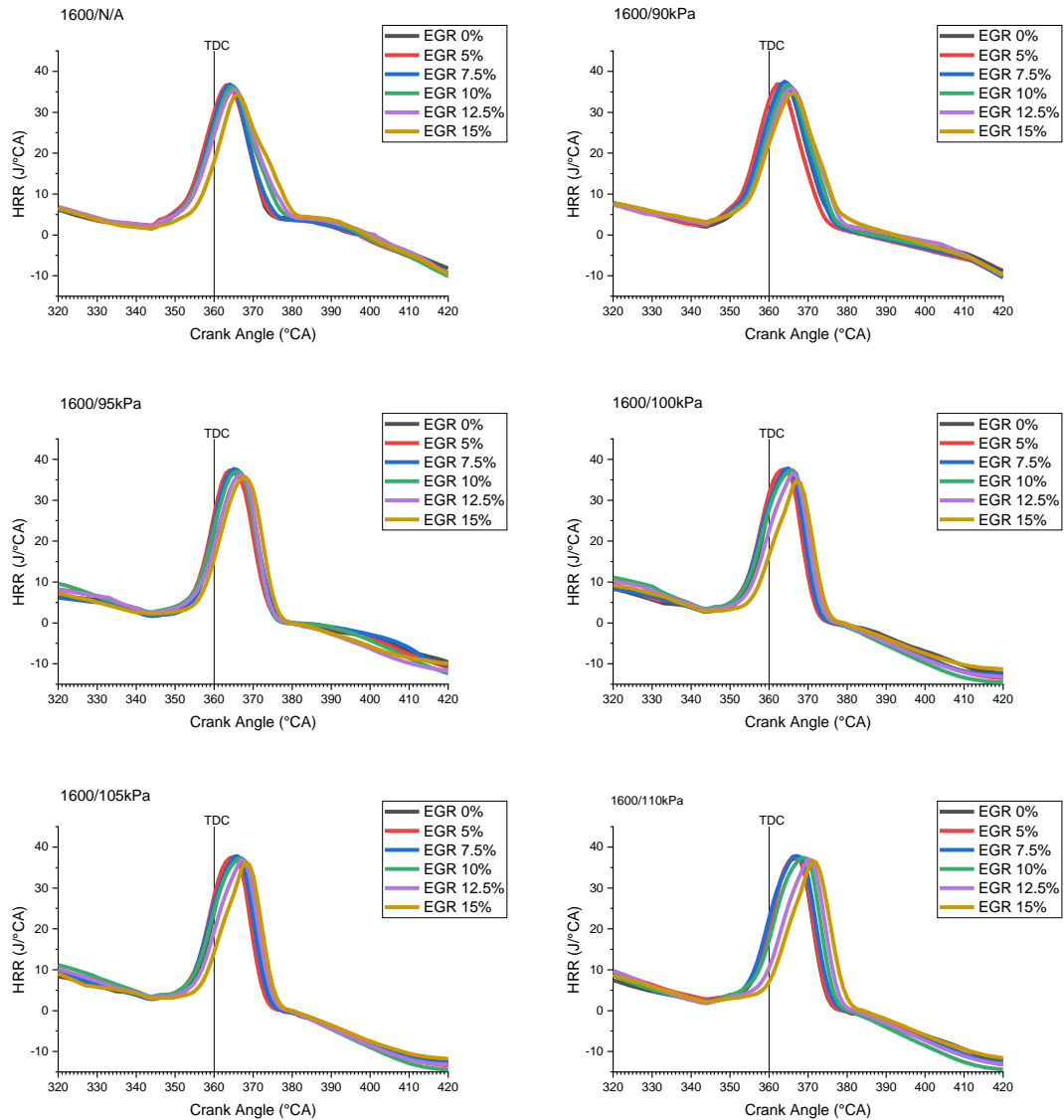
Figure 4.40.HRR varying with crank angle and EGR at various MAP at 1600rpm

When the MAP is boosted, it increases η_{vol}. Hence, a large amount of cold air enters, absorbing initial combustion chamber heat; combustion slows down, leading to extended combustion duration. Hence, peak HRR retards. In addition, a larger mass of fuel is supplied to maintain ϕ; therefore, despite long CA10, a large amount of fuel/ºCA burns, leading to increase HRR. This increases cylinder temperature near TDC, which helps fast-burning after TDC, further increasing the HRR and higher peak HRR is achieved.

93
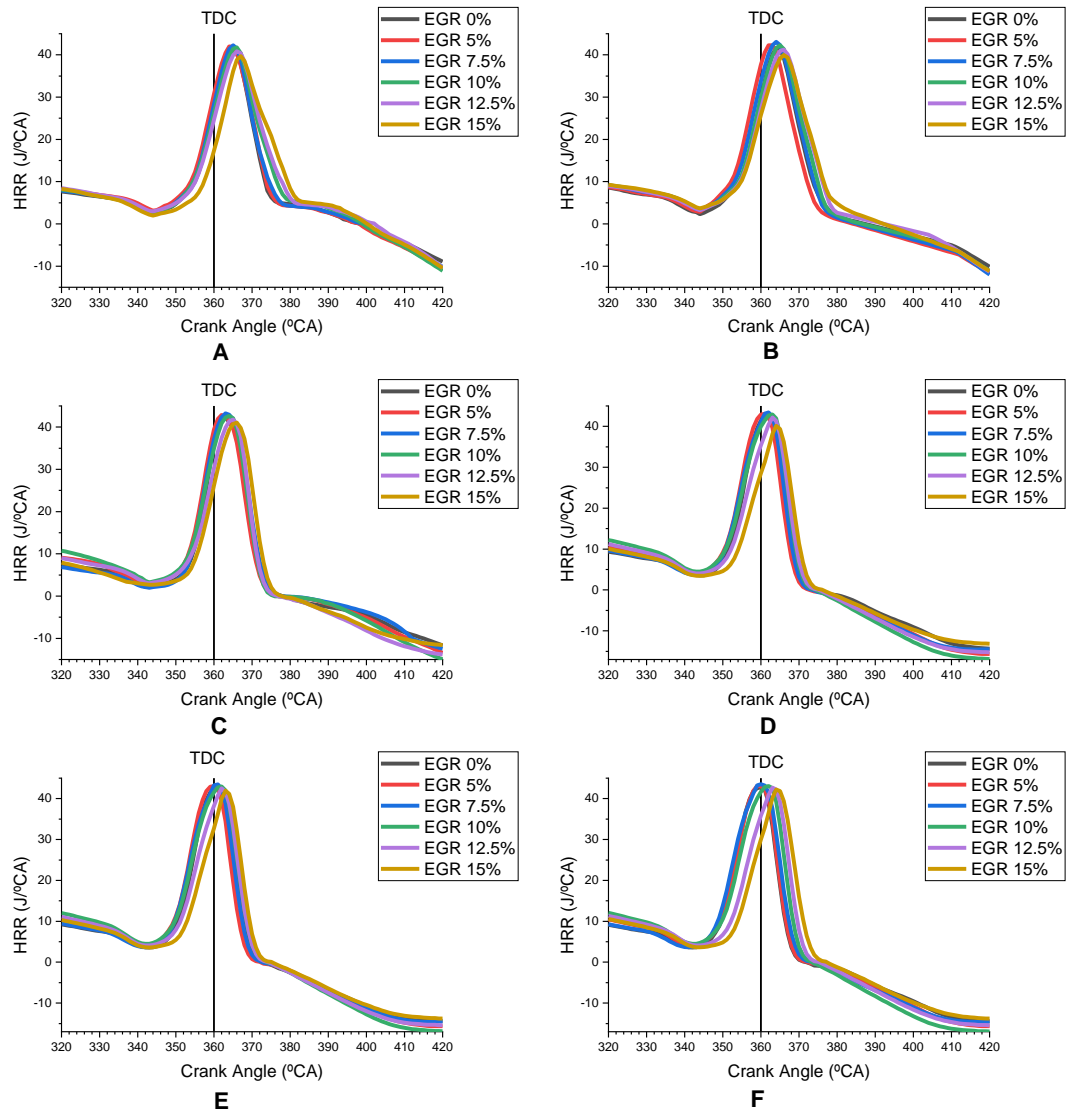
Figure 4.41.HRR varying with crank angle and EGR at various MAP at 1800rpm

4.3.7. Peak cylinder temperature (T_{max})

T_{max} is represented in Figure 4.42; there is a continuous increase in T_{max} by increasing MAP at any speed. However, the increment rate is discrete and depends on speed. T_{max} increases almost statically at low speed, while it first increases with MAP boost at high speed and then drops. An average 3.27% increase/5kPa MAP boost is observed at 1800rpm at 0% EGR. Since MGT increases with engine speed due to insufficient time available for engine cooling, it further adds up to T_{max}. In addition, the increased MGT

94

also reduces combustion duration; hence, T_{max} is further increased. While EGR is implemented, there is a small increment in T_{max} up to a specific EGR rate depending on MAP; at low MAP, the EGR rate corresponding to increasing T_{max} is larger. However, a further MAP boost leads to a larger recirculation mass, leading to high dilution; hence, T_{max} is continuously reducing with EGR at 110kPa. On the other hand, T_{max} drops rapidly for higher EGR rates, and the drop rate gradually increases with speed. Further, boosting MAP intensifies the EGR effect, as T_{max} drops more rapidly with increasing EGR by boosting MAP. It is observed that T_{max} for 110kPa is recorded as less than MAP 100kPa and 105kPa at EGR rates over 10%.
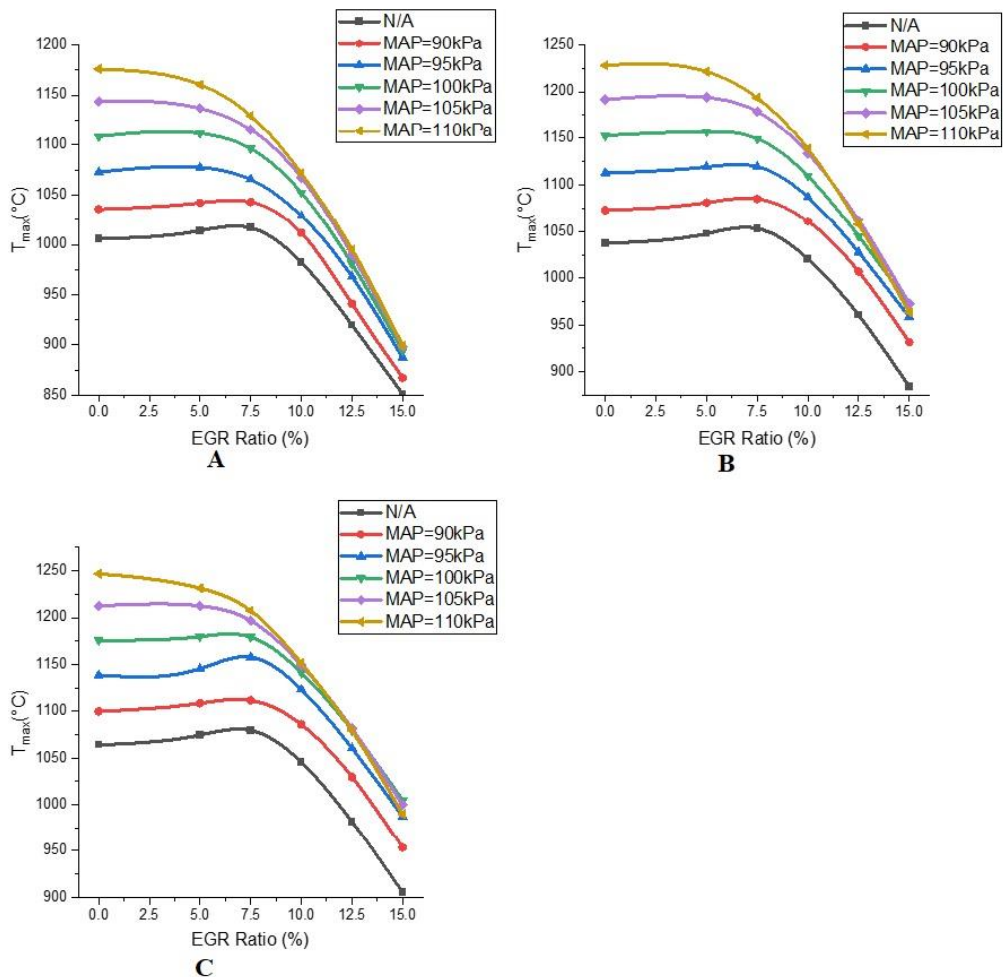
Figure 4.42.T_{max} varies with EGR and MAP (A-1400rpm, B-1600rpm, C-1800rpm)

4.3.8. Coefficient of variation in IMEP (CoV$_{imep}$)

CoV$_{imep}$ is observed to reduce by low EGR rates, as it reduces the combustion duration by increasing the MGT (Figure 4.43). At N/A conditions, combustion durations are long, resulting in large mass burning in the expansion stroke. Therefore, the fuel-burning rate is suppressed, and the cyclic variations increase.
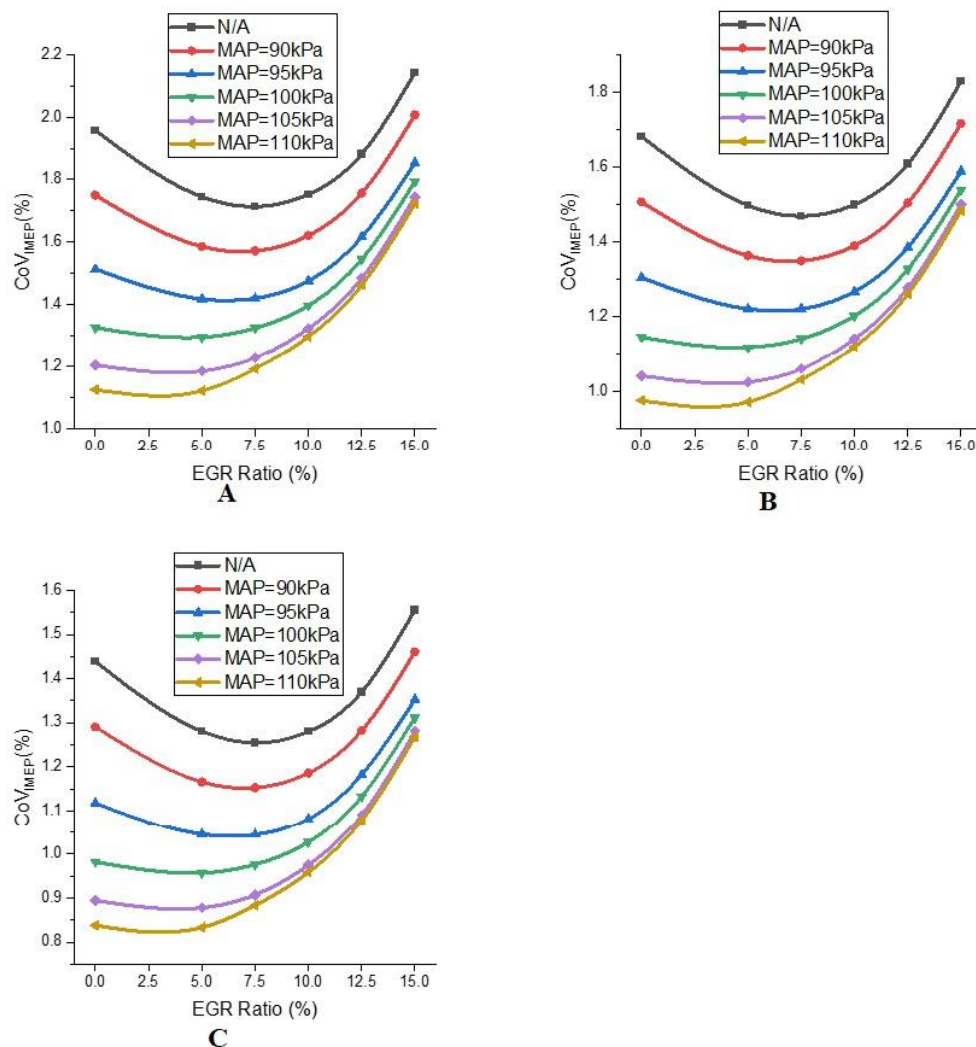
Figure 4.43. CoV$_{imep}$ varies with EGR and MAP (A-1400rpm, B-1600rpm, C-1800rpm)

On the other hand, EGR increases MGT, leading to fast burning and reduction of CoV$_{imep}$. At 5% EGR there is an average 22% reduction in CoV$_{imep}$. However, a higher EGR results in elongated combustion due to heterogeneity; hence, the cyclic variation increases, it increases CoV$_{imep}$ as at 15% EGR, there is 12.7% increase from 12.5%

EGR. With the increase of speed, combustion speed reduces, leading to shortening combustion; hence CoV_{imep} reduces. However, boosting MAP cools the combustion chamber, and regularizes fuel burning. Hence, CoV_{imep} is reduced, an average 62.3% CoV_{imep} drop at 110kPa from N/A is observed. The increasing speed has no significant impact on the MAP effects on CoV_{imep}; however, the impact of EGR reduces with MAP boosting. The EGR rate corresponding to minimum CoV_{imep} is observed to reduce with MAP boost; even at MAP 110kPa, the CoV_{imep} increases continuously with EGR.

4.3.9. Exhaust gas temperature (EGT)
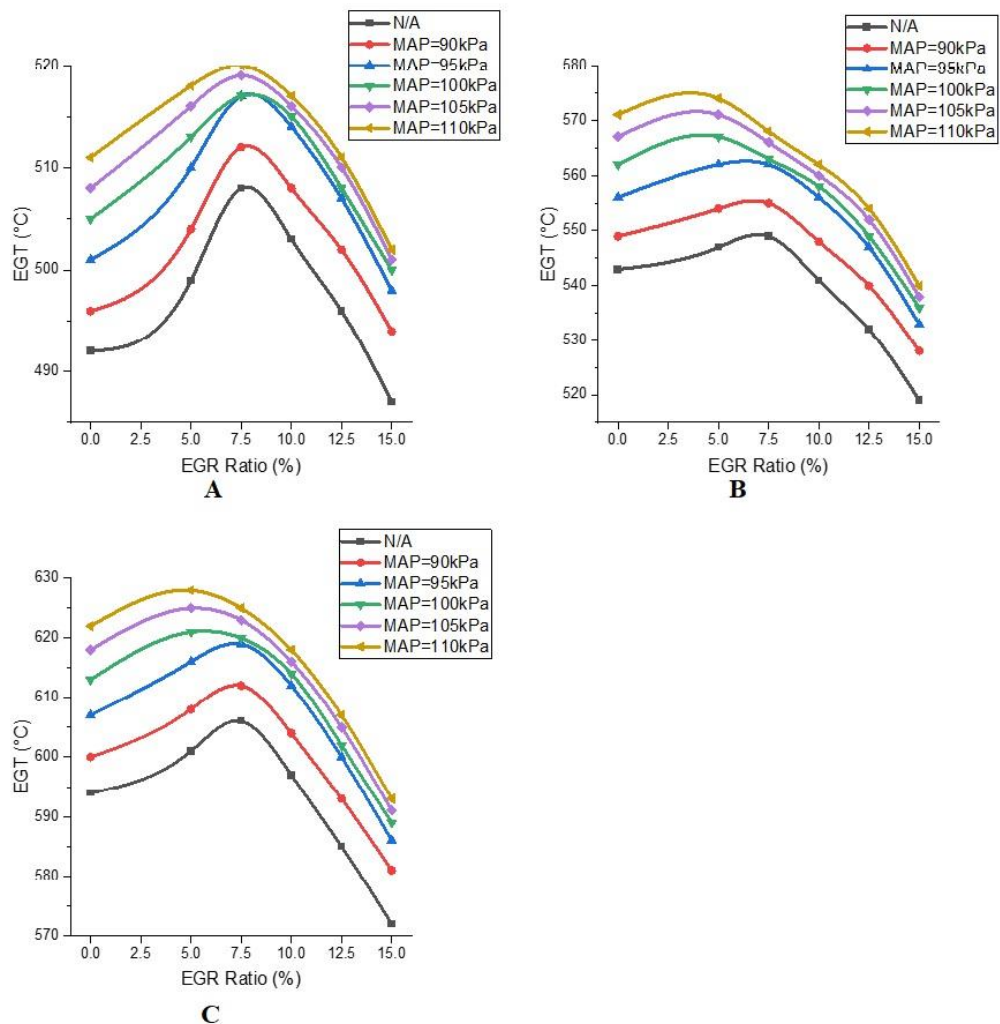
Figure 4.44.EGT varies with EGR and MAP (A-1400rpm, B-1600rpm, C-1800rpm)

EGT, as depicted in Figure 4.44, increases with initial EGR due to higher HRR leading to heat the working fluid to a great extent. Since low EGR promotes combustion, many high heat capacity gases are liberated, and HRR is also extensive; hence, a very high fraction of this energy is used to sensibly heat these exhaust gases like H_2O vapor, which carries out heat with it during exhaust. Hence, EGT increases. However, a further increase in EGR results in longer combustion, which increases heat loss to the cylinder wall, leading to reducing the sensible heating of these gases, EGT reduces. There is 0.87% increase noticed for 5% EGR, which changes to 2.2% drop for 15% EGR at N/A conditions. On the other hand, MAP boosting increases fuel supply and combustion speed; hence, more energy liberates, and the quantity of high heat capacity gases in exhaust increases. Therefore, EGT gets increased. An average 3.27% increase in EGT for 110kPa from N/A is noticed. The EGR rate corresponding to maximum EGT reduces with MAP. Similarly, the drop rate of EGT by EGR increases with MAP. EGT is also observed to increase with speed; even impact of EGR is observed to reduce with engine speed. However, MAP impact reduces continuously with engine speed.

4.3.10. NO$_x$ emissions

The NO$_x$ emission depends upon T_{max} and the residence time, and since the combustion period is very short in SI, the residence time plays an insignificant role. Hence, NO$_x$ formation is directly proportional to T_{max}. Figure 4.45 shows specific NO$_x$ emissions. From previous sections, it is noticed that a small EGR fraction improves combustion, resulting in increased P_{max}; however, the cylinder wall losses also occur; hence, the reflection in T_{max} is not that impressive. Therefore, NO$_x$ reduces slightly with EGR. The increment in BP is probably higher than the increase in NO$_x$ ppm, resulting in low specific NO$_x$. While the EGR is increased further, the dilution reduces T_{max} by elongated combustion and a considerable reduction in available oxygen. Therefore, the amount of nascent airborne nitrogen and oxidation becomes difficult, leading to reduced NO$_x$.

In addition, rapid increment in stratification reduces T_{max} severely, which effectively curbs the NO$_x$ formation. MAP boosting helps increase combustion, resulting in high T_{max} and increasing NO$_x$. However, with boosting MAP, the dilution ratio increases due to EGR, which does not allow excessive NO$_x$. Also, BP is improved significantly,

leading to lower specific NO_x compared to N/A at higher EGR rates. The increasing speed increases T_{max}, resulting in higher NO_x emissions; with higher MAP, more oxygen is supplied, leading to an increase. However, the impact of EGR is insignificant for speed change. The NO_x at MAP 110kPa is observed to reduce by 42.79% from N/A conditions at 15% EGR rates.
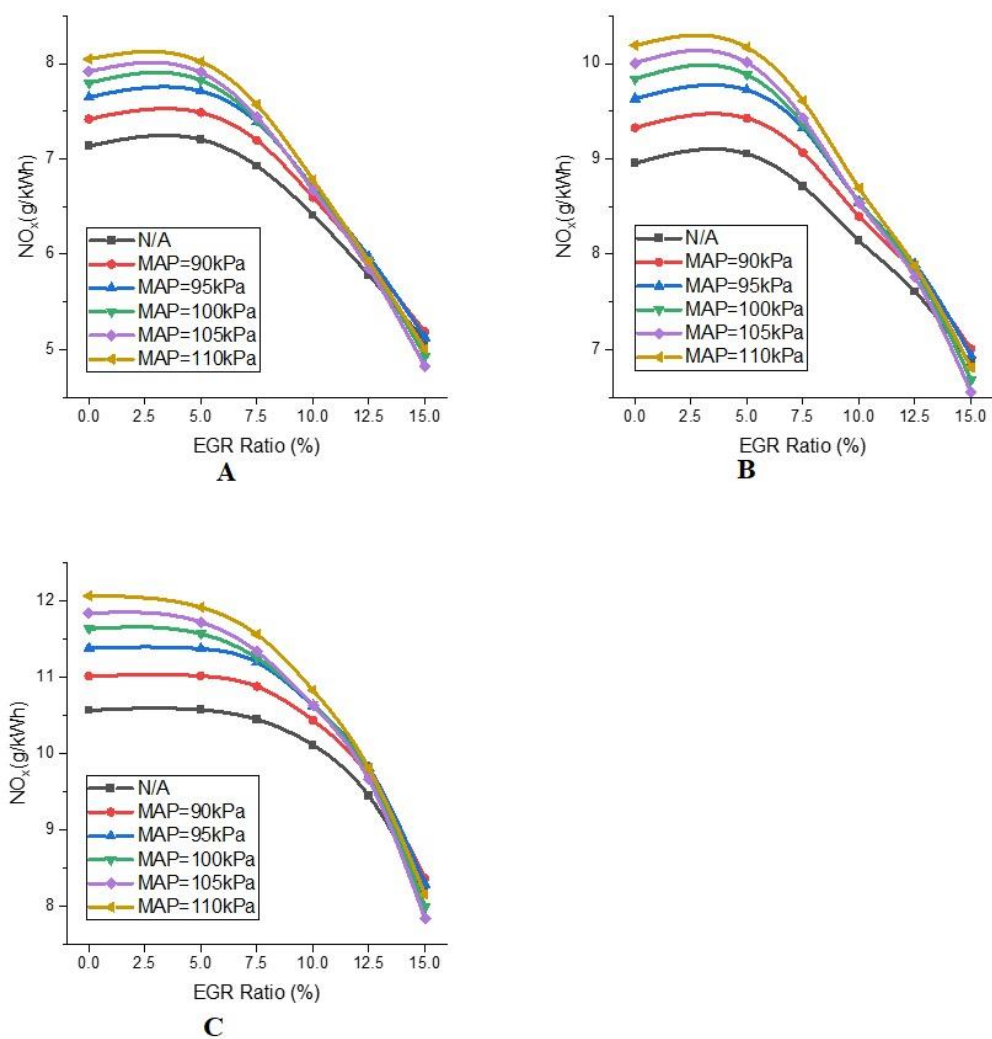
Figure 4.45.NO_x varies with EGR and MAP (A-1400rpm, B-1600rpm, C-1800rpm)

4.3.11. Conclusion of section 4.3

The results are discussed above in brief, and a summary of the outcomes is concluded as follows;

- A low EGR rate enhances BP and BTE; however, the performance deteriorates severely with increasing EGR. It leads to heat the incoming air, and expansion occurs in the mixing unit, which restricts a relatively large air intake, reducing η_{vol}.

- CA10, CA10-90, and late burning periods are observed to reduce with low EGR due to high cylinder temperature at the time of ignition. A further increase in EGR reduces oxygen reach, resulting in increased combustion durations.

- HRR, CP, and EGT are first increased and then reduced intensively with EGR.

- EGR reduces specific NO_x continuously; at low EGR, BP increases larger than volumetric NO_x increase; hence, specific NO_x reduces. At high EGR, it controls the oxidation of nascent nitrogen and reduces T_{max}; therefore, NO_x is reduced to a very low.

- MAP boosting helps reduce the volumetric losses, allowing more fuel to supply and fast combustion; hence, BP and BTE are increased; however, CA10, CA10-90, and Late burning are increased due to a larger amount of intake air and fuel supply.

- The combustion and BTE loss due to high EGR is reduced by MAP, which increases the operating pressure and MGT.

- The dilution ratio increases with MAP at high EGR, reducing NO_x; also, BP is increased; hence, specific NO_x is reduced at 110kPa MAP than N/A and low MAP.

A boosted MAP allows higher EGR to operate; hence, 110kPa is observed as the best MAP boost, considering CoV and NO_x emissions, at an optimal EGR of 12.5%, decided through a trade-off between NO_x control and BTE.

CHAPTER 5

CONCLUSION

The conclusions from the outcomes of the experimental study are made section-wise in the previous chapter; however, the entire research outcomes are summarised below;

- The drawbacks of hydrogen fuelling, such as low η_{vol} and power output, are solved by enhancing CR.

- Hydrogen can be operated on higher CR than gasoline within the safe limit, allowing a larger fuel supply under lean conditions. It improves power output.

- At high CR, better combustion speed due to higher MGT helps rapid fuel-burning, resulting in better efficiency.

- High CR and ϕ>0.8 has adverse effects on combustion and performance due to large replacement of air and increased probability of flame compression.

- At CR14 and moderate ϕ (0.75-0.8), BP is observed to be 5.68% higher than gasoline for a delayed ignition (18ºCA-16ºCA).

- The combustion duration is 13.48% less, which is reflected in a rapid rise in the HRR curve, it rises rapidly up to CR14. However, retarding ignition helps improve ignition delay; it elongates combustion duration by shifting a large amount of fuel burning in expansion stroke.

- The NO_x emissions are increased by 143% for ϕ=0.7-0.8 by raising CR from 10 to 14 due to 19% increased T_{max}, which is slightly controlled by 2ºCA-6ºCA delayed ignition.

- A largely delayed ignition controls NO_x efficiently, but BTE drops by 9.67%. A trade-off between BTE and NO_x has been laid to CR14 and 16ºCA bTDC.

- The EGR helps control NO_x, even at a 10% rate despite significant compromise with performance, NO_x dropped by 29%.

- Performance improves at low EGR, despite a continuous NO_x drop, while at high EGR (>10%), NO_x drops below 50% at the stake of a slight power drop.

- MAP boosting promotes fast combustion, improving BTE; however, combustion durations increase due to larger intake air and increased fuel supply.

- MAP boosting also increases dilution at high EGR, reducing NO_x below N/A conditions.

5.1. Future Scope

Though there are satisfactory results obtained from the research, there are still more challenges to solve. The power improvement is slight compared to gasoline, while η_{vol} is also a concern. The optimal conditions of MAP 110kPa and EGR 12.5% are suitable for NO_x control; lower η_{vol} is needed to improve. Hence, there are still some limitations in performance that can be improved. There are some techniques described below that can improve HICE.

- An electronically monitored high-pressure hydrogen injection directly to the combustion chamber can be a good option. It would not affect the air replacement; hence, η_{vol} may improve.
- Hydrogen requires a larger amount of air than gasoline, which increases with lean-extent. In such a case, a variable MAP controlling supercharging/ turbocharging mechanism may help in allowing more air to supply, improving performance.
- Though EGR implementation limits NO_x emissions, it does not drop them to near zero without compromising performance. Therefore, some after-treatment processes such as SCR could limit it to zero.
- The PM emissions are not studied due to limited technology; hence, they can be studied, and technology to reduce it would be studied too.

CHAPTER 6

REFERENCES

Abdalla, A. M., Hossain, S., Nis, O. B., & Azad, A. T. (2018). *Hydrogen production , storage , transportation and key challenges with applications : A review*. *165*(April), 602–627. https://doi.org/10.1016/j.enconman.2018.03.088

Açikgöz, B., Çelik, C., Soyhan, H. S., Gökalp, B., & Karabal, B. (2015). Emission characteristics of an hydrogen-CH4 fuelled spark ignition engine. *Fuel*, *159*(x), 298–307. https://doi.org/10.1016/j.fuel.2015.06.043

Ağbulut, Ü., Sarıdemir, S., & Albayrak, S. (2019). Experimental investigation of combustion, performance and emission characteristics of a diesel engine fuelled with diesel–biodiesel–alcohol blends. *Journal of the Brazilian Society of Mechanical Sciences and Engineering*, *41*(9). https://doi.org/10.1007/s40430-019-1891-8

Akansu, S. O., Tangöz, S., Kahraman, N., İlhak, M. İ., & Açıkgöz, S. (2017). Experimental study of gasoline-ethanol-hydrogen blends combustion in an SI engine. *International Journal of Hydrogen Energy*, *42*(40), 25781–25790. https://doi.org/10.1016/j.ijhydene.2017.07.014

Akif Ceviz, M., Sen, A. K., Küleri, A. K., & Volkan Öner, I. (2012). Engine performance, exhaust emissions, and cyclic variations in a lean-burn SI engine fueled by gasoline-hydrogen blends. *Applied Thermal Engineering*, *36*(1), 314–324. https://doi.org/10.1016/j.applthermaleng.2011.10.039

Alger, T., Gingrich, J., & Mangold, B. (2007). The effect of hydrogen enrichment on EGR tolerance in spark ignited engines. *SAE Technical Papers*, (724). https://doi.org/10.4271/2007-01-0475

Alrazen, H. A., & Ahmad, K. A. (2018). HCNG fueled spark-ignition (SI) engine with its e ff ects on performance and emissions. *Renewable and Sustainable*

Energy Reviews, *82*(September 2017), 324–342.
https://doi.org/10.1016/j.rser.2017.09.035

Ayad, S. M. M. E., Belchior, C. R. P., da Silva, G. L. R., Lucena, R. S., Carreira, E.
S., & de Miranda, P. E. V. (2020). Analysis of performance parameters of an
ethanol fueled spark ignition engine operating with hydrogen enrichment.
International Journal of Hydrogen Energy, *45*(8), 5588–5606.
https://doi.org/10.1016/j.ijhydene.2019.05.151

Bai-Gang, S., Hua-Yu, T., & Fu-Shui, L. (2014). The distinctive characteristics of
combustion duration in hydrogen internal combustion engine. *International
Journal of Hydrogen Energy*, *39*(26), 14472–14478.
https://doi.org/10.1016/j.ijhydene.2014.04.013

Bakhtyari, A., Makarem, M. A., & Rahimpour, M. R. (2018). *Hydrogen Production
Through Pyrolysis*.

Balki, M. K., & Sayin, C. (2014). The effect of compression ratio on the performance,
emissions and combustion of an SI (spark ignition) engine fueled with pure
ethanol, methanol and unleaded gasoline. *Energy*, *71*, 194–201.
https://doi.org/10.1016/j.energy.2014.04.074

Barbir, F. (2005). PEM electrolysis for production of hydrogen from renewable
energy sources. *Solar Energy*, *78*(5), 661–669.
https://doi.org/10.1016/j.solener.2004.09.003

Barelli, L. Ã., Bidini, G., Gallorini, F., & Servili, S. (2008). *Hydrogen production
through sorption-enhanced steam methane reforming and membrane
technology : A review*. *33*, 554–570.
https://doi.org/10.1016/j.energy.2007.10.018

Bergthorson, J. M., & Thomson, M. J. (2015). A review of the combustion and
emissions properties of advanced transportation biofuels and their impact on
existing and future engines. *Renewable and Sustainable Energy Reviews*, *42*,
1393–1417. https://doi.org/10.1016/j.rser.2014.10.034

Bhasker, J. P., & Porpatham, E. (2017). Effects of compression ratio and hydrogen
addition on lean combustion characteristics and emission formation in a
Compressed Natural Gas fuelled spark ignition engine. *Fuel*, *208*, 260–270.
https://doi.org/10.1016/j.fuel.2017.07.024

Binjuwair, S., & Alkudsi, A. (2016). The effects of varying spark timing on the
performance and emission characteristics of a gasoline engine: A study on Saudi
Arabian RON91 and RON95. *Fuel*, *180*, 558–564.
https://doi.org/10.1016/j.fuel.2016.04.071

Boggio, S. D. M., Lacava, P. T., Merola, S., Pe, A., & Irimescu, A. (2018).
*ScienceDirect Characterization of flame front propagation during early and late
combustion for methane-hydrogen fueling of an optically accessible SI engine*. *3*.
https://doi.org/10.1016/j.ijhydene.2018.10.167

Catapano, F., Iorio, S. Di, Sementa, P., & Vaglieco, B. M. (2016). Analysis of energy
ef fi ciency of methane and hydrogen-methane blends in a PFI / DI SI research
engine. *Energy*, *117*, 378–387. https://doi.org/10.1016/j.energy.2016.06.043

Ceper, B. A. (2012). Experimental investigation of the effect of spark plug gap on a
hydrogen fueled SI engine. *International Journal of Hydrogen Energy*, *37*(22),
17310–17320. https://doi.org/10.1016/j.ijhydene.2012.08.070

Chen, Z., Wang, L., Zhang, Q., Zhang, X., Yang, B., & Zeng, K. (2019). Effects of
spark timing and methanol addition on combustion characteristics and emissions
of dual-fuel engine fuelled with natural gas and methanol under lean-burn
condition. *Energy Conversion and Management*, Vol. 181, pp. 519–527.
https://doi.org/10.1016/j.enconman.2018.12.040

Cong, X., Ji, C., & Wang, S. (2021). Investigation into engine performance of a
hydrogen-dimethyl ether spark-ignition engine under various dimethyl ether
fractions. *Fuel*, *306*(June), 121429. https://doi.org/10.1016/j.fuel.2021.121429

Curry, S. (1963). A three-dimensional study of flame propagation in a spark ignition
engine. *SAE Technical Papers*, *71*(1963), 628–650.

https://doi.org/10.4271/630487

Das, L. M. (1990). *H Y D R O G E N ENGINES : A VIEW OF THE PAST A N D A LOOK INTO THE F U T U R E. 15*(6).

Davies, G. (2012). The role of demonstration, concept and competition cars. In *Materials for Automobile Bodies*. https://doi.org/10.1016/b978-0-08-096979-4.00004-9

Dhyani, V., & Subramanian, K. A. (2018). Experimental investigation on effects of knocking on backfire and its control in a hydrogen fueled spark ignition engine. *International Journal of Hydrogen Energy*, *43*(14), 7169–7178. https://doi.org/10.1016/j.ijhydene.2018.02.125

Dhyani, V., & Subramanian, K. A. (2019a). Control of backfire and NOx emission reduction in a hydrogen fueled multi-cylinder spark ignition engine using cooled EGR and water injection strategies. *International Journal of Hydrogen Energy*, *44*(12), 6287–6298. https://doi.org/10.1016/j.ijhydene.2019.01.129

Dhyani, V., & Subramanian, K. A. (2019b). Fundamental characterization of backfire in a hydrogen fuelled spark ignition engine using CFD and experiments. *International Journal of Hydrogen Energy*, *44*(60), 32254–32270. https://doi.org/10.1016/j.ijhydene.2019.10.077

Dhyani, V., & Subramanian, K. A. (2021). Development of online control system for elimination of backfire in a hydrogen fuelled spark ignition engine. *International Journal of Hydrogen Energy*, *46*(27), 14757–14763. https://doi.org/10.1016/j.ijhydene.2020.08.148

Diéguez, P. M. M., Urroz, J. C. C., Marcelino-Sádaba, S., Pérez-Ezcurdia, A., Benito-Amurrio, M., Sáinz, D., & Gandía, L. M. M. (2014). Experimental study of the performance and emission characteristics of an adapted commercial four-cylinder spark ignition engine running on hydrogen – methane mixtures. *Applied Energy*, *113*, 1068–1076. https://doi.org/10.1016/j.apenergy.2013.08.063

Dinesh, M. H., Pandey, J. K., & Kumar, G. N. (2022). Effect of parallel LPG fuelling in a methanol fuelled SI engine under variable compression ratio. *Energy*, *239*, 122134. https://doi.org/10.1016/j.energy.2021.122134

Duan, J., liu, F., Yang, Z., Sun, B., Chen, W., & Wang, L. (2017). Study on the NOx emissions mechanism of an HICE under high load. *International Journal of Hydrogen Energy*, *42*(34), 22027–22035. https://doi.org/10.1016/j.ijhydene.2017.07.048

Duan, X., Deng, B., Liu, Y., Zou, S., Liu, J., & Feng, R. (2020). An experimental study the impact of the hydrogen enrichment on cycle-to-cycle variations of the large bore and lean burn natural gas spark-ignition engine. *Fuel*, *282*(July), 118868. https://doi.org/10.1016/j.fuel.2020.118868

Duan, X., Li, Y., Liu, J., Guo, G., Fu, J., Zhang, Q., … Liu, W. (2019). Experimental study the effects of various compression ratios and spark timing on performance and emission of a lean-burn heavy-duty spark ignition engine fueled with methane gas and hydrogen blends. *Energy*, *169*, 558–571. https://doi.org/https://doi.org/10.1016/j.energy.2018.12.029

Duan, X., Liu, Y., Lai, M. C., Guo, G., Liu, J., Chen, Z., & Deng, B. (2019). Effects of natural gas composition and compression ratio on the thermodynamic and combustion characteristics of a heavy-duty lean-burn SI engine fueled with liquefied natural gas. *Fuel*, Vol. 254. https://doi.org/10.1016/j.fuel.2019.115733

Duan, X., Liu, Y., Liu, J., Lai, M. C., Jansons, M., Guo, G., … Tang, Q. (2019). Experimental and numerical investigation of the effects of low-pressure, high-pressure and internal EGR configurations on the performance, combustion and emission characteristics in a hydrogen-enriched heavy-duty lean-burn natural gas SI engine. *Energy Conversion and Management*, *195*(March), 1319–1333. https://doi.org/10.1016/j.enconman.2019.05.059

Eitel, J., Kramer, W., & Lutz, R. (2007). EXHAUST GAS RECIRCULATION STRATEGY IN THE HYDROGEN SI ENGINE. *Journal of KONES Powertrain*

and Transport, *14*(2), 457–464. https://doi.org/10.1007/bf03224626

Elsemary, I. M. M., Attia, A. A. A., Elnagar, K. H., & Elsaleh, M. S. (2017). Spark timing effect on performance of gasoline engine fueled with mixture of hydrogen–gasoline. *International Journal of Hydrogen Energy*, *42*(52), 30813–30820. https://doi.org/10.1016/j.ijhydene.2017.10.125

Fu, J., Zhong, L., Zhao, D., Liu, Q., Shu, J., Zhou, F., & Liu, J. (2021). Effects of hydrogen addition on combustion , thermodynamics and emission performance of high compression ratio liquid methane gas engine. *Fuel*, *283*(September 2020), 119348. https://doi.org/10.1016/j.fuel.2020.119348

Gao, J., Tian, G., Ma, C., Huang, L., & Xing, S. (2021). Explorations of the impacts on a hydrogen fuelled opposed rotary piston engine performance by ignition timing under part load conditions. *International Journal of Hydrogen Energy*, *46*(21), 11994–12008. https://doi.org/10.1016/j.ijhydene.2021.01.030

Gao, J., Tian, G., Ma, C., Xing, S., & Huang, L. (2021). Three-dimensional numerical simulations on the effect of ignition timing on combustion characteristics, nitrogen oxides emissions, and energy loss of a hydrogen fuelled opposed rotary piston engine over wide open throttle conditions. *Fuel*, *288*(September 2020), 119722. https://doi.org/10.1016/j.fuel.2020.119722

García-Morales, J., Cervantes-Bobadilla, M., Escobar-Jimenez, R. F., Gómez-Aguilar, J. F., & Olivares-Peregrino, V. H. (2017). Experimental implementation of a control scheme to feed a hydrogen-enriched E10 blend to an internal combustion engine. *International Journal of Hydrogen Energy*, *42*(39), 25026–25036. https://doi.org/10.1016/j.ijhydene.2017.08.110

Goel, S., Sharma, R., & Rathore, A. K. (2021). A review on barrier and challenges of electric vehicle in India and vehicle to grid optimisation. *Transportation Engineering*, *4*(February). https://doi.org/10.1016/j.treng.2021.100057

Gómez Montoya, J. P., Amador Diaz, G. J., & Amell Arrieta, A. A. (2018). Effect of equivalence ratio on knocking tendency in spark ignition engines fueled with

fuel blends of biogas, natural gas, propane and hydrogen. *International Journal of Hydrogen Energy*, *3*(51), 1–9. https://doi.org/10.1016/j.ijhydene.2018.10.117

Gong, C., Li, Z., Chen, Y., Liu, J., Liu, F., & Han, Y. (2019). Influence of ignition timing on combustion and emissions of a spark-ignition methanol engine with added hydrogen under lean-burn conditions. *Fuel*, *235*(July 2018), 227–238. https://doi.org/10.1016/j.fuel.2018.07.097

Gong, C., Li, Z., Sun, J., & Liu, F. (2020). Evaluation on combustion and lean-burn limit of a medium compression ratio hydrogen/methanol dual-injection spark-ignition engine under methanol late-injection. *Applied Energy*, *277*(July), 115622. https://doi.org/10.1016/j.apenergy.2020.115622

Gong, C., Li, Z., Yi, lin, Huang, K., & Liu, F. (2020). Research on the performance of a hydrogen/methanol dual-injection assisted spark-ignition engine using late-injection strategy for methanol. *Fuel*, *260*(October 2019), 116403. https://doi.org/10.1016/j.fuel.2019.116403

Gong, C., Li, Z., Yi, L., & Liu, F. (2020). Experimental investigation of equivalence ratio effects on combustion and emissions characteristics of an H2/methanol dual-injection engine under different spark timings. *Fuel*, *262*(October 2019), 116463. https://doi.org/10.1016/j.fuel.2019.116463

Government of Japan. (2017). Basic Hydrogen Strategy, Ministerial Council on Renewable Energy, Hydrogen and Related Issues. *Ministerial Council on Renewable Energy of Japan*, 1–37. Retrieved from http://www.meti.go.jp/english/press/2017/pdf/1226_003b.pdf

Greenwood, J. B., Erickson, P. A., Hwang, J., & Jordan, E. A. (2014). Experimental results of hydrogen enrichment of ethanol in an ultra-lean internal combustion engine. *International Journal of Hydrogen Energy*, *39*(24), 12980–12990. https://doi.org/10.1016/j.ijhydene.2014.06.030

Gürbüz, H., & Akçay, İ. H. (2021). Evaluating the effects of boosting intake-air pressure on the performance and environmental-economic indicators in a

hydrogen-fueled SI engine. *International Journal of Hydrogen Energy*, *46*(56), 28801–28810. https://doi.org/10.1016/j.ijhydene.2021.06.099

Hagos, F. Y., A. Aziz, A. R., Sulaiman, S. A., & Mamat, R. (2019). Engine speed and air-fuel ratio effect on the combustion of methane augmented hydrogen rich syngas in DI SI engine. *International Journal of Hydrogen Energy*, *44*(1), 477–486. https://doi.org/10.1016/j.ijhydene.2018.02.093

Heywood, J. B. (2018). *Internal Combustion Engine Fundamentals, Second Edition* (2nd editio). New York: McGraw-Hill Education.

Ivanič, Ž., Ayala, F., Goldwitz, J., & Heywood, J. B. (2005). Effects of hydrogen enhancement on efficiency and NOx emissions of lean and EGR-diluted mixtures in a SI engine. *SAE Technical Papers*, *114*(May 2022), 138–149. https://doi.org/10.4271/2005-01-0253

Jeeragal, R., & Subramanian, K. A. (2019). Experimental Investigation for NOx Emission Reduction in Hydrogen Fueled Spark Ignition Engine Using Spark Timing Retardation, Exhaust Gas Recirculation and Water Injection Techniques. *Journal of Thermal Science*, *28*(4), 789–800. https://doi.org/10.1007/s11630-019-1099-3

Ji, C., & Wang, S. (2010). Experimental study on combustion and emissions performance of a hybrid hydrogen – gasoline engine at lean burn limits. *International Journal of Hydrogen Energy*, *35*(3), 1453–1462. https://doi.org/10.1016/j.ijhydene.2009.11.051

Ji, C., & Wang, S. (2013). Combustion and emissions performance of a hydrogen engine at idle and lean conditions. *International Journal of Energy Research*, *37*, 468–474. https://doi.org/10.1002/er.3020

Ji, C., Wang, S., & Zhang, B. (2010). Effect of spark timing on the performance of a hybrid hydrogen-gasoline engine at lean conditions. *International Journal of Hydrogen Energy*, *35*(5), 2203–2212. https://doi.org/10.1016/j.ijhydene.2010.01.003

Keçebaş, A., & Kayfeci, M. (2019). Hydrogen properties. *Solar Hydrogen Production: Processes, Systems and Technologies*, 3–29. https://doi.org/10.1016/B978-0-12-814853-2.00001-1

Kim, J., Min, K., Song, S., Baek, H., & Woo, S. (2018). Hydrogen effects on the combustion stability , performance and emissions of a turbo gasoline direct injection engine in various air / fuel ratios. *Applied Energy*, *228*(May), 1353–1361. https://doi.org/10.1016/j.apenergy.2018.06.129

Kosmadakis, G. M., Rakopoulos, D. C., & Rakopoulos, C. D. (2021). Assessing the cyclic-variability of spark-ignition engine running on methane-hydrogen blends with high hydrogen contents of up to 50%. *International Journal of Hydrogen Energy*, *46*(34), 17955–17968. https://doi.org/10.1016/j.ijhydene.2021.02.158

Krishna, V. M., Reddy, A. H., Kumar, M. S., & Raghu, A. (2020). ScienceDirect Effect of hydroxy gas addition on performance and exhaust emissions in variable compression spark ignition engine. *Materials Today: Proceedings*, *24*, 930–936. https://doi.org/10.1016/j.matpr.2020.04.404

Lattimore, T., Herreros, J. M., Xu, H., & Shuai, S. (2016). Investigation of compression ratio and fuel effect on combustion and PM emissions in a DISI engine. *Fuel*, *169*, 68–78. https://doi.org/10.1016/j.fuel.2015.10.044

Lebrouhi, B. E., Khattari, Y., Lamrani, B., Maaroufi, M., Zeraouli, Y., & Kousksou, T. (2021). Key challenges for a large-scale development of battery electric vehicles: A comprehensive review. *Journal of Energy Storage*, *44*(PB), 103273. https://doi.org/10.1016/j.est.2021.103273

Lee, J., Park, C., Bae, J., Kim, Y., Choi, Y., & Lim, B. (2019). Effect of different excess air ratio values and spark advance timing on combustion and emission characteristics of hydrogen-fueled spark ignition engine. *International Journal of Hydrogen Energy*, *44*(45), 25021–25030. https://doi.org/10.1016/j.ijhydene.2019.07.181

Lee, J., Park, C., Kim, Y., Choi, Y., Bae, J., & Lim, B. (2019). Effect of turbocharger

on performance and thermal efficiency of hydrogen-fueled spark ignition engine. *International Journal of Hydrogen Energy*, *44*(8), 4350–4360. https://doi.org/10.1016/j.ijhydene.2018.12.113

Lee, S., Park, C., Park, S., & Kim, C. (2013). Comparison of the effects of EGR and lean burn on an SI engine fueled by hydrogen-enriched low calorific gas. *International Journal of Hydrogen Energy*, *39*(2), 1086–1095. https://doi.org/10.1016/j.ijhydene.2013.10.144

Lim, G., Lee, S., Park, C., Choi, Y., & Kim, C. (2014). Effect of ignition timing retard strategy on NOx reduction in hydrogen-compressed natural gas blend engine with increased compression ratio. *International Journal of Hydrogen Energy*, *39*(5), 2399–2408. https://doi.org/10.1016/j.ijhydene.2013.11.131

Liu, W., Placke, T., & Chau, K. T. (2022). Overview of batteries and battery management for electric vehicles. *Energy Reports*, *8*, 4058–4084. https://doi.org/10.1016/j.egyr.2022.03.016

Luo, Qing-he he, Hu, J. Bin, Sun, B. gang, Liu, F. shui, Wang, X., Li, C., & Bao, L. zhi. (2018). Experimental investigation of combustion characteristics and NOx emission of a turbocharged hydrogen internal combustion engine. *International Journal of Hydrogen Energy*, *44*(11), 5573–5584. https://doi.org/10.1016/j.ijhydene.2018.08.184

Luo, Qing he, Hu, J. Bin, Sun, B. gang, Liu, F. shui, Wang, X., Li, C., & Bao, L. zhi. (2019). Effect of equivalence ratios on the power, combustion stability and NOx controlling strategy for the turbocharged hydrogen engine at low engine speeds. *International Journal of Hydrogen Energy*, *44*(31), 17095–17102. https://doi.org/10.1016/j.ijhydene.2019.03.245

Ma, F., He, Y., Deng, J., Jiang, L., Naeve, N., Wang, M., & Chen, R. (2011). Idle characteristics of a hydrogen fueled SI engine. *International Journal of Hydrogen Energy*, *36*(7), 4454–4460. https://doi.org/10.1016/j.ijhydene.2010.12.121

Ma, F., Li, S., Zhao, J., Qi, Z., Deng, J., Naeve, N., … Zhao, S. (2012). Effect of compression ratio and spark timing on the power performance and combustion characteristics of an HCNG engine. *International Journal of Hydrogen Energy*, *37*(23), 18486–18491. https://doi.org/10.1016/j.ijhydene.2012.08.134

Ma, F., & Wang, Y. (2008). Study on the extension of lean operation limit through hydrogen enrichment in a natural gas spark-ignition engine. *International Journal of Hydrogen Energy*, *33*(4), 1416–1424. https://doi.org/10.1016/j.ijhydene.2007.12.040

Ma, F., Wang, Y., Liu, H., Li, Y., Wang, J., & Ding, S. (2008). Effects of hydrogen addition on cycle-by-cycle variations in a lean burn natural gas spark-ignition engine. *International Journal of Hydrogen Energy*, *33*(2), 823–831. https://doi.org/10.1016/j.ijhydene.2007.10.043

Maintenance, P., Şöhret, Y., Gürbüz, H., & Akçay, İ. H. (2019). Energy and exergy analyses of a hydrogen fueled SI engine: Effect of ignition timing and compression ratio. *Energy*, *175*, 410–422. https://doi.org/10.1016/j.energy.2019.03.091

Manigandan, S., Ponnusamy, V. K., Devi, P. B., Oke, S. A., Sohret, Y., Venkatesh, S., … Gunasekar, P. (2020). Effect of nanoparticles and hydrogen on combustion performance and exhaust emission of corn blended biodiesel in compression ignition engine with advanced timing. *International Journal of Hydrogen Energy*, *45*(4), 3327–3339. https://doi.org/10.1016/j.ijhydene.2019.11.172

Martin, J. C., Millington, P., Campbell, B., Barron, L., & Fisher, S. (2019). On-board generation of hydrogen to improve in-cylinder combustion and after-treatment efficiency and emissions performance of a hybrid hydrogen–gasoline engine. *International Journal of Hydrogen Energy*, *44*(25), 12880–12889. https://doi.org/10.1016/j.ijhydene.2018.12.164

Martínez-Merino, V., Gil, M. J., & Cornejo, A. (2013). Biological Hydrogen Production. *Renewable Hydrogen Technologies: Production, Purification,*

Storage, Applications and Safety, 171–199. https://doi.org/10.1016/B978-0-444-56352-1.00008-8

Millet, P., & Grigoriev, S. (2013). Water Electrolysis Technologies. *Renewable Hydrogen Technologies: Production, Purification, Storage, Applications and Safety*, 19–41. https://doi.org/10.1016/B978-0-444-56352-1.00002-7

Murthy, S. S. (2016). *Report on Hydrogen Storage and Applications Other Than*. 200.

Nadaleti, W. C., Przybyla, G., Vieira, B., Leandro, D., Gadotti, G., Quadro, M., … Castro, A. (2018). Efficiency and pollutant emissions of an SI engine using biogas-hydrogen fuel blends: BIO60, BIO95, H20BIO60 and H20BIO95. *International Journal of Hydrogen Energy*, *43*(14), 7190–7200. https://doi.org/10.1016/j.ijhydene.2018.02.133

Nande, A. M., Szwaja, S., & Naber, J. D. (2008). Impact of EGR on combustion processes in a hydrogen fuelled SI engine. *SAE Technical Papers*, *2008*(724). https://doi.org/10.4271/2008-01-1039

Naruke, M., Morie, K., Sakaida, S., Tanaka, K., & Konno, M. (2019). Effects of hydrogen addition on engine performance in a spark ignition engine with a high compression ratio under lean burn conditions. *International Journal of Hydrogen Energy*, *44*(29), 15565–15574. https://doi.org/10.1016/j.ijhydene.2019.04.120

Natkin, R. J., Tang, X., Boyer, B., Oltmans, B., Denlinger, A., & Heffel, J. W. (2003). Hydrogen IC engine boosting performance and NOX study. *SAE Technical Papers*, *112*, 865–875. https://doi.org/10.4271/2003-01-0631

Navale, S. J., Kulkarni, R. R., & Thipse, S. S. (2017). An experimental study on performance, emission and combustion parameters of hydrogen fueled spark ignition engine with the timed manifold injection system. *International Journal of Hydrogen Energy*, *42*(12), 8299–8309. https://doi.org/10.1016/j.ijhydene.2017.01.059

Nguyen, D., Choi, Y., Park, C., Kim, Y., & Lee, J. (2020). Effect of supercharger

system on power enhancement of hydrogen-fueled spark-ignition engine under low-load condition. *International Journal of Hydrogen Energy*, *46*(9), 6928–6936. https://doi.org/10.1016/j.ijhydene.2020.11.144

Nitnaware, P. T., & Suryawanshi, J. G. (2016). Effects of MBT spark timing on performance emission and combustion characteristics of S.I engine using hydrogen-CNG blends. *International Journal of Hydrogen Energy*, *41*(1), 666–674. https://doi.org/10.1016/j.ijhydene.2015.11.074

Nouni, M. R., Jha, P., Sarkhel, R., Banerjee, C., Tripathi, A. K., & Manna, J. (2021). Alternative fuels for decarbonisation of road transport sector in India: Options, present status, opportunities, and challenges. *Fuel*, *305*(June), 121583. https://doi.org/10.1016/j.fuel.2021.121583

Nuthan Prasad, B. S., Pandey, J. K., & Kumar, G. N. (2020). Impact of changing compression ratio on engine characteristics of an SI engine fueled with equi-volume blend of methanol and gasoline. *Energy*, *191*, 116605. https://doi.org/10.1016/j.energy.2019.116605

Oh, Sechul, Park, C., Nguyen, D., Kim, S., Kim, Y., Choi, Y., & Lee, J. (2021). Investigation on the operable range and idle condition of hydrogen-fueled spark ignition engine for unmanned aerial vehicle (UAV). *Energy*, *237*, 121645. https://doi.org/10.1016/j.energy.2021.121645

Oh, Seungmook, Kim, C., Lee, Y., Yoon, S., Lee, J., & Kim, J. (2019). Experimental investigation of the hydrogen-rich offgas spark ignition engine under the various compression ratios. *Energy Conversion and Management*, *201*(July), 112136. https://doi.org/10.1016/j.enconman.2019.112136

Oikawa, M., Kojiya, Y., Sato, R., Goma, K., Takagi, Y., & Mihara, Y. (2021). Effect of supercharging on improving thermal efficiency and modifying combustion characteristics in lean-burn direct-injection near- zero-emission hydrogen engines. *International Journal of Hydrogen Energy*, *47*(2), 1319–1327. https://doi.org/10.1016/j.ijhydene.2021.10.061

Pal, A., & Agarwal, A. K. (2015). Effect of compression ratio on combustion, performance and emissions of a laser ignited single cylinder hydrogen engine. *International Journal of Hydrogen Energy*, *40*(36), 12531–12540. https://doi.org/10.1016/j.ijhydene.2015.07.051

Panagariya, A. (2004). India's Trade Reform. *India Policy Forum: Columbia University*, 1–68.

Pollet, B. G., Kocha, S. S., & Staffell, I. (2019). Current status of automotive fuel cells for sustainable transport. *Current Opinion in Electrochemistry*, *16*, 90–95. https://doi.org/10.1016/j.coelec.2019.04.021

Polverino, P., D'Aniello, F., Arsie, I., & Pianese, C. (2019). Study of the energetic needs for the on-board production of Oxy-Hydrogen as fuel additive in internal combustion engines. *Energy Conversion and Management*, *179*(October 2018), 114–131. https://doi.org/10.1016/j.enconman.2018.09.082

Porpatham, E., Ramesh, A., & Nagalingam, B. (2007). Effect of hydrogen addition on the performance of a biogas fuelled spark ignition engine. *International Journal of Hydrogen Energy*, *32*(12), 2057–2065. https://doi.org/10.1016/j.ijhydene.2006.09.001

Porpatham, E., Ramesh, A., & Nagalingam, B. (2012). Effect of compression ratio on the performance and combustion of a biogas fuelled spark ignition engine. *Fuel*, *95*, 247–256. https://doi.org/10.1016/j.fuel.2011.10.059

Prasad, B. S. N., Pandey, J. K., & Kumar, G. N. (2021). Effect of hydrogen enrichment on performance, combustion, and emission of a methanol fueled SI engine. *International Journal of Hydrogen Energy*, *46*(49), 25294–25307. https://doi.org/10.1016/j.ijhydene.2021.05.039

Qiao, J., Li, Y., Wang, S., Wang, P., & Liu, J. (2020). Experimental investigation and numerical assessment the effects of EGR and hydrogen addition strategies on performance, energy and exergy characteristics of a heavy-duty lean-burn NGSI engine. *Fuel*, *275*(April), 117824. https://doi.org/10.1016/j.fuel.2020.117824

Qing-he, L., Bai-gang, S., Yong-li, G., Xi, W., Han, W., Ji-bin, H., … Chao, L. (2019). The effect of equivalence ratio , temperature and pressure on the combustion characteristics of hydrogen-air pre-mixture with turbulent jet induced by pre-chamber sparkplug. *International Journal of Hydrogen Energy*, *44*(36), 20470–20481. https://doi.org/10.1016/j.ijhydene.2019.05.238

Ravi, K., Pradeep Bhasker, J., Porpatham, E., Pradeep Bhasker, J., Porpatham, E., Bhasker, J. P., & Porpatham, E. (2017). Effect of compression ratio and hydrogen addition on part throttle performance of a LPG fuelled lean burn spark ignition engine. *Fuel*, *205*, 71–79. https://doi.org/10.1016/j.fuel.2017.05.062

Raviteja, S., & Kumar, G. N. (2015). Effect of hydrogen addition on the performance and emission parameters of an SI engine fueled with butanol blends at stoichiometric conditions. *International Journal of Hydrogen Energy*, *40*(30), 9563–9569. https://doi.org/10.1016/j.ijhydene.2015.05.171

Sadiq Al-Baghdadi, M. A. R. (2004). Effect of compression ratio, equivalence ratio and engine speed on the performance and emission characteristics of a spark ignition engine using hydrogen as a fuel. *Renewable Energy*, *29*(15), 2245–2260. https://doi.org/10.1016/j.renene.2004.04.002

Salvi, B. L., & Subramanian, K. A. (2016a). Experimental investigation on effects of compression ratio and exhaust gas recirculation on backfire , performance and emission characteristics in a hydrogen fuelled spark ignition engine. *International Journal of Hydrogen Energy*, *41*(13), 5842–5855. https://doi.org/10.1016/j.ijhydene.2016.02.026

Salvi, B. L., & Subramanian, K. A. (2016b). Experimental investigation on effects of exhaust gas recirculation on flame kernel growth rate in a hydrogen fuelled spark ignition engine. *Applied Thermal Engineering*, *107*, 48–54. https://doi.org/10.1016/j.applthermaleng.2016.06.125

Sarıkoç, S. (2021). Effect of H2 addition to methanol-gasoline blend on an SI engine at various lambda values and engine loads: A case of performance, combustion,

and emission characteristics. *Fuel*, *297*(March), 120732. https://doi.org/10.1016/j.fuel.2021.120732

Sayin, C. (2012). The impact of varying spark timing at different octane numbers on the performance and emission characteristics in a gasoline engine. *Fuel*, *97*(x), 856–861. https://doi.org/10.1016/j.fuel.2012.03.013

Senturk Acar, M., & Arslan, O. (2017). Exergo-economic Evaluation of a new drying system Boosted by Ranque-Hilsch vortex tube. *Applied Thermal Engineering*, *124*, 1–16. https://doi.org/10.1016/j.applthermaleng.2017.06.010

Shi, C., Ji, C., Wang, S., Yang, J., & Wang, H. (2021). Experimental and numerical study of combustion and emissions performance in a hydrogen-enriched Wankel engine at stoichiometric and lean operations. *Fuel*, *291*(January), 120181. https://doi.org/10.1016/j.fuel.2021.120181

Shivaprasad, K. V., Chitragar, P. R., & Kumar, G. N. (2015). Effect of Hydrogen Addition on Combustion and Emission Characteristics of High Speed Spark Ignition Engine- An Experimental Study. *SAE Technical Papers*, *2015-April*(April). https://doi.org/10.4271/2015-01-1684

Singh, R., & Das, L. M. (2019). Performance and emission assessment of a multi-cylinder S . I engine using CNG & HCNG as fuels. *International Journal of Hydrogen Energy*, *44*(38), 21181–21192. https://doi.org/10.1016/j.ijhydene.2019.03.137

Singh, S., Jain, S., Ps, V., Tiwari, A. K., Nouni, M. R., Pandey, J. K., & Goel, S. (2015). *Hydrogen : A sustainable fuel for future of the transport sector*. *51*, 623–633. https://doi.org/10.1016/j.rser.2015.06.040

Su, T., Ji, C., Wang, S., Cong, X., & Shi, L. (2018). Research on performance of a hydrogen/n-butanol rotary engine at idling and varied excess air ratios. *Energy Conversion and Management*, *162*(January), 132–138. https://doi.org/10.1016/j.enconman.2018.02.042

Subramanian, V., Mallikarjuna, J. M., & Ramesh, A. (2007). Intake charge dilution effects on control of nitric oxide emission in a hydrogen fueled SI engine. *International Journal of Hydrogen Energy*, *32*(12), 2043–2056. https://doi.org/10.1016/j.ijhydene.2006.09.039

Sun, B. G., Zhang, D. S., & Liu, F. S. (2013). Cycle variations in a hydrogen internal combustion engine. *International Journal of Hydrogen Energy*, *38*(9), 3778–3783. https://doi.org/10.1016/j.ijhydene.2012.12.126

Sun, X., Liu, H., Duan, X., Guo, H., Li, Y., Qiao, J., … Liu, J. (2022). Effect of hydrogen enrichment on the flame propagation, emissions formation and energy balance of the natural gas spark ignition engine. *Fuel*, *307*(2), 121843. https://doi.org/10.1016/j.fuel.2021.121843

Sun, Z. Y., & Li, G. X. (2016). Propagation characteristics of laminar spherical flames within homogeneous hydrogen-air mixtures. *Energy*, *116*, 116–127. https://doi.org/10.1016/j.energy.2016.09.103

Tangöz, S., Kahraman, N., & Akansu, S. O. (2017). The effect of hydrogen on the performance and emissions of an SI engine having a high compression ratio fuelled by compressed natural gas. *International Journal of Hydrogen Energy*, *42*(40), 25766–25780. https://doi.org/10.1016/j.ijhydene.2017.04.076

Technologies, B. (2013). Multi-Year Program Plan. *Office, Bioenergy Technologies*, (April).

Valiev, D. M., Akkerman, V., Kuznetsov, M., Eriksson, L. E., Law, C. K., & Bychkov, V. (2013). Influence of gas compression on flame acceleration in the early stage of burning in tubes. *Combustion and Flame*, *160*(1), 97–111. https://doi.org/10.1016/j.combustflame.2012.09.002

Verhelst, S. (2013). Recent progress in the use of hydrogen as a fuel for internal combustion engines. *International Journal of Hydrogen Energy*, *39*(2), 1071–1085. https://doi.org/10.1016/j.ijhydene.2013.10.102

Verhelst, S, Maesschalck, P., Rombaut, N., & Sierens, R. (2009). Increasing the power output of hydrogen internal combustion engines by means of supercharging and exhaust gas recirculation. *International Journal of Hydrogen Energy*, *34*(10), 4406–4412. https://doi.org/10.1016/j.ijhydene.2009.03.037

Verhelst, S, Vancoillie, J., Naganuma, K., Paepe, M. De, Dierickx, J., Huyghebaert, Y., & Wallner, T. (2012). Setting a best practice for determining the EGR rate in hydrogen internal combustion engines. *International Journal of Hydrogen Energy*, *38*(5), 2490–2503. https://doi.org/10.1016/j.ijhydene.2012.11.138

Verhelst, Sebastian, & Wallner, T. (2009). Hydrogen-fueled internal combustion engines. *Progress in Energy and Combustion Science*, *35*(6), 490–527. https://doi.org/10.1016/j.pecs.2009.08.001

Verma, T. N., Shrivastava, P., Rajak, U., Dwivedi, G., Jain, S., Zare, A., … Verma, P. (2021). A comprehensive review of the influence of physicochemical properties of biodiesel on combustion characteristics, engine performance and emissions. *Journal of Traffic and Transportation Engineering (English Edition)*, *8*(4), 510–533. https://doi.org/10.1016/j.jtte.2021.04.006

Wang, L., Yang, Z., Huang, Y., Liu, D., Duan, J., Guo, S., & Qin, Z. (2017). The effect of hydrogen injection parameters on the quality of hydrogen–air mixture formation for a PFI hydrogen internal combustion engine. *International Journal of Hydrogen Energy*, *42*(37), 23832–23845. https://doi.org/10.1016/j.ijhydene.2017.04.086

Wang, S., Ji, C., & Zhang, B. (2010). Effects of hydrogen addition and cylinder cutoff on combustion and emissions performance of a spark-ignited gasoline engine under a low operating condition. *Energy*, *35*(12), 4754–4760. https://doi.org/10.1016/j.energy.2010.09.015

Wang, S., Ji, C., Zhang, B., & Liu, X. (2014). Lean burn performance of a hydrogen-blended gasoline engine at the wide open throttle condition. *Applied Energy*, *136*, 43–50. https://doi.org/10.1016/j.apenergy.2014.09.042

Wang, Z., Liu, H., & Reitz, R. D. (2017). Knocking combustion in spark-ignition engines. *Progress in Energy and Combustion Science*, *61*, 78–112. https://doi.org/10.1016/j.pecs.2017.03.004

Xu, P., Ji, C., Wang, S., Bai, X., & Cong, X. (2018). Realizing low NOx emissions on a hydrogen-fuel spark ignition engine at the cold start period through excess air ratios control. *International Journal of Hydrogen Energy*, *43*(46), 21617–21626. https://doi.org/10.1016/j.ijhydene.2018.09.136

Xu, P., Ji, C., Wang, S., Bai, X., Cong, X., Su, T., & Shi, L. (2019). Realizing low emissions on a hydrogen-fueled spark ignition engine at the cold start period under rich combustion through ignition timing control. *International Journal of Hydrogen Energy*, *44*(16), 8650–8658. https://doi.org/10.1016/j.ijhydene.2019.01.275

Xu, P., Ji, C., Wang, S., Cong, X., Ma, Z., Tang, C., … Shi, C. (2020). Effects of direct water injection on engine performance in engine fueled with hydrogen at varied excess air ratios and spark timing. *Fuel*, *269*(November 2019), 117209. https://doi.org/10.1016/j.fuel.2020.117209

Yang, J., Ji, C., Wang, S., Zhang, Z., Wang, D., & Ma, Z. (2017). Numerical investigation of the effects of hydrogen enrichment on combustion and emissions formation processes in a gasoline rotary engine. *Energy Conversion and Management*, *151*(August), 136–146. https://doi.org/10.1016/j.enconman.2017.08.070

Yilmaz, İ., & Taştan, M. (2018). Investigation of hydrogen addition to methanol-gasoline blends in an SI engine. *International Journal of Hydrogen Energy*, *43*(44), 20252–20261. https://doi.org/10.1016/j.ijhydene.2018.07.088

Yousufuddin, S., & Masood, M. (2009). Effect of ignition timing and compression ratio on the performance of a hydrogen – ethanol fuelled engine. *International Journal of Hydrogen Energy*, *34*(16), 6945–6950. https://doi.org/10.1016/j.ijhydene.2009.05.122

Yu, X., Guo, Z., He, L., Dong, W., & Sun, P. (2019). Study on lean-burn characteristics of an SI engine with hydrogen / gasoline combined injection and EGR. *International Journal of Hydrogen Energy*, *44*(26), 13988–13998. https://doi.org/10.1016/j.ijhydene.2019.03.236

Yu, X., Li, D., Sun, P., Li, G., Yang, S., & Yao, C. (2021). Energy and exergy analysis of a combined injection engine using gasoline port injection coupled with gasoline or hydrogen direct injection under lean-burn conditions. *International Journal of Hydrogen Energy*, *46*(11), 8253–8268. https://doi.org/10.1016/j.ijhydene.2020.12.022

Zareei, J., Rohani, A., Mahmood, W. M. F. B. W., & Abdullah, S. (2020). Effect of Ignition Timing and Hydrogen Fraction in Natural Gas Blend on Performance and Exhaust Emissions in a DI Engine. *Iranian Journal of Science and Technology - Transactions of Mechanical Engineering*, *44*(3), 737–747. https://doi.org/10.1007/s40997-019-00296-x

Zhang, B., Ji, C., & Wang, S. (2015). Combustion analysis and emissions characteristics of a hydrogen-blended methanol engine at various spark timings. *International Journal of Hydrogen Energy*, *40*(13), 4707–4716. https://doi.org/10.1016/j.ijhydene.2015.01.142

Zhang, R., Chen, L., Wei, H., Pan, J., Li, J., Yang, P., & Chen, R. (2021). Optical study on the effects of the hydrogen injection timing on lean combustion characteristics using a natural gas/hydrogen dual-fuel injected spark-ignition engine. *International Journal of Hydrogen Energy*, *46*(39), 20777–20789. https://doi.org/10.1016/j.ijhydene.2021.03.171

Zhao, H., Stone, R., & Zhou, L. (2010). *Analysis of the particulate emissions and combustion performance of a direct injection spark ignition engine using hydrogen and gasoline mixtures*. *5*, 2–12. https://doi.org/10.1016/j.ijhydene.2010.02.087

Zhao, J., Ma, F., Xiong, X., Deng, J., Wang, L., & Naeve, N. (2013). Effects of

compression ratio on the combustion and emission of a hydrogen enriched natural gas engine under different excess air ratio. *Energy*, *59*(x), 658–665. https://doi.org/10.1016/j.energy.2013.07.033

Zhen, X., Tian, Z., Wang, Y., Liu, D., & Li, X. (2021). A model to determine the effects of low proportion of hydrogen and the flame kernel radius on combustion and emission performance of direct injection spark ignition engine. *Process Safety and Environmental Protection*, *147*(x), 1110–1124. https://doi.org/10.1016/j.psep.2021.01.040

Zheng, J., Huang, Z., Wang, J., Wang, B., Ning, D., & Zhang, Y. (2009). Effect of compression ratio on cycle-by-cycle variations in a natural gas direct injection engine. *Energy and Fuels*, *23*(11), 5357–5366. https://doi.org/10.1021/ef900651p

----

List of Publications based on PhD Research Work

[to be filled-in by the Research Scholar and to be enclosed with Synopsis submission Form]

Sl. No.	Title of the paper	Authors (in the same order as in the paper. Underline the Research Scholar's name)	Name of the Journal/ Conference/ Symposium, Vol., No., Pages	Month & Year of Publication	Category *
1.	Jayashish Kumar Pandey, G.N. Kumar	Effect of variable compression ratio and equivalence ratio on performance, combustion and emission of hydrogen port injection SI engine	Energy, Volume 239, Part E, 122468	January, 2022	1
2.	Jayashish Kumar Pandey, G.N. Kumar	Effects of hydrogen assisted combustion of EBNOL in SI engines under variable compression ratio and ignition timing	Energy, Volume 246, 123364	May, 2022	1
3.	Jayashish Kumar Pandey, G.N. Kumar	Consequences of ignition timing on a hydrogen-fueled engine at various equivalence ratio	Energy Sources Part A: Recovery, Utilization, and Environmental Effects, Vol. 44, No. 3, 6556–6567	June, 2022	1
4.	B.S. Nuthan Prasad, Jayashish Kumar Pandey, G.N. Kumar	Effect of hydrogen enrichment on performance, combustion, and emission of a methanol fueled SI engine	International Journal of Hydrogen Energy, Vol. 46, Issue 49, 25294-25307	July, 2021	1
5.	Jayashish Kumar Pandey, G.N. Kumar	Studying the effects of manifold pressure boosting and EGR on combustion and NO_x emission of hydrogen-fuelled SI engine	International Journal of Engine Research, IJER-22-0282	Accepted, January 03, 2022	1
6.	Jayashish Kumar Pandey, G.N. Kumar	Study of combustion and emission of a SI engine at various CR fuelled with different ratios of biobutanol/hydrogen fuel	Fuel, JFUE-D-23-00080	Under Review	2

* Category: 1: Journal paper, full paper reviewed
               2: Journal paper, Abstract reviewed
               3: Conference/Symposium paper, full paper reviewed
               4: Conference/Symposium paper, abstract reviewed
               5: others (including papers in Workshops, NITK Research Bulletins, Short notes etc.)

(If the paper has been accepted for publication but yet to be published, the supporting documents must be attached.)

Research Scholar   Research Guide(s)
Name & Signature, with Date   Name & Signature, with Date

BIO-DATA

Jayashish Kumar Pandey

Assistant Professor, Room-327, AB-1,
Department of Aeronautical and Automobile Engineering,
Manipal Insittute of Technology, Manipal, Udupi-576104,
Karnataka, India

Contact:
pandeyjayashish@gmail.com
Jayashish.pandey@manipal.edu.in
+91 9540897775, +91 8987214604

Orcid ID: - 0000-0003-3810-7922

❖ **Educational Qualifications**

- **Matriculation, 2002**
  Bihar Secondary Examination Board, Patna

- **Intermediate Science (Math), 2005**
  Bihar Intermediate Examination Council, Patna

- **B. Tech (Mechanical Engineering), 2010**
  ORISSA ENGINEERING COLLEGE, Rourkela

- **M. Tech (Thermal Engineering), 2013**
  NATIONAL INSTITUTE OF TECHNOLOGY KARNATAKA (NITK)

- **Ph.D. (Mechanical Engineering), 2022**
  NATIONAL INSTITUTE OF TECHNOLOGY KARNATAKA (NITK)

❖ **Research Publications (2018-22)**

- **Jayashish Kumar Pandey** and G.N. Kumar, "Effect of variable compression ratio and equivalence ratio on performance, combustion and emission of hydrogen port injection SI engine", *Energy*, Volume 239, Part E, 122468, *IF: 8.857,* https://doi.org/10.1016/j.energy.2021.122468

- **Jayashish Kumar Pandey** and G.N. Kumar, "Effects of hydrogen assisted combustion of EBNOL IN SI engines under variable compression ratio and ignition timing", *Energy*, Volume 246, 123364, *IF: 8.857,* https://doi.org/10.1016/j.energy.2022.123364

- **Jayashish Kumar Pandey**, Dinesh M.H. and G.N. Kumar, "Consequences of varying compression ratio and ignition timing on engine fuelled with E-MEBANOL", *International Journal of Engine Research, 1–20, 2022*, *IF: 5.21,* https://doi.org/10.1177/14680874221091676

- **Jayashish Kumar Pandey** and G.N. Kumar, "Consequences of ignition timing on a hydrogen-fueled engine at various equivalence ratio", *Energy Sources Part A: Recovery, Utilization, and Environmental Effects*, 2022, VOL. 44, NO. 3, 6556–6567, *IF: 3.447,* https://doi.org/10.1080/15567036.2022.2100519

- **Jayashish Kumar Pandey** and G.N. Kumar, "Studying the effects of manifold pressure boosting and EGR on combustion and NO_x emission of hydrogen-fuelled SI engine", *International Journal of Engine Research*, *In-proof, January 2023,* *IF: 5.21, https://doi.org/10.1177/14680874231153209*

- **Jayashish Kumar Pandey**, Dinesh M.H. and G.N. Kumar, "Study of bio-methanol as sustainable replacement of Autogas at variable ignition timing", *HELIYON, Volume 8, Issue 10, October 2022*, e-10865, *IF: 3.776,* https://doi.org/10.1016/j.heliyon.2022.e10865

- Dinesh M.H., **Jayashish Kumar Pandey** and G.N. Kumar, "Effect of parallel LPG fuelling in a methanol fuelled SI engine under variable compression ratio", *Energy*, Volume 239, Part C, 122134, *IF: 8.857,* https://doi.org/10.1016/j.energy.2021.122134

- Dinesh M.H., **Jayashish Kumar Pandey** and G.N. Kumar, "Study of performance, combustion, and NO_x emission behavior of an SI engine fueled with ammonia/hydrogen blends at various compression ratio", ***International Journal of Hydrogen Energy***, Volume 47, Issue 60, 25391-25403, ***IF: 7.139,*** https://doi.org/10.1016/j.ijhydene.2022.05.287
- B.S. Nuthan Prasad, **Jayashish Kumar Pandey** and G.N. Kumar, "Impact of changing compression ratio on engine characteristics of an SI engine fueled with equi-volume blend of methanol and gasoline", ***Energy***, Volume 191, 116605, ***IF: 8.857,*** https://doi.org/10.1016/j.energy.2019.116605
- B.S. Nuthan Prasad, **Jayashish Kumar Pandey** and G.N. Kumar, "Effect of hydrogen enrichment on performance, combustion, and emission of a methanol fueled SI engine", ***International Journal of Hydrogen Energy,*** Volume 46, Issue 49, Pages 25294-25307, ***IF: 7.139,*** https://doi.org/10.1016/j.ijhydene.2021.05.039